

# INVESTIGATION ON THE FLOW DISTRIBUTION WITHIN THE ROD BUNDLE OF AHWR

*By*

MOHIT PRAMOD SHARMA

ENGG 01201104005

Bhabha Atomic Research Centre, Mumbai

*A thesis submitted to the  
Board of Studies in Engineering Sciences*

*In partial fulfillment of requirements*

*for the Degree of*

**DOCTOR OF PHILOSOPHY**

*of*

**HOMI BHABHA NATIONAL INSTITUTE**

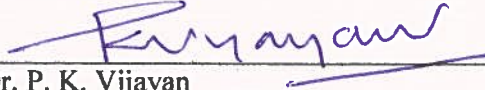
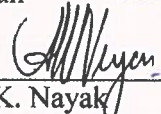
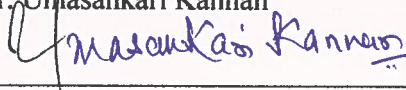
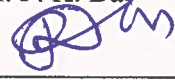
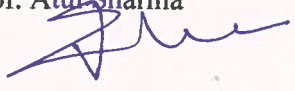


**September, 2016**

# Homi Bhabha National Institute

## Recommendations of the Viva Voce Committee

As members of the Viva Voce Committee, we certify that we have read the dissertation prepared by Mr. Mohit Pramod Sharma entitled "Investigation on the flow distribution within the rod bundle of AHWR" and recommend that it may be accepted as fulfilling the thesis requirement for the award of Degree of Doctor of Philosophy.

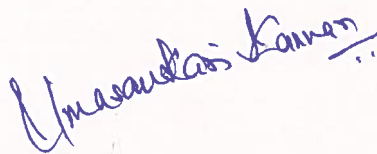
|   |                |
|---|----------------|
| <br>Chairman – Dr. P. K. Vijayan       | Date: 2/9/16   |
| <br>Guide / Convener – Dr. A. K. Nayak | Date: 2-9-16   |
| <br>Co-guide - Dr. Umasankari Kannan   | Date: 2/9/2016 |
| <br>Examiner – Prof. P. K. Das         | Date: 2.9.16   |
| <br>Member 1- Dr. K. Velusamy        | Date: 2/9/2016 |
| <br>Member 2- Prof. Atul Sharma      | Date: 2/9/16   |

Final approval and acceptance of this thesis is contingent upon the candidate's submission of the final copies of the thesis to HBNI.

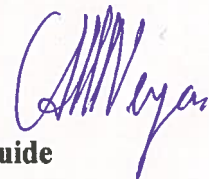
I/We hereby certify that I/we have read this thesis prepared under my/our direction and recommend that it may be accepted as fulfilling the thesis requirement.

Date: 2-9-2016

Place: Mumbai



Co-guide



Guide

## STATEMENT BY AUTHOR

This dissertation has been submitted in partial fulfillment of requirements for an advanced degree at Homi Bhabha National Institute (HBNI) and is deposited in the Library to be made available to borrowers under rules of the HBNI.

Brief quotations from this dissertation are allowable without special permission, provided that accurate acknowledgement of source is made. Requests for permission for extended quotation from or reproduction of this manuscript in whole or in part may be granted by the Competent Authority of HBNI when in his or her judgment the proposed use of the material is in the interests of scholarship. In all other instances, however, permission must be obtained from the author.



Mohit P sharma

## **DECLARATION**

I, hereby declare that the investigation presented in the thesis has been carried out by me. The work is original and has not been submitted earlier as a whole or in part for a degree / diploma at this or any other Institution / University.



Mohit P.Sharma

## **List of Publications arising from the thesis**

### **International Journals**

1. Sharma, M.P., Nayak A.K., 2016. "Experimental investigation of two phase turbulent mixing rate under bubbly flow regime in simulated subchannels of a natural circulation pressure tube type BWR". Experimental Thermal and Fluid Science (Elsevier), Vol. 76, Pages 228–237.
2. Sharma, M.P., Nayak A.K., 2015. "Determination of single phase turbulent mixing rate in simulated subchannels of a natural circulation pressure tube type BWR". Nuclear Science and Engineering (ANS), Vol. 180, 175-185.
3. Sharma, M.P., Nayak A.K., 2014. "Assessment and development of two phase turbulent mixing models for subchannel analysis relevant to BWR". World Journal Nuclear Science and Technology, Vol. 4, 195-207.
4. Sharma, M.P., Nayak A.K., 2014. "Assessment of two phase turbulent mixing model subchannel analysis relevant to BWR". Journal of Nuclear Engineering and Technology, Vol. 4, 25-44.
5. Sharma, M.P., Nayak A.K., 2016. "Determination of two phase turbulent mixing rate in simulated subchannels of a natural circulation pressure tube type BWR". Nuclear Science and Engineering (ANS), Target Vol. 184, issue 2. **In press**
6. Sharma, M.P., Nayak A.K., 2016. "Experimental investigation of void drift in simulated subchannels of a natural circulation pressure tube type BWR". Paper submitted in Nuclear Technology (ANS). **Accepted**
7. Sharma, M.P., Nayak A.K., 2016. "Experimental investigation of diversion cross flow in simulated subchannels of a natural circulation pressure tube type BWR". Nuclear Engineering and Radiation Science. (ASME). **Communicated (Accepted with modification)**

### **International Conferences**

1. Sharma, M.P., Nayak A.K., Kannan U. "Development of two phase turbulent mixing models for subchannel analysis relevant to BWR". Proceedings of New Horizons in Nuclear Reactor Thermal Hydraulics and Safety, January 13-15, 2014, Mumbai, India.
2. Sharma, M.P., Nayak A.K., Kannan U. "Determination of single phase turbulent mixing rate in a simulated AHWR subchannels". Proceedings of New Horizons in Nuclear Reactor Thermal Hydraulics and Safety, January 13-15, 2014, Mumbai, India.

  
Mohit P.Sharma

# DEDICATION

*I dedicate this thesis to my guide*

**Gurur Brahmaa Gurur Vishnuh Gurur Devo Maheshvarah;  
Gurur Sakshat Param Brahma Tasmai Shree Guruve Namah**

## ACKNOWLEDGEMENTS

I would like to acknowledge and express gratitude to my guide **Dr. A. K. Nayak**, Head, THS, Reactor Engineering Division, BARC, for his motivation, immense knowledge and his invaluable suggestions in carrying out my PhD studies. This thesis would not have been completed without his advice, support and encouragement. He always used to say “you will get Ph.D only if you give your heart to Ph.D work”. This line always motivates me for my research work. He guided me not only for research but also guided me spiritually. I learned from him how to do work under pressure and meet the deadline. He gave me moral support during the difficult times in my life. I could not have imagined having a better advisor and mentor for my Ph.D study.

I am also very thankful to my co-guide **Dr. Umasankari Kannan**, my doctoral committee chairman **Dr. P.K.Vijayan** and members **Dr. K. Velusamy** and **Dr. J.C. Mandal** for their valuable suggestion time to time

My sincere thanks to **Shri D. G. Belokar, Smt Rajalaxmi, Mr. Mahesh Bajaj, Mr. Arnab Das Gupta, Shri V.K. Gupta, Shri Ananthan, Dr. Parimal Kulkarni** and **Dr. D. K. Chandraker** for their support and suggestion during my experimental work

I express my gratitude to my friends *Mr. Abhijit P. Deokule, Mr. Jayaraj, Miss Paridhi, Mr. Sunil Kumar, Miss Sapna Singh* and *Mr. V. S. Yellapu* for their needful help.

My special thanks to *Mr. Avinash Moharana* and *Mr. Nitendra Singh* for helping me during my experimental work.

I would like to thank my father *Shri Pramod Sharma* and specially my mother *Smt. Snehlata Sharma* for her blessing, my brother *Rohit Sharma*, my lovely son *Chaitransh Sharma* and my wife *Anita Sharma* for keeping patience and her belief on me. I am very thankful to my family for supporting me emotionally throughout my Ph.D duration and my life in general.

Finally, I would like to thank all the staff members of RED, Bhabha Atomic Research Centre and Homi Bhabha National Institute

**Mohit P. Sharma**

ENGG01201104005

# CONTENTS

|   |       |
|---|-------|
| Synopsis .....  | i     |
| Abstract .....  | xv    |
| List of Figures .....   | xviii |
| List of Tables .....  | xxii  |
| Nomenclature .....  | xxv   |
| <b>CHAPTER 1 INTRODUCTION</b> .....   | 1     |
| 1.1 Introduction .....  | 1     |
| 1.1.1 Introduction to inter-subchannel mixing phenomena .....                                       | 1     |
| 1.2 Review of literature .....  | 3     |
| 1.2.1 Turbulent mixing .....  | 3     |
| 1.2.2 Void drift .....  | 15    |
| 1.2.3 Diversion Cross flow .....  | 20    |
| 1.3 Assessment of two phase turbulent mixing models .....   | 22    |
| 1.4 Motivation for Ph.D work .....  | 40    |
| 1.5 Objective and solution strategy .....   | 43    |
| 1.6 Development of a new model for turbulent mixing in rod bundle. ....                             | 44    |
| 1.7 Organization of thesis .....  | 58    |
| 1.8 Closure .....   | 60    |
| <b>CHAPTER 2 SCALING OF TEST FACILITY TO SIMULATE MIXING PHENOMENA IN<br/>AHWR ROD BUNDLE</b> ..... | 61    |
| 2.1 Introduction .....  | 61    |
| 2.2 Scaling of Test Facility .....  | 62    |
| 2.3 Experimental flow condition .....   | 64    |
| 2.3.1 Bubbly-Slug transition .....  | 65    |
| 2.3.2 Slug- Annular transition .....  | 65    |
| 2.4 Mixing model to evaluate turbulent mixing rate .....  | 66    |
| 2.4.1 Selection of tracer .....   | 73    |
| 2.5 Closure .....   | 74    |

**CHAPTER 3 EXPERIMENTAL TEST FACILITY AND EXPERIMENTAL PROCEDURE.. 75**

3.1 Introduction..... 75

3.2 Experimental Test Facility..... 75

    3.2.1 Test section ..... 78

    3.2.2 Mixer..... 79

    3.2.3 Separator ..... 80

    3.2.4 Tubes and fitting. .... 82

    3.2.5 Needle valve..... 82

    3.2.6 Rotameter ..... 82

3.3 Measurement of experimental variable..... 82

3.4 Experimental procedure for inter-subchannel mixing phenomena..... 85

3.5 Closure ..... 91

**CHAPTER 4 STUDY OF SINGLE PHASE TURBULENT MIXING RATE IN AHWR ROD**

*BUNDLE*..... 92

4.1 Introduction..... 92

4.2 Experiments conducted..... 93

4.3 Results and discussion ..... 94

4.4 Assessment of existing model to simulate single phase turbulent mixing rate..... 96

4.5 Model development ..... 100

4.6 Closure ..... 103

**CHAPTER 5 STUDY OF TWO PHASE TURBULENT MIXING RATE IN AHWR ROD**

*BUNDLE*..... 104

5.1 Introduction..... 104

5.2 Experiments conducted..... 106

5.3 Results and discussion ..... 108

5.4 Assessment of existing model to simulate two phase turbulent mixing rate ..... 112

5.5 Model development ..... 117

    5.5.1 Liquid phase turbulent mixing rate ..... 118

    5.5.2 Gas phase turbulent mixing rate ..... 122

5.6 Closure ..... 125

|  |     |
|--|-----|
| <b>CHAPTER 6</b> <i>STUDY OF VOID DRIFT IN AHWR ROD BUNDLE</i> .....                                       | 126 |
| 6.1 Introduction.....  | 126 |
| 6.2 Experiments conducted.....   | 129 |
| 6.3 Results and discussion .....   | 131 |
| 6.4 Determination of void diffusion coefficient .....  | 134 |
| 6.5 Assessment of existing model to simulate equilibrium void fraction distribution due to void drift..... | 136 |
| 6.6 Closure .....  | 141 |
| <br>   |     |
| <b>CHAPTER 7</b> <i>STUDY OF SINGLE AND TWO PHASE DIVERSION CROSS FLOW IN AHWR ROD BUNDLE</i> .....        | 142 |
| 7.1 Introduction.....  | 142 |
| 7.2 Experiments conducted.....   | 144 |
| 7.3 Results and discussion .....   | 145 |
| 7.3.1 Single phase diversion cross flow.....   | 146 |
| 7.3.2 Two phase diversion cross flow.....  | 147 |
| 7.4 Assessment of existing model to simulate diversion cross flow resistance.....                          | 148 |
| 7.5 Closure .....  | 156 |
| <br>   |     |
| <b>CHAPTER 8</b> <i>CONCLUSION AND FUTURE WORK</i> .....   | 157 |
| 8.1 Conclusion .....   | 157 |
| 8.2 Future Work .....  | 161 |
| <br>   |     |
| References.....  | 162 |
| APPENDIX 1 .....   | 170 |
| APPENDIX 2.....  | 181 |
| APPENDIX 3.....  | 185 |



1. Name of the Student: Mohit Pramod Sharma
2. Name of the Constituent Institution: Bhabha Atomic Research Centre
3. Enrolment Number: ENGG 01201104005
4. Title of the thesis: Investigation on the Flow Distribution within the Rod Bundle of AHWR
5. Board of studies: Engineering Sciences

## **Synopsis**

The Advanced Heavy Water Reactor (AHWR) is a vertical pressure tube type, heavy water moderated and boiling light water cooled natural circulation based reactor. The fuel bundle of AHWR contains 54 fuel rods arranged in three concentric rings of 12, 18 and 24 fuel rods. Evaluation of the coolant flow distribution under single and two phase flow condition is very important for AHWR rod bundle to ensure its safety and performance. Single phase flow condition exists in reactor rod bundle during start-up condition and up to certain length of rod bundle when it is operating at full power under boiling condition. Being a natural circulation BWRs, transition from single phase to two phase flow condition occurs in reactor rod bundle with increase in power. The determination of inter-subchannel mixing of coolant amongst these subchannels is important for evaluation thermal margin and safety of the reactor. The inter-subchannel mixing consists of three independent phenomena; turbulent mixing, void drift and diversion cross flow (Lahey and Moody (1993), Hotta et al. (2005)).

Of course, two phase turbulent mixing studies are not new especially for conventional BWRs. However it is important to assess the models developed so far, for their accuracy and applicability to AHWR condition. In this study, assessment of two phase turbulent mixing models applicable to BWRs has been performed against existing experimental data for various subchannel geometries of BWRs. An assessment of these models gives the following findings:

1. There are large differences among the data of turbulent mixing rate from one subchannel array to another.
2. There are large differences among the models when it is compared with the same experimental data as shown in table 1.

Table 1: Error analysis between calculated and measured turbulent mixing rate.

| Model                  | Liquid mixing rate |                 |                 | Gas mixing rate |                 |                 |
|------------------------|--------------------|-----------------|-----------------|-----------------|-----------------|-----------------|
|                        | Maximum error %    | Minimum error % | Average error % | Maximum error % | Minimum error % | Average error % |
| Bues (1972)            | +4320              | -93             | +515.4          | +412            | -93             | -52.1           |
| Kazimi and Kelly(1983) | +1480              | -86             | +153.2          | +2810           | -99             | -41.8           |
| Kawahara et al. (2000) | +9370              | -71.9           | +1200           | +7940           | -78.3           | +637            |
| Carlucci et al. (2003) | +1900              | -95             | -15.6           | +8910           | -96             | +104            |

Because of large error in the models, a new model for turbulent mixing rate was proposed from first principle. The turbulent mixing rate is expressed in terms of mixing number. The mixing number ( $N_{mix}$ ) for single phase flow which is function of Reynolds number (Re), gap (s) and centroidal distance ( $\delta$ ) between subchannel is considered. The equation can be represented by

$$N_{mix} = C Re^a \left( \frac{S}{\delta} \right)^b \quad (1)$$

The model for two phase turbulent mixing rate is modified by replacing single phase flow properties with two phase flow properties. Thus liquid and gas turbulent mixing number for two phase flow in subchannels is a function of mixture Reynolds number ( $Re_{mix}$ ), gap (S) and centroidal distance ( $\delta$ ) between subchannels. In addition the volumetric fraction ( $\beta$ ) needs to be incorporated in the model. The subchannel array effect ( $F_{gc}$ ) which is function of gap (S), centroidal distance ( $\delta$ ) and volumetric fraction ( $\beta$ ) and pressure effect ( $F_p$ ) which is function surface tension ( $\sigma$ ) of fluid is considered in present model. The equation for liquid and gas phase turbulent mixing rate can be represented by

$$N_{l,mix} = F_{l,gc} \times F_p \times 0.00104 Re^{1.80} \quad (2)$$

$$N_{g,mix} = F_{l,gc} \times F_p \times 0.0000749 (\ln(Re \times \beta))^{5.14} \quad (3)$$

The coefficient and exponent is obtained by fitting existing test data for different subchannel array. Hence the model could predict within average error of  $\pm 4\%$  for all the test data available for triangular-triangular, square-square, rectangular-rectangular subchannel array. The model was also tested even for steam-water high pressure data and found that it can predict within average error of  $\pm 9.94\%$ . These errors are significantly less than that predicted by previous models.

It may be notated that, the subchannel geometry of AHWR rod bundle is completely different from conventional BWRs. The rods in AHWR bundle are arranged in circular subchannel array unlike conventional BWRs geometry in which rods are arranged in square-square, rectangular-rectangular and square-rectangular subchannel array as shown in figure 1(a) and 1(b). The Steam generator heavy water reactor (SGHWR) bundle even though has similar geometry like AHWR rod bundle, however, there are almost no studies performed on inter-subchannel mixing studies for this reactor.

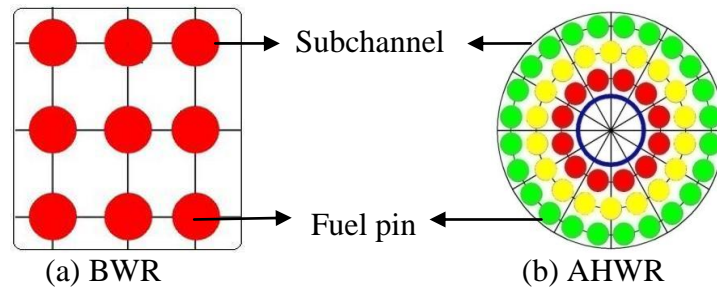


Fig.1. BWR and AHWR lattice

In addition, AHWR being a natural circulation BWR, the mass flux condition in the subchannels can vary from close to zero to rated condition depending on the power, which is different from conventional BWRs wherein the mass flux in the subchannel is more or less constant irrespective of power. Effect of variation of mass flux in the subchannels on two phase mixing phenomena typical to AHWR specific geometry has never been investigated. In the view of above, data obtained from conventional BWRs cannot be used for AHWR.

The objective of the thesis is to determine the mixing in subchannels of AHWR rod bundle due to turbulent mixing, void drift and diversion cross flow.

The strategy for solving these issues in AHWR rod bundle is carried out in following steps

1. Experiments performed in 1:1 scaled test facility simulating the subchannels of AHWR rod bundle for each component of inter-subchannel mixing i.e. turbulent mixing, void drift and diversion cross flow applicable to AHWR rod bundle
2. Assessment of existing models against present experiment data for turbulent mixing, void drift and diversion cross flow applicable to AHWR rod bundle
3. Development of new models for turbulent mixing, void drift and diversion cross flow, if existing models cannot predict measured values of present experiment applicable to AHWR rod bundle.

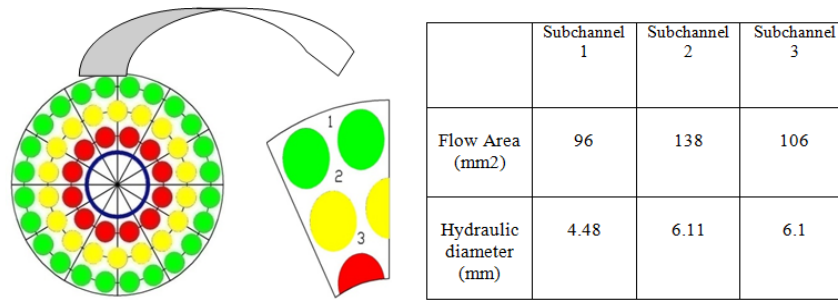


Fig. 2. 1/12<sup>th</sup> segment of AHWR fuel rod bundle

To simulate mixing phenomena, a test facility has been designed. The subchannel geometry simulated consists of 1/12<sup>th</sup> model of AHWR as shown in figure 2 (Dasgupta et al (2006)). The rods used in the subchannel mixing studies have the same size and pitch as that of actual rod bundle of AHWR. Three subchannels are considered in 1/12<sup>th</sup> symmetric cross section of the actual rod bundle. Table 2 shows comparison of the dimensions of rod bundle between model and prototype.

Table 2 Scaling of present experiment

| Properties   | Prototype           | Model               |
|--|---------------------|---------------------|
| Fluid  | Steam-water         | Air-water           |
| Fuel rod diameter                                  | 11.2 mm             | 11.2 mm             |
| Gap  | 2.3 mm              | 2.3 mm              |
| Height   | 3.5 m               | 3.5 m               |
| Subchannel Hydraulic diameter (1/12 section)       | 5.9 mm              | 5.9 mm              |
| Flow Area (1/12 section)                           | 340 mm <sup>2</sup> | 340 mm <sup>2</sup> |
| Liquid velocity in single phase ( $V_l$ )          | 0 to 1.2 m/s        | 0 to 1.2 m/s        |
| Superficial liquid velocity in two phase ( $J_l$ ) | 0 to 1 m/s          | 0 to 1 m/s          |
| Void fraction range                                | 0 to 0.8            | 0 to 0.8            |

The flow schematic of experimental loop is shown in figure 3.

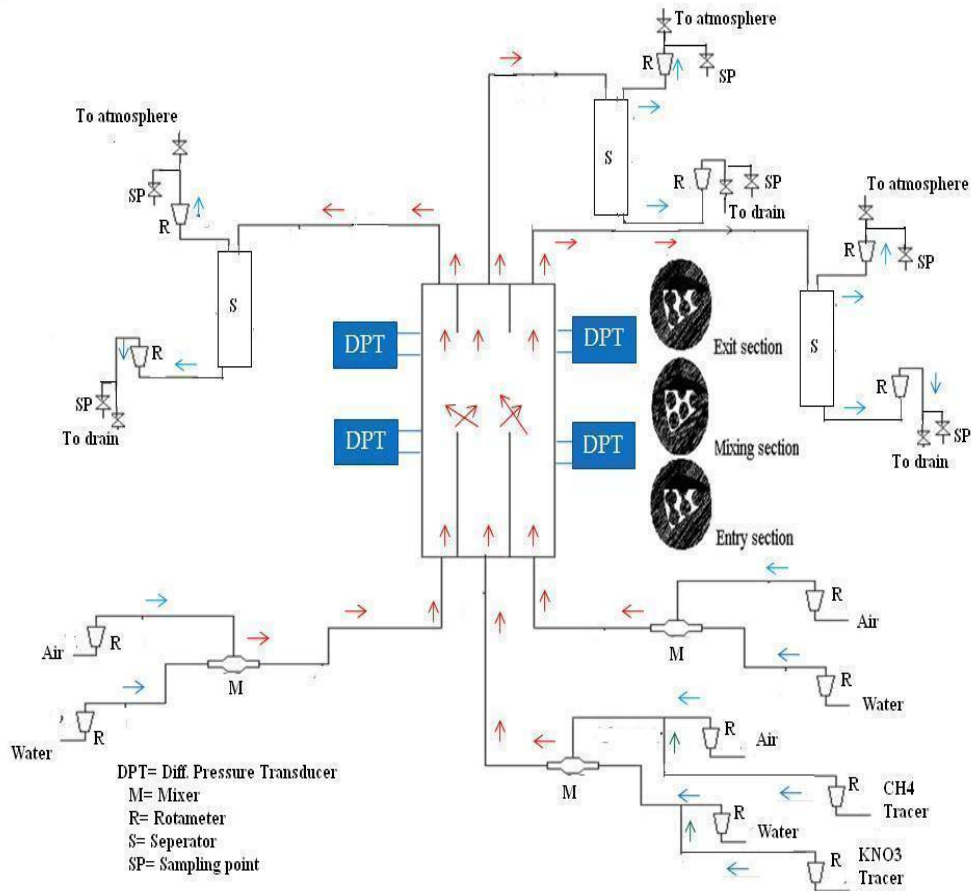


Fig. 3 Test rig schematic

The facility consists of a test section along with air-water mixer and separator. The vertical test channel of 3.5 m long is divided into three sections; entry section (1.5 m), mixing section (1.5 m) and discharge section (0.5 m) from bottom to the top of channel. In entry section and exit section, subchannels are completely separated by a 4 mm partition and in mixing section; subchannels are completely free from partition to allow mixing between subchannels. Potassium nitrate used as a tracer for water and methane gas is used as a tracer for air to simulate turbulent mixing among the subchannels. There are six rotameters used to measure air flow rate, six rotameters are used to measure water flow rate and two rotameters are used to measure tracer flow rate. Four differential pressure transmitters (DPT 1 to DPT 4) are provided to measure radial pressure difference between the subchannels. The accuracy of water rotameter is  $\pm 2\%$  over the full span of 20 lpm and for air rotameter is  $\pm 1\%$  over the

full span of 10 lpm. The accuracy of potassium nitrate tracer rotameter is  $\pm 2\%$  over the full span of 0.6 lpm and methane gas tracer rotameter is  $\pm 1\%$  over the full span of 1 lpm. The accuracy of differential pressure transmitters is  $\pm 0.2\%$ . The analysis of tracer concentration in collected sample of liquid was carried out by absorption spectrophotometer and for gas through gas chromatograph. The instrument was calibrated prior to each set of analysis with standard solution. Analysis was reproducible within  $\pm 1\%$ .

**(i) Determination of turbulent mixing rate in AHWR rod bundle**

The single phase turbulent mixing rate among the subchannels of AHWR rod bundle is measured for different liquid flow rate. Figure 4 shows variation of measured mixing rate with average Reynolds number.

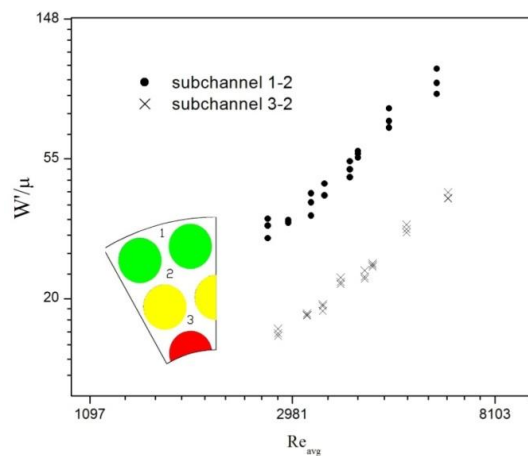


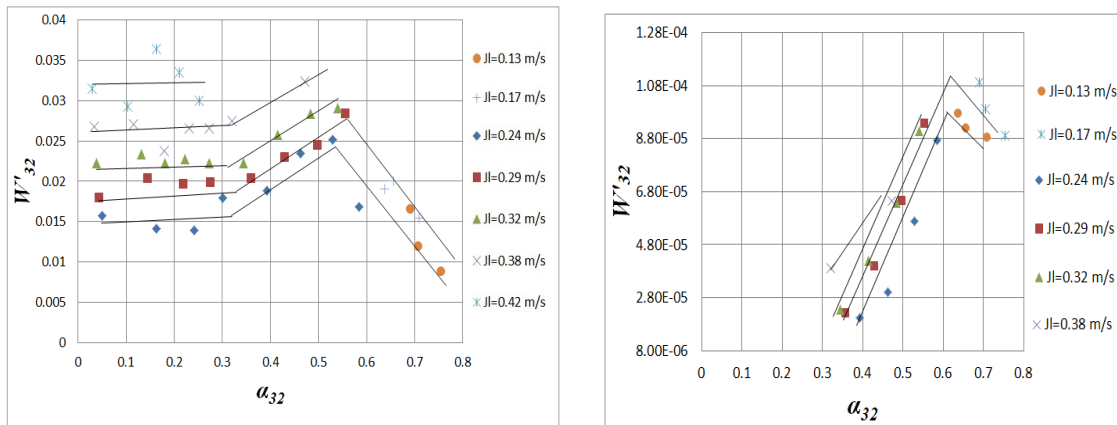
Fig. 4 Comparison of  $W'/\mu$  against  $Re_{avg}$

The main findings are as follows

1. The turbulent mixing rate is found to increase with increase in mass flux or Reynolds number, which is function of mass flux in the subchannels of rod bundle.
2. It also indicates that the turbulent mixing rate between subchannel 1-2 i.e.  $W'_{12}$  is higher as compared to subchannel 3-2 i.e.  $W'_{32}$  because subchannel 1-2 has higher gap to centroidal ratio ( $S/\delta$ ) as compared to subchannel 3-2.

An assessment of existing models against present experimental data has been carried out and found that none of these models predict measured turbulent mixing rate for AHWR rod bundle. There are errors between measured and predicted value by  $-92\%$  to  $+327\%$  (average error) depends on the models. The model presented earlier in equation (1) was used and modified by changing the coefficient and exponent by fitting the present test data which predicts turbulent mixing rate quite accurately within  $\pm 7\%$ .

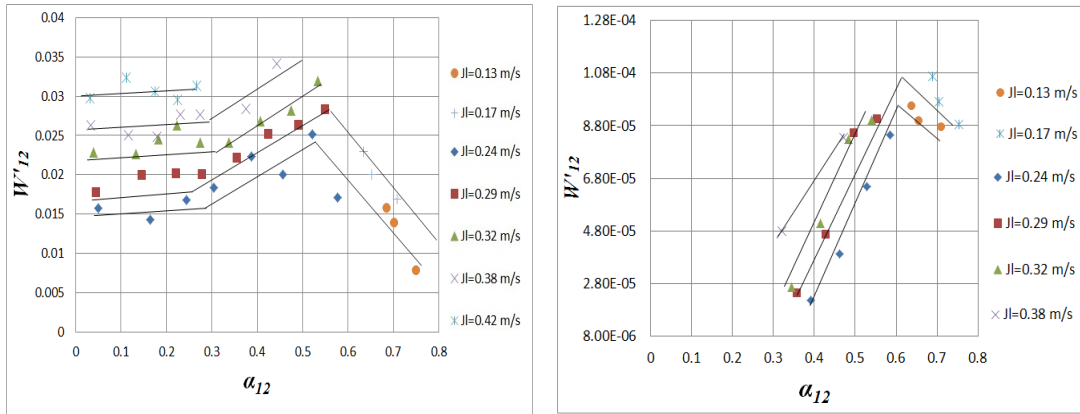
Figures 5 and 6 show variation of two phase turbulent mixing rate against average void fraction between the subchannels of AHWR rod bundle. The turbulent mixing rate in two phase flow is sum of liquid and gas phase turbulent mixing rate in two phase flow. The liquid and gas phase turbulent mixing rate in subchannel 1-2 and subchannel 3-2 is measured for void fraction ranging from 0 to 0.8 by varying superficial liquid velocity. It was difficult to measure turbulent mixing rate accurately beyond void fraction of  $\alpha=0.55$  at superficial liquid velocity equal to 0.2. This is because above this limit, the two phase air-water mixture is found to be unstable and difficult to quantify the mixing rate in the test.



(a) Liquid phase

(b) Gas phase

Fig. 5 Turbulent mixing rate vs average void fraction between subchannel 3-2



(a) Liquid phase

(b) Gas phase

Fig. 6 Turbulent mixing rate vs average void fraction between subchannel 1-2.

The main findings of these experiments are as follows

1. The liquid phase turbulent mixing rate is more or less constant up to average void fraction of 0.3 which is in bubbly flow regime, and then increases and reaches to a maximum at void fraction equal to 0.55 which is in slug-churn flow regime; afterwards it decreases till it reaches void fraction equal to 0.8.
2. The gas phase turbulent mixing rate increases with increase in average void fraction and reaches maximum at void fraction equal to 0.65. Afterwards, it decreases till it reaches void fraction equal to 0.8. However the gas phase turbulent mixing is difficult to measure in bubbly flow due to low air flow (void fraction equal to 0.3)
3. The results indicate that turbulent mixing rate increases with increase in superficial liquid velocity.
4. The test data were compared with existing models. It was found that existing models could not predict the measured turbulent mixing rate in the rod bundle of AHWR.

An assessment of existing models against present experimental data has been carried out and found that none of these models predict measured turbulent mixing rate for AHWR rod bundle. There are errors between measured and predicted value by  $-68\%$  to  $+567\%$

(average error) depends on the models. The model presented earlier in equation (2) and (3) was used and modified by changing the coefficient and exponent by fitting the present test data which predicts turbulent mixing rate quite accurately within average error of  $\pm 2\%$ .

### (ii) Determination of void drift in AHWR rod bundle

The void drift among the subchannels of AHWR rod bundle was measured by varying non-equilibrium flow at inlet and measuring subsequent equilibrium flow at outlet of individual subchannel.

The net change in gas mass flux between the subchannels due to void drift can be expressed by (Lahey and Moody (1993))

$$G_{g,ij} = \rho_g D [(\alpha_i - \alpha_j) - (\alpha_i - \alpha_j)_{eq}] / S_{ij} \quad (3)$$

Where  $G_{g,ij}$  is net change in mass flux due to void drift,  $\rho_g$  is the density of gas,  $D$  is void diffusion coefficients,  $(\alpha_i - \alpha_j)$  is void fraction difference in non-equilibrium flow,  $(\alpha_i - \alpha_j)_{eq}$  is void fraction difference in equilibrium flow and  $S_{ij}$  is gap between the subchannels.

Figure 7 shows variation of equilibrium void fraction (at outlet) with non-equilibrium (at inlet) void fraction.

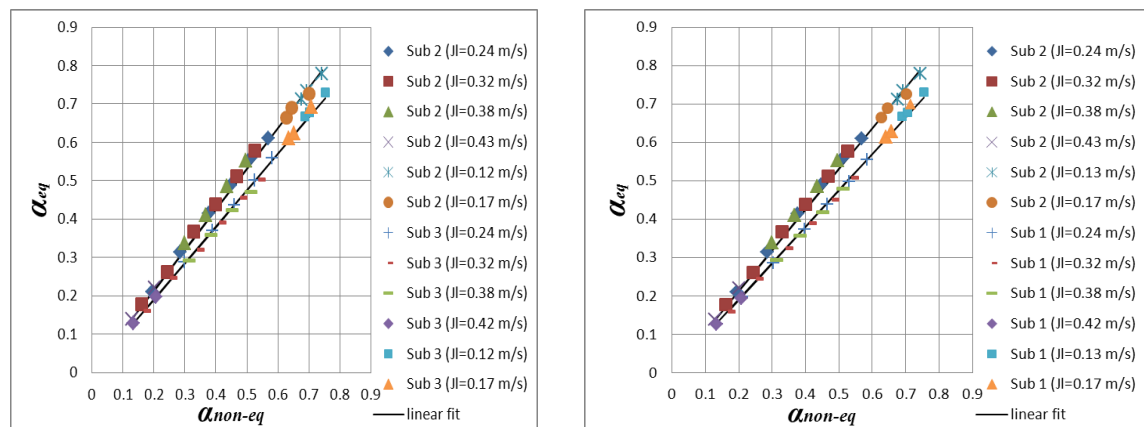


Fig. 7 Equilibrium void fraction vs non equilibrium void fraction for subchannel 3-2 and subchannel1-2

The main findings of these experiments are as follows.

1. The equilibrium void fraction is more in subchannel 2 as compared to subchannel 3 and subchannel 1. This is because ratio of flow area of subchannel 2 ( $A_2$ ) to the total area ( $A_t=A_1+A_2+A_3$ ) is more for subchannel 2 ( $A_2/A_t=0.40$ ) as compared to subchannel 3 ( $A_3/A_t = 0.29$ ) and subchannel 1 ( $A_1/A_t=0.31$ ).
2. The variation in equilibrium and non-equilibrium void fraction is very less with respect to liquid superficial velocity.
3. In both the cases of void drift i.e. subchannel 1-2 and subchannel 3-2, the difference in equilibrium and non-equilibrium void fraction of individual subchannels is less when void fraction is equal to 0.3 and this difference is more at void fraction greater than 0.3. This means that voids drift more in slug-churn as compared to bubbly flow.

Figure 8 shows the variation of void diffusion coefficient between the subchannels with average void fraction.

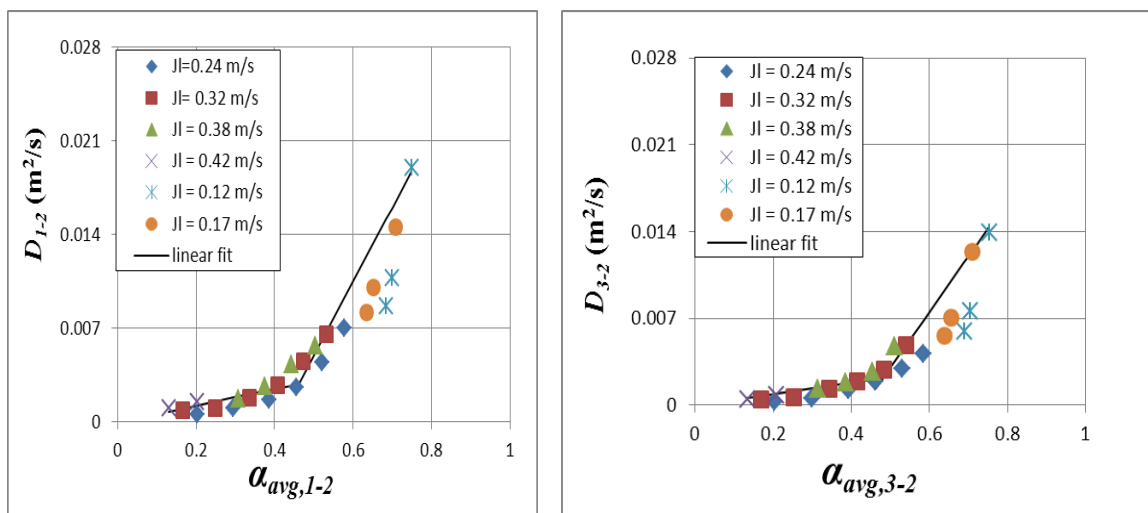


Fig. 8 Variation of void diffusion coefficient between the subchannel 1-2 and subchannel 3-2 with average void fraction.

The main findings are as follows.

1. The void diffusion coefficient is more or less constant or little increases with increase in average void fraction up to  $\alpha \approx 0.45$ . Beyond void fraction  $\alpha \approx 0.45$ , there is a steep increase in void diffusion coefficient with increase in average void fraction.
2. The trends of void diffusion coefficient found to be same for subchannel 1-2 and subchannel 3-2.
3. Also the magnitude of diffusion coefficient found to be increase with increase in superficial liquid velocity.

The capability of existing correlation is checked to predict the measured equilibrium void fraction. The test data were compared with existing models in literature. It was found that existing models could predict the measured equilibrium void fraction in the rod bundle of reactor within range (average error) of +8 % to -14 %.

### **(iii) Determination of diversion cross flow in AHWR rod bundle.**

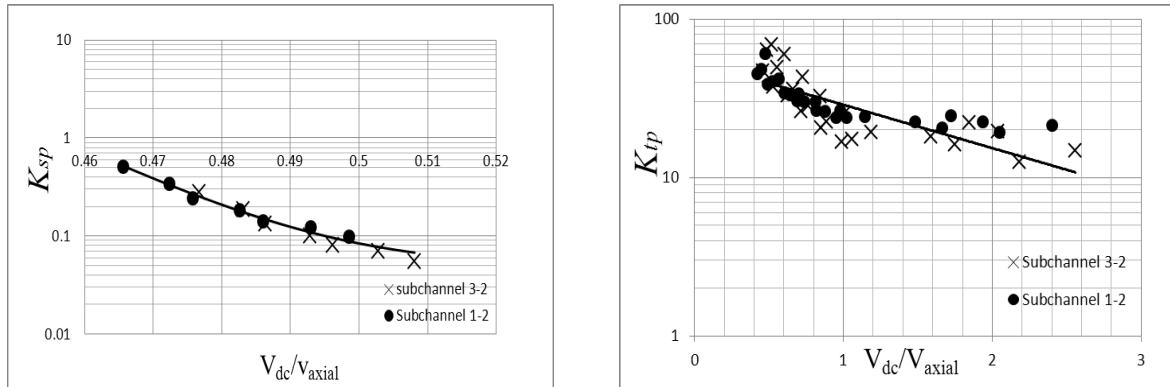
The diversion cross flow is an inter-subchannel mixing phenomena which occurs only due to lateral pressure difference between adjacent subchannels. In this phenomenon, there is a net flow from one subchannel to the other at their common boundary. The radial pressure difference between the subchannels is generally related to density and cross flow velocity between the subchannels by a factor  $K$  which is called as transverse resistance coefficient or cross flow resistance coefficient represented as

$$K = \frac{\Delta P}{\frac{1}{2} \rho V_{dc}^2} \quad (4)$$

Where  $\Delta P$  is radial pressure difference between subchannel

$\rho_l$  = Density of liquid and  $V_{dc}$  = diversion cross flow velocity

Figure 9 (a) and 9 (b) shows the variation of transverse resistance coefficient ( $K$ ), for single phase and two phase flows. The transverse resistance coefficient ( $K$ ) is plotted against a ratio of diversion cross flow velocity to the axial velocity ( $V_{dc}/V_{axial}$ ).



(a) Single phase

(b) Two phase

Fig. 9 Transverse resistance coefficient vs Ratio of cross flow velocity to the axial velocity

The main findings are as follows.

1. The cross flow resistance coefficient decreases with increase in ratio of cross flow velocity to the axial velocity both in single and two phase flow condition.
2. Also cross flow resistance coefficient in two phase flow is higher as compared to single phase flow.

The capability of existing correlation is checked to predict the measured cross flow resistance coefficient and found that none of these models predict measured cross flow resistance coefficient for AHWR rod bundle. There are errors between measured and predicted value by  $-100\%$  to  $+571\%$  (average error) depends on the models. In the view of this, a new model applicable to AHWR has been presented which predicts cross flow resistance coefficient quite accurately within average error of  $\pm 9\%$ .

In summary, an assessment of turbulent mixing models has been carried out and found that there is large discrepancy between predictions by models and existing experimental data relevant to conventional BWRs. This is because turbulent mixing phenomena are highly geometry and operating condition dependent. The average errors in existing models as

compared to test data are found to be -52% to +1200%. Because of large error in the models, a new model for turbulent mixing was proposed from first principle. The model could predict within average error of  $\pm 4\%$  for all the test data available for triangular-triangular, square-square, rectangular-rectangular subchannel array. The model was tested even for steam-water high pressure data and found that it can predict within average error of  $\pm 9.94\%$ . However the AHWR rod bundle is completely different from conventional BWRs. In addition being a natural circulation BWR, the flow velocity in the subchannel can vary over a wide range unlike that of conventional BWRs. The test data and models are not applicable to AHWR condition. This has necessitated measurement in 1:1 condition of AHWR rod bundle and develops AHWR specific models which can later use for AHWR thermal margin and safety analysis.

Study of inter-subchannel mixing phenomena for AHWR rod bundle gives important conclusion which are enlisted here

- i. The turbulent mixing and void drift both are found to be dependent on void fraction and flow regimes even for low mass flux condition typical to AHWR geometry.
- ii. The magnitude of turbulent mixing rate and diffusion coefficient is found to be higher for AHWR subchannels geometry compared to conventional BWRs geometry for the same mass flux.
- iii. Also the magnitude of turbulent mixing rate and diffusion coefficient found to be increase with increase in superficial liquid velocity.
- iv. None of existing models found to predict measured test data of turbulent mixing rate and cross flow resistance. Hence a new model has been developed applicable to AHWR geometry and operating condition which predicts quite accurately.

## Abstract

The Advanced Heavy Water Reactor (AHWR) is a vertical pressure tube type, heavy water moderated and boiling light water cooled natural circulation based reactor. The fuel bundle of AHWR contains 54 fuel rods arranged in three concentric rings of 12, 18 and 24 fuel rods. The coolant flow distribution in single and two phase flow condition is very important for AHWR rod bundle to ensure its safety and performance. Single phase flow condition exists in reactor rod bundle during start-up condition and up to certain length of rod bundle when it is operating at full power. However, being a natural circulation BWR, transition from single phase to two phase flow condition occurs in reactor rod bundle with increase in power. Prediction of thermal margin of the reactor has necessitated the determination of inter-subchannel mixing of coolant amongst these subchannels. The inter-subchannel mixing consists of three independent phenomena; turbulent mixing, void drift and diversion cross flow.

Of course, two phase turbulent mixing studies are not new especially for conventional BWRs. However it is important to assess the models developed so far for these reactors for their accuracy and applicability to AHWR condition. In this study, assessment of two phase turbulent mixing models applicable to BWRs has been performed against existing experimental data for various subchannel geometries of BWRs. It is found that there are large errors between predictions by the empirical models and measured experimental data by an average error of +1200 % to -52 %. Even there are large differences in prediction among the models and experimental data of turbulent mixing rate from one subchannel array to another. This is because mixing phenomena are highly geometry and operating condition dependent. It may be noted that, the subchannel geometry of AHWR rod bundle is completely different from conventional BWRs. The rods in AHWR bundle are arranged in circular subchannel array unlike conventional BWRs geometry in which rods are arranged in square-square,

rectangular-rectangular and square-rectangular subchannel array. In the view of above, data obtained from conventional BWRs cannot be used for AHWR.

In addition, AHWR being a natural circulation BWR, the mass flux condition in the subchannels can vary depending on the power, which is different from conventional BWRs where the mass flux in the subchannel is more or less constant irrespective of power. Effect of variation of mass flux in the subchannels on two phase mixing phenomena for AHWR specific geometry has never been investigated.

The objective of present work is to establish mixing in subchannels of AHWR rod bundle due to turbulent mixing, void drift and diversion cross flow. Since it is difficult to develop mechanistic model for different aspects of mixing (i.e. turbulent mixing, void drift and diversion cross flow) in the rod bundle, experiments were carried out in a scaled test facility of AHWR rod bundle. The facility simulates 1:1 geometry of 1/12<sup>th</sup> symmetrical section of AHWR rod bundle. Water and air was used as the working fluid and the inter-subchannel mixing tests were carried out. The turbulent mixing rate, void drift and diversion cross flow was experimentally measured for AHWR operating condition.

The mass flow rate in actual rod bundle of AHWR varies from 0 to 4.7 kg/sec depending on operating condition. So if we consider three subchannels in 1/12 segment, the mass flow rate can vary in the range 0 to 0.12 kg/sec and correspondingly range of mean velocity is around 0 to 1.2 m/s. The void fraction in two phase flow is varied from 0 to 0.8 which is same as that of actual bundle. The mean superficial liquid velocity is varied from 0 to 0.42 m/s and mean superficial gas velocity is varied from 0 to 1.3 m/s.

Our results indicate that:

- i. The turbulent mixing and void drift both are found to be dependent on void fraction and flow regimes even for low mass flux condition typical to AHWR geometry.

ii. The magnitude of turbulent mixing rate due to turbulent mixing and diffusion coefficient due to void drift is found to be higher for AHWR subchannels geometry compared to conventional BWRs geometry for the same mass flux.

iii. Also the magnitude of turbulent mixing rate and diffusion coefficient found to be increase with increase in superficial liquid velocity

iv The cross flow resistance coefficient due to diversion cross flow in two phase flow is higher as compared to single phase flow.

In the present work, empirical models were developed based on experimental data which could predict the inter-subchannel mixing quite accurately with an average error of  $\pm 9\%$ .

These models can be used to assess AHWR flow distribution and thermal margin.

## List of Figures

| Caption  | Page no. |
|--|----------|
| <b>Fig 1.1</b> Subchannel mixing phenomena in rod bundle   | 03       |
| <b>Fig. 1.2 (a)</b> Comparison of the predictions of Bues (1972) model against subchannel experiments for liquid phase turbulent mixing rate in two phase flow             | 24       |
| <b>Fig. 1.2 (b)</b> Comparison of the predictions of Bues (1972) model against subchannel experiments for gas phase turbulent mixing rate in two phase flow                | 26       |
| <b>Fig. 1.3 (a)</b> Comparison of the predictions of Kazimi and Kelly (1983) model against subchannel experiments for liquid phase turbulent mixing rate in two phase flow | 28       |
| <b>Fig. 1.3 (b)</b> Comparison of the predictions of Kazimi and Kelly (1983) model against subchannel experiments for gas phase turbulent mixing rate in two phase flow    | 30       |
| <b>Fig. 1.4 (a)</b> Comparison of the predictions of Kawahara et al. (2000) model against subchannel experiments for liquid phase turbulent mixing rate in two phase flow  | 32       |
| <b>Fig. 1.4 (b)</b> Comparison of the predictions of Kawahara et al. (2000) model against subchannel experiments for gas phase turbulent mixing rate in two phase flow     | 33       |
| <b>Fig. 1.5 (a)</b> Comparison of the predictions of Carlucci et al. (2003) model against subchannel experiments for liquid phase turbulent mixing rate in two phase flow  | 35       |
| <b>Fig. 1.5 (b)</b> Comparison of the predictions of Carlucci et al. (2003) model against subchannel experiments for gas phase turbulent mixing rate in two phase flow     | 37       |

|  |    |
|--|----|
| <b>Fig. 1.6</b> BWR and AHWR lattice   | 42 |
| <b>Fig. 1.7</b> Representation of geometrical parameter in R-R, S-S and T-T subchannel array   | 45 |
| <b>Fig. 1.8</b> Liquid phase turbulent mixing rate   | 48 |
| <b>Fig. 1.9</b> Gas phase turbulent mixing rate  | 49 |
| <b>Fig. 1.10</b> The coefficient $C_1$ and exponent $a_1$ for various subchannel geometry in liquid phase mixing rate                                  | 51 |
| <b>Fig. 1.11</b> The coefficient $C_1$ and exponent $a_1$ for various subchannel geometry in gas phase turbulent mixing rate                           | 53 |
| <b>Fig. 1.12</b> Comparison of the predictions of present model against subchannel experiment for liquid phase turbulent mixing rate in two phase flow | 55 |
| <b>Fig. 1.13</b> Comparison of the predictions of present model against subchannel experiment for gas phase turbulent mixing rate in two phase flow    | 56 |
| <b>Fig. 1.14</b> Comparison of the predictions of present model against subchannel experiment for total turbulent mixing rate in two phase flow        | 58 |
| <b>Fig. 2.1 (a)</b> AHWR fuel rod bundle   | 62 |
| <b>Fig. 2.1 (b)</b> 1/12 <sup>th</sup> segment of AHWR fuel rod bundle   | 62 |
| <b>Fig. 2.2</b> Mixing flow diagram  | 68 |
| <b>Fig. 3.1</b> AHWR fuel rod bundle (1/12 <sup>th</sup> segment)  | 76 |
| <b>Fig. 3.2</b> Test rig schematic   | 77 |
| <b>Fig. 3.3</b> Schematic of test section  | 78 |
| <b>Fig. 3.4</b> Schematic of mixer   | 80 |
| <b>Fig. 3.5</b> Schematic of separator   | 81 |
| <b>Fig. 3.6</b> Radial pressure difference measurement of subchannels  | 84 |

|   |     |
|---|-----|
| <b>Fig. 4.1</b> Comparison of $W'/\mu$ against $Re_{avg}$   | 96  |
| <b>Fig. 4.2</b> Comparison of existing models against present experimental data   | 99  |
| <b>Fig 4.3</b> $\ln(N_{mix})$ vs $\ln(Re_{avg})$  | 101 |
| <b>Fig. 4.4</b> $\ln(N_{mix})$ vs $\ln(Re_{avg} \times (S/\delta))$   | 102 |
| <b>Fig. 4.5</b> Comparison of the predictions of model against experiment for liquid phase turbulent mixing rate  | 103 |
| <b>Fig. 5.1</b> Turbulent mixing rate vs average void fraction between subchannel 3-2   | 109 |
| <b>Fig. 5.2</b> Turbulent mixing rate vs average void fraction between subchannel 1-2   | 111 |
| <b>Fig.5.3 (a)</b> Comparison of the predictions of Bues model (1972) against subchannel experiments for turbulent mixing rate in two phase flow          | 114 |
| <b>Fig. 5.3 (b)</b> Comparison of the predictions of Kazimi and Kelly's (1983) against subchannel experiments for turbulent mixing rate in two phase flow | 115 |
| <b>Fig. 5.3 (c)</b> Comparison of the predictions of Carlucci et al. (2003) against subchannel experiments for turbulent mixing rate in two phase flow    | 116 |
| <b>Fig. 5.4 (a)</b> Liquid phase mixing rate ( $0 \leq \alpha \leq 0.3$ )   | 119 |
| <b>Fig 5.4 (b)</b> Liquid phase mixing rate ( $0.3 \leq \alpha \leq 0.55$ )   | 120 |
| <b>Fig 5.4 (c)</b> Liquid phase mixing rate ( $0.55 \leq \alpha \leq 0.8$ )   | 121 |
| <b>Fig 5.5 (a)</b> Gas phase mixing rate ( $0.3 \leq \alpha \leq 0.65$ )  | 122 |
| <b>Fig 5.5 (b)</b> Gas phase mixing rate ( $0.65 \leq \alpha \leq 0.8$ )  | 123 |
| <b>Fig. 5.6</b> Comparison of the predictions of present model against subchannel experiments for turbulent mixing rate in two phase flow                 | 124 |
| <b>Fig. 6.1</b> Equilibrium flow vs non-equilibrium flow for gas and liquid phase   | 132 |
| <b>Fig. 6.2 (a)</b> Equilibrium void fraction vs non-equilibrium void fraction for subchannel 3-2   | 133 |

|  |     |
|--|-----|
| <b>Fig. 6.2 (b)</b> Equilibrium void fraction vs non-equilibrium void fraction for subchannel 1-2  | 133 |
| <b>Fig. 6.3 (a)</b> Variation of void diffusion coefficient between the subchannel 1-2 with average void fraction 1-2  | 135 |
| <b>Fig. 6.3 (b)</b> Variation of void diffusion coefficient between the subchannel 3-2 with average void fraction 3-2  | 135 |
| <b>Fig. 6.4</b> Comparison of the predictions of Rowe et al. (1990) model against subchannels experiments for equilibrium void fraction in two phase flow                                | 138 |
| <b>Fig. 6.5</b> Comparison of the predictions of Carlucci et al. (2003) model against subchannels experiments for equilibrium void fraction in two phase flow                            | 139 |
| <b>Fig. 6.6</b> Comparison of ratio of equilibrium void fraction difference to average void fraction vs ratio of equilibrium mass flux difference to average mass flux in two phase flow | 140 |
| <b>Fig. 7.1</b> Transverse resistance coefficient in single phase flow vs Ratio of cross flow velocity to the axial velocity   | 146 |
| <b>Fig. 7.2</b> Transverse resistance coefficient in two phase flow vs Ratio of cross flow velocity to the axial velocity  | 147 |

## List of Tables

| Caption   | Page no. |
|---|----------|
| <b>Table 1.1</b> Review of correlations for different types of subchannel array   | 7        |
| <b>Table 1.2</b> Description of available data on two phase turbulent mixing rate   | 10       |
| <b>Table 1.3</b> Description of two phase turbulent mixing models   | 14       |
| <b>Table 1.4</b> Description of void drift models   | 20       |
| <b>Table 1.5</b> Error analysis between calculated liquid phase turbulent mixing rate (Bues (1972) model) and measured liquid phase turbulent mixing rate in two phase flow             | 25       |
| <b>Table 1.6</b> Error analysis calculated gas phase turbulent mixing rate (Bues (1972) model) from measured gas phase turbulent mixing rate in two phase flow                          | 27       |
| <b>Table 1.7</b> Error analysis between calculated liquid phase turbulent mixing rate (Kazimi and Kelly (1983) model) and measured liquid phase turbulent mixing rate in two phase flow | 29       |
| <b>Table 1.8</b> Error analysis between calculated gas phase turbulent mixing rate (Kazimi and Kelly (1983) model) from measured gas phase turbulent mixing rate in two phase flow      | 31       |
| <b>Table 1.9</b> Error analysis between calculated liquid phase turbulent mixing rate (Kawahara et al. (2000) model) and measured liquid phase turbulent mixing rate in two phase flow  | 33       |
| <b>Table 1.10</b> Error analysis between calculated gas phase turbulent mixing rate (Kawahara et al. (2000) model) and measured gas phase turbulent mixing rate in two phase flow       | 34       |
| <b>Table 1.11</b> Error analysis between calculated liquid phase turbulent mixing rate  | 36       |

|  |     |
|--|-----|
| Carlucci et al. (2003) model and measured liquid phase turbulent mixing rate in two phase flow   |     |
| <b>Table 1.12</b> Error analysis between calculated gas turbulent mixing rate Carlucci et al. (2003) model) and measured gas turbulent mixing rate in two phase flow | 37  |
| <b>Table 1.13</b> Error analysis between calculated liquid turbulent mixing and measured liquid turbulent mixing rate in two phase flow                              | 39  |
| <b>Table 1.14</b> Major thermal hydraulic parameters of AHWR and ESBWR   | 42  |
| <b>Table 1.15</b> Error analysis between calculated liquid phase turbulent mixing and measured liquid turbulent mixing rate in two phase flow                        | 56  |
| <b>Table 1.16</b> Error analysis between calculated gas turbulent mixing and measured gas turbulent mixing rate in two phase flow                                    | 57  |
| <b>Table 2.1</b> Scaling of present experiment   | 63  |
| <b>Table 3.1</b> Experimental test matrix for single phase turbulent mixing  | 86  |
| <b>Table 3.2</b> Experimental test matrix for two phase turbulent mixing   | 87  |
| <b>Table 3.3</b> Experimental test matrix for void drift   | 89  |
| <b>Table 3.4</b> Experimental test matrix for single phase diversion cross flow  | 90  |
| <b>Table 3.5</b> Experimental test matrix for two phase diversion cross flow   | 91  |
| <b>Table 4.1</b> Experimental test matrix for single phase turbulent mixing  | 93  |
| <b>Table 4.2</b> Error analysis for various correlations for single phase mixing rate  | 98  |
| <b>Table 5.1</b> Experimental test matrix for two phase turbulent mixing   | 107 |
| <b>Table 6.1</b> Experimental test matrix for void drift   | 130 |
| <b>Table 7.1</b> Experimental test matrix for single phase diversion cross flow  | 144 |
| <b>Table 7.2</b> Experimental test matrix for two phase diversion cross flow   | 145 |
| <b>Table 7.3</b> Comparison of prediction by Kawahara et al. (2007) model and  | 150 |

|   |     |
|---|-----|
| measured value of transverse resistance coefficient in single phase diversion cross flow  |     |
| <b>Table 7.4</b> Comparison of prediction by Kim and Park (1995) model and measured value of transverse resistance coefficient in single phase diversion cross flow     | 151 |
| <b>Table 7.5</b> Comparison of present model against experimental data of subchannels 1-2 and subchannel 3-2  | 152 |
| <b>Table 7.6</b> Comparison of prediction by Kawahara et al. (2007) model against measured value of transverse resistance coefficient in two phase diversion cross flow | 153 |
| <b>Table 7.7</b> Comparison of prediction by Iwamura et al. (1986) model against measured value of transverse resistance coefficient in two phase diversion cross flow  | 154 |
| <b>Table 7.8</b> Comparison of present model against experimental data of subchannel 1-2 and subchannel 3-2.  | 155 |

## Nomenclature

|               |   |
|---------------|---|
| $A$           | flow area ( $\text{m}^2$ )                            |
| $B_I$         | empirical constant                                    |
| $C$           | Concentration (ppm)                                   |
| $D$           | diffusion coefficient ( $\text{m}^2/\text{s}$ )       |
| $D_h$         | hydraulic diameter (m)                                |
| $d$           | rod diameter (m)                                      |
| $d_c$         | critical bubble diameter                              |
| $d_{CD}^{Br}$ | Brodkey critical bubble diameter                      |
| $E$           | Error (%)   |
| $F^*$         | subchannel geometry factor                            |
| $F_{G,P}$     | mass flux and pressure factor                         |
| $F_{gap}$     | gap factor  |
| $F_{gc}$      | gap to centroid factor                                |
| $F_p$         | pressure factor                                       |
| $F_{obs}$     | obstruction factor                                    |
| $f$           | friction factor                                       |
| $G$           | mass flux ( $\text{kg}/\text{m}^2\text{s}$ )          |
| $g$           | acceleration due to gravity ( $\text{m}/\text{s}^2$ ) |
| $J$           | superficial velocity (m/s)                            |
| $k$           | obstruction loss factor                               |
| $K$           | transverse resistance coefficient                     |
| $l$           | length (m)  |
| $m$           | mass flow rate (kg/s)                                 |

|           |   |
|-----------|---|
| $N_{mix}$ | Mixing number   |
| $p$       | pitch (m)   |
| $Q$       | volumetric flow rate (1lpm = $10^{-3}$ m <sup>3</sup> /s) |
| Re        | Reynolds number   |
| RMS       | root mean square  |
| R-R       | Rectangular-Rectangular                                   |
| S-S       | Square-Square   |
| $s$       | slip ratio  |
| $S$       | gap (m)   |
| T-T       | Triangular-Triangular                                     |
| $W'$      | total turbulent mixing rate (kg/m <sup>2</sup> s)         |
| $x$       | quality   |
| $z$       | axial distance(m)   |
| 1-C       | 1 centre  |
| 2-S       | 2 side  |

### **Greek letters**

|               |  |
|---------------|--|
| $\alpha$      | void fraction                            |
| $\mu$         | dynamic viscosity (N-s/m <sup>2</sup> )  |
| $\nu$         | kinematic viscosity (m <sup>2</sup> /s)  |
| $\rho$        | density (kg/m <sup>3</sup> )             |
| $\varepsilon$ | turbulent diffusivity(m <sup>2</sup> /s) |
| $\theta$      | two phase multiplier                     |
| $\gamma$      | correlation coefficient                  |
| $\beta$       | volumetric fraction                      |

$\Sigma$  summation  
 $\sigma$  surface tension

### **Subscript**

*avg* average  
*cal* calculated  
CB critical bubble size  
*ct* convective transfer  
*exp* experimental  
*g* gas  
*hom* homogenous  
*ij,* subchannel identifier  
123 subchannel identifier  
*inc* incremental  
*l* liquid  
*mix* mixture  
*p* peak  
*pd* pressure difference  
*q* phase identifier  
*sp* single phase  
*tp* two phase  
*td* turbulent diffusion  
R.T. reference temperature (ambient temperature)  
H.T. high temperature

# CHAPTER 1

## *INTRODUCTION*

---

---

### **1.1 Introduction**

This chapter gives a brief introduction to different mixing phenomena in a rod bundle i.e. turbulent mixing, void drift and diversion cross flow followed by detailed background literature of each component of inter-subchannel mixing. It also provides motivation and objective of research work. In this chapter, assessment of models against existing experimental data relevant to BWRs geometry has been done. A new model has been developed from first principle for the two phases turbulent mixing and compared against all the test data generated so far in literature.

#### **1.1.1 Introduction to inter-subchannel mixing phenomena**

The flow rate of coolant in the reactor rod bundle is very important for evaluating enthalpy distribution and thermal margin. A lot of research has already been dedicated to understand the coolant flow and enthalpy distribution in rod bundle geometries. This study reveals that study of mixing process between subchannels is very important. Due to mixing between subchannels, enthalpy of fluid decreases in hotter subchannel. In

subchannel analysis, the lateral cross sectional area of rod bundle along the length is divided into number of imaginary flow tubes called subchannels. Once subchannels are formed, appropriate conservation equations are solved to get flow rate and enthalpy in the subchannels.

The fluid transfer between subchannels is explained by three mechanisms i.e. turbulent mixing, void drift and diversion cross flow (Lahey and Moody (1993), Hotta et al. (2005)). Turbulent mixing is an oscillating component of flow in the transverse direction between subchannels expressed in units of mass per unit time per unit length. In this phenomenon, neither net mass transfer nor net volume transfer of each phase occurs between subchannels. The second mechanism is void drift which occurs even in absence of pressure difference. Void drift is due to redistribution of non-equilibrium flow to attain equilibrium flow or in other words we can say that non-equilibrium void fraction to attain equilibrium void fraction. Equilibrium void fraction means that the voids are constant in every subchannel and does not vary along the respective subchannels. The third mechanism is diversion cross flow which occurs due to lateral pressure difference between adjacent subchannels. In this phenomenon, there is a net flow from one subchannel to the other subchannel, which occurs at their common boundary. Fig 1.1 shows subchannel mixing phenomena i.e. turbulent mixing, void drift and diversion cross flow in the rod bundle of nuclear reactor.

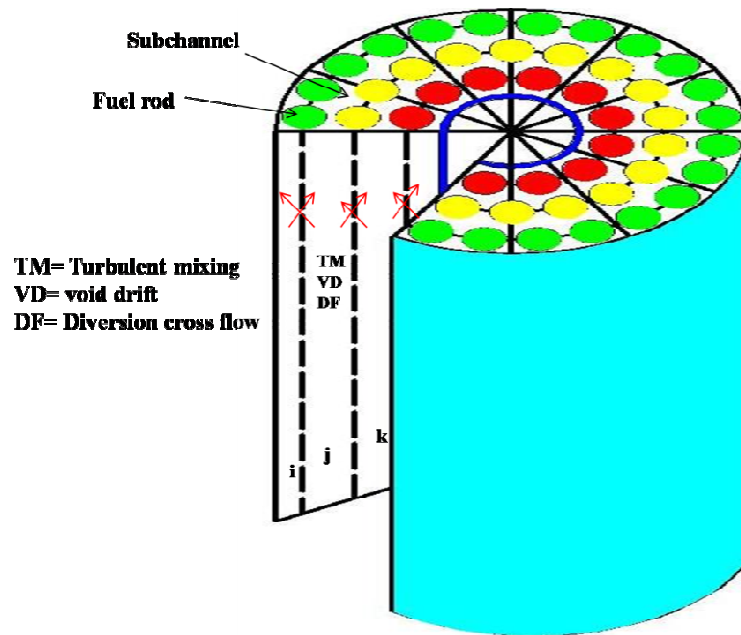


**Fig 1.1** Subchannel mixing phenomena in rod bundle

## 1.2 Review of literature

### 1.2.1 Turbulent mixing

#### (i) Review of single phase turbulent mixing experiments

Single phase turbulent mixing experiments were performed by Petrunik (1968), Walton (1969), Rowe and Angle (1969), Galibert and Knudsen (1971), Singh (1972), Castellana et al. (1974), Rogers and Tahir (1975), Kelly and Todreas (1977), Sadatomi et al. (2004) and Kawahara et al. (2006). These experiments were performed with various subchannel arrays like square-square, triangular-triangular, rectangular-rectangular, square-rectangular and square-triangular.

Petrunik (1968) determined the single phase turbulent mixing rate between rectangular-rectangular subchannel array. Water was used working fluid. The turbulent mixing rate was determined by tracer technique. He found that mixing rate increases with increases in Reynolds number. The range of Reynolds number was  $1.35 \times 10^3$  to  $3.08 \times 10^4$ . Petrunik (1968) also demonstrated that entrance effect at the interconnection length were negligible after the entrance length of 13 equivalent hydraulic diameters. Rowe and Angle (1969) determined the single phase turbulent mixing rate between square- square and square-triangular subchannel array. Water was used working fluid. The turbulent mixing rate was determined by comparing the enthalpy values at the test section exit with the prediction from COBRA code. Thus mixing rate is depends on mathematical model. They also found that mixing rate increases with increases in Reynolds number. The range of Reynolds number was  $4.2 \times 10^4$  to  $1.80 \times 10^5$ . In addition to this, Rowe and Angle (1969) shows depended of mixing rate on subchannel array. They reported that turbulent mixing rate in square-square subchannel is lower than square-triangular subchannel array. Walton (1969) determined single phase turbulent mixing rate between triangular-triangular subchannel array. Water was used working fluid. The turbulent mixing rate was determined by tracer technique. He also found that mixing rate increases with increases in Reynolds number. The range of Reynolds number was  $1.9 \times 10^3$  to  $9.1 \times 10^4$ . Castellana et al. (1974) determined single phase turbulent mixing rate between aquare-square. Water was used as working fluid. The turbulent mixing rate was determined by measuring precisely subchannel exit temperatures over a range of test conditions. Their analysis of experimental results found that turbulent mixing rate is function of Reynolds numbers, gap spacing and average mass flux between subchannels. The range of

Reynolds number was  $9 \times 10^4$  to  $4.90 \times 10^5$ . Singh (1972) determined single phase turbulent mixing rate between triangular-triangular array, triangular-square and square-square array. Water was used working fluid. The turbulent mixing rate was determined by tracer technique. He also found that mixing rate increases with increases in Reynolds number. The range of Reynolds number was  $1.3 \times 10^3$  to  $3.80 \times 10^4$ . Singh (1972) reported that turbulent mixing rate is dependent on subchannel array. The turbulent mixing rate was found to be the lowest in triangular-triangular array and increased for triangular-square and square-square array in ascending order while keeping gap spacing between subchannels constant. Galibert and Knudsen (1971) determined single phase mixing rate between adjacent subchannels in a simulated rod bundle made by placing 1 inch diameter in square-square subchannel array. The turbulent mixing rate was determined by tracer technique. Five different gaps were used. They concluded that turbulent mixing rate increases with rod spacing and Reynolds number. The range of Reynolds number was  $8 \times 10^3$  to  $3 \times 10^4$ . Kelly and Todreas (1977) determined single phase mixing rate between adjacent subchannel arranged in triangular rod arrays. The turbulent mixing rate was determined by tracer technique. They found that turbulent mixing rate increases as the Reynolds number increases. They also found that mixing rate increases with increases in Reynolds number. The range of Reynolds number was  $2.0 \times 10^3$  to  $2.4 \times 10^4$ . Rogers and Tahir (1975) determined single phase turbulent mixing rate between square-square and triangular-triangular subchannel array. Air was used working fluid. The turbulent mixing rate was determined by tracer technique. They also found that mixing rate increases with increases in Reynolds number. The range of Reynolds number was  $8.1 \times 10^3$  to  $4.95 \times 10^4$ . Sadatomi et al. (2004) performed experiment with multiple subchannels having square

and rectangular subchannel array. . Water was used working fluid. The turbulent mixing rate was determined by tracer technique. They also found that mixing rate increases with increases in Reynolds number. The range of Reynolds number was  $7 \times 10^3$  to  $2 \times 10^4$ . They also reported that turbulent mixing rate in square-square and rectangular-rectangular is lower (about 20 %) than square-rectangular subchannel array. Kawahara et al. (2006) determined single phase turbulent mixing rate between triangular-triangular subchannel array. Water was used working fluid. They also found that mixing rate increases with increases in Reynolds number. The turbulent mixing rate was determined by tracer technique. The range of Reynolds number was  $1.7 \times 10^3$  to  $2.4 \times 10^5$ . The turbulent mixing rate was determined by tracer technique.

The main findings of these experiments are as follows.

1. Results show that the magnitude of turbulent mixing rate increases with increase in average Reynolds number.
2. The turbulent mixing rate is very much geometry and operating condition dependent.

#### **(ii) Review of single phase turbulent mixing models**

Numerous correlations have been proposed based on the single phase turbulent mixing experiments to predict the magnitude of single phase turbulent mixing rate for various subchannel geometry (i.e. square-square, triangular-triangular, rectangular-rectangular, square-rectangular and square-triangular) of reactor rod bundle as shown in Table 1.1. These correlations are mainly function of average Reynolds number and geometry of subchannel.

**Table 1.1** Review of correlations for different types of subchannel array

| Authors                       | Subchannel geometry | Hydraulic diameter of subchannel $D_h$ (m) | Correlation in form of $W'/\mu$   |
|-------------------------------|---------------------|--|---|
| Roger and Tahir 1 (1975)      | S-S                 | -  | $\frac{W'_{ij}}{\mu} = 0.0050 \text{Re}^{0.9} \left(\frac{S}{d}\right)^{0.106}$ |
| Roger and Tahir 2 (1975)      | T-T                 | 0.0294                                     | $\frac{W'_{ij}}{\mu} = 0.0018 \text{Re}^{0.9} \left(\frac{S}{d}\right)^{-0.4}$  |
| Peterniuk (1968)              | R-R                 | 0.0203                                     | $\frac{W'_{ij}}{\mu} = 0.009 \text{Re}^{0.827}$                                 |
| Galibert and Knudsen 1 (1971) | S-S                 | 0.0112                                     | $\frac{W'_{ij}}{\mu} = 0.0001 \text{Re}^{1.23}$                                 |
| Galibert and Knudsen 2 (1971) | S-S                 | 0.012 4                                    | $\frac{W'_{ij}}{\mu} = 0.00037 \text{Re}^{1.12}$                                |
| Galibert and Knudsen 3(1971)  | S-S                 | 0.0147                                     | $\frac{W'_{ij}}{\mu} = 0.0050 \text{Re}^{1.12}$                                 |
| Galibert and Knudsen 4 (1971) | S-S                 | 0.018 3                                    | $\frac{W'_{ij}}{\mu} = 0.00190 \text{Re}^{1.01}$                                |
| Kelly and Todreas (1977)      | T-T                 | 0.0127                                     | $\frac{W'_{ij}}{\mu} = 0.0021 \text{Re}^{0.935}$                                |
| Rowe and Angel 1(1969)        | S-S                 | 0.0051                                     | $\frac{W'_{ij}}{\mu} = \frac{0.063 \text{Re}^{-0.1} \overline{SG}}{\mu}$        |
| Rowe and Angel 2 (1969)       | S-T                 | 0.0073                                     | $\frac{W'_{ij}}{\mu} = \frac{0.021 \text{Re}^{-0.1} \overline{SG}}{\mu}$        |

|                   |     |        |  |
|-------------------|-----|--------|--|
| Castellana (1974) | S-S | 0.0135 | $\frac{W'_{ij}}{\mu} = \frac{0.027 \text{Re}^{-0.1} S\bar{G}}{\mu}$                            |
| Rehme (1992)      | -   | -      | $\frac{W'_{ij}}{\mu} = 0.0075 \text{Re}^{0.9} \frac{S}{\delta} \left( \frac{0.7}{S/d} \right)$ |
| Seale 1 (1979)    | S-S | 0.027  | $\frac{W'_{ij}}{\mu} = \frac{0.02968 \text{Re}^{-0.1} S\bar{G}}{\mu}$                          |
| Seale 2 (1979)    | S-S | 0.057  | $\frac{W'_{ij}}{\mu} = \frac{0.01683 \text{Re}^{-0.1} S\bar{G}}{\mu}$                          |
| Seale 3 (1979)    | S-S | 0.125  | $\frac{W'_{ij}}{\mu} = \frac{0.009225 \text{Re}^{-0.1} S\bar{G}}{\mu}$                         |

### (iii) Review of two phase turbulent mixing experiments

The two phase turbulent mixing experiments (Walton (1969), Rudzinski (1970), Singh K.S. (1972), Kawahara et al. (1997 (b)), Sadatomi et al. (2004), Kawahara et al. (2006)) show that the turbulent mixing is strongly related to flow regimes.

Walton (1969) determined two phase turbulent mixing rate between triangular-triangular subchannel array. Water and air was used working fluid. The total mass flux varies from 90 to 1000 (kg/m<sup>2</sup>s). The flow pattern observed is annular flow. The tracer technique is used for finding out turbulent mixing rate. The turbulent mixing rate was determined by tracer technique. He found that mixing rate decreases with increases in quality in annular region. He also discussed the criterion of fully developed flow in each subchannel is achieved by keeping the entry length more than 127 times hydraulic diameter. Rudzinski

(1970) determined two phase turbulent mixing rate between square-square and triangular-triangular subchannel array. Water and air was used working fluid. The total mass flux varies from 680 to 2030 ( $\text{kg /m}^2\text{s}$ ). The flow pattern observed was bubbly, slug and annular flow. The tracer technique is used for finding out turbulent mixing rate. He found that the liquid phase turbulent mixing rate starts at zero quality, which increases in bubbly flow reaches maximum value in slug churn and then decreases beyond churn-annular flow transition. The gas phase turbulent mixing rate starts near zero value of quality, reaches maximum in slug churn flow and then decreases with increase in quality.

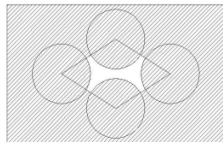
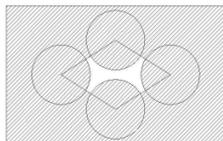
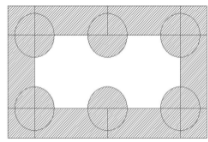
Singh (1972) determined two phase turbulent mixing rate between triangular-triangular array, triangular-square and square-square array. Water and air was used working fluid. The total mass flux varies from 40 to 1080 ( $\text{kg /m}^2\text{s}$ ). The flow pattern observed was bubbly, slug and annular flow. The tracer technique is used for finding out the turbulent mixing rate. He also found that mixing rate is flow regime dependent and geometry dependent.

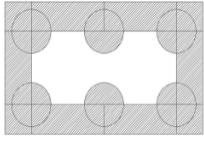
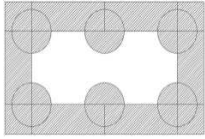
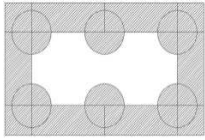
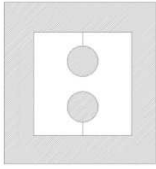
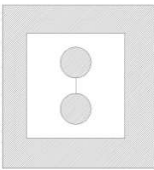
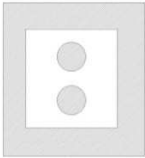
Kawahara et al. (2000) determined two phase turbulent mixing rate between two identical rectangular subchannel of 1-centre gap, 2-side gap and 3 gap. Water and air was used working fluid. The total mass flux varies from 100 to 1000 ( $\text{kg /m}^2\text{s}$ ). The flow pattern observed was bubbly, slug and annular flow. The tracer technique is used for finding out turbulent mixing rate. They also found that mixing rate is flow regime dependent. In addition to it, they observed that two phase mixing rate depends on gap between the subchannels. On increasing the gap between the subchannels, mixing rate increases.

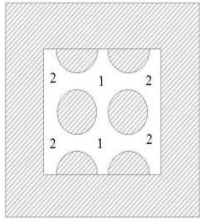
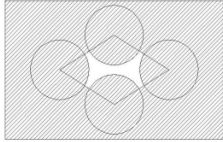
Sadatomi et al. (2004) performed experiment with multiple subchannels having square and rectangular subchannel array. Water and air was used working fluid. The total mass flux varies from 100 to 2000 ( $\text{kg /m}^2\text{s}$ ). The flow pattern observed was bubbly, slug

and annular flow. The turbulent mixing rate was determined by tracer technique. . They also found that mixing rate is flow regime dependent. Kawahara (2006) determined two phase turbulent mixing rate between triangular-triangular subchannel array. Water and air was used working fluid. The total mass flux varies from 100 to 2000 (kg/m<sup>2</sup>s). The flow pattern observed was bubbly, slug and annular flow. The tracer technique is used for finding out turbulent mixing rate. They also found that mixing rate is flow regime dependent. The experiments on two phase turbulent mixing rate between adjacent subchannels are listed in Table 1.2.

**Table 1.2** Description of available data on two phase turbulent mixing rate.

| S.No. | Experiment  | Subchannel array  | Geometrical Description  | Working Fluid | Total mass flux                   |
|-------|---|---|--|---------------|-----------------------------------|
| 1.    | Walton (1969)<br>[T-T subchannel experiment]            |  | $d = 19.7 \times 10^{-3} \text{m}$<br>$S = 1.02 \times 10^{-3} \text{m}$<br>$D_h = 3.9 \times 10^{-3} \text{m}$<br>$P/d = 1.05$<br>$A = 33.9 \times 10^{-6} \text{m}^2$  | Water and air | 90 to 1000 (kg/m <sup>2</sup> s)  |
| 2.    | Rudzinski (1970)<br>[T-T and S-S subchannel experiment] |  | $d = 19.7 \times 10^{-3} \text{m}$<br>$S = 1.02 \times 10^{-3} \text{m}$<br>$D_h = 3.9 \times 10^{-3} \text{m}$<br>$P/d = 1.05$<br>$A = 33.9 \times 10^{-6} \text{m}^2$  | Water and air | 680 to 2030 (kg/m <sup>2</sup> s) |
|       |   |  | $d = 20.8 \times 10^{-3} \text{m}$<br>$S = 0.89 \times 10^{-3} \text{m}$<br>$D_h = 8.75 \times 10^{-3} \text{m}$<br>$P/d = 1.04$<br>$A = 52.4 \times 10^{-6} \text{m}^2$ |               |                                   |

|    |   |   |   |                  |   |
|----|---|---|---|------------------|---|
| 3. | Singh (1972)<br>[S-S<br>subchannel<br>experiment<br>with varying<br>gap width]  |    | $d = 19.8 \times 10^{-3} \text{ m}$<br>$S = 2.03 \times 10^{-3} \text{ m}$<br>$D_h = 9.6 \times 10^{-3} \text{ m}$<br>$P/d = 1.10$<br>$A = 1.69 \times 10^{-4} \text{ m}^2$ | Water<br>and air | 40 to<br>1080<br>(kg<br>/m <sup>2</sup> s)  |
|    |   |    | $d = 20.8 \times 10^{-3} \text{ m}$<br>$S = 0.89 \times 10^{-3} \text{ m}$<br>$D = 8.7 \times 10^{-3} \text{ m}$<br>$P/d = 1.04$<br>$A = 1.52 \times 10^{-4} \text{ m}^2$   |                  |   |
|    |   |   | $d = 21.3 \times 10^{-3} \text{ m}$<br>$S = 0.38 \times 10^{-3} \text{ m}$<br>$D = 8.3 \times 10^{-3} \text{ m}$<br>$P/d = 1.02$<br>$A = 1.43 \times 10^{-4} \text{ m}^2$   |                  |   |
| 4. | Kawahara et al.<br>(1997b)<br>[R-R<br>subchannel<br>experiment<br>with varying<br>gap number i.e.<br>1 center, 2 side<br>and 3 gap] |  | $d = 12 \times 10^{-3} \text{ m}$<br>$S = 2.1 \times 10^{-3} \text{ m}$<br>$D = 15.7 \times 10^{-3} \text{ m}$<br>$P/d = 1.17$<br>$A = 4.07 \times 10^{-4} \text{ m}^2$     | Water<br>and air | 100 to<br>1000<br>(kg<br>/m <sup>2</sup> s) |
|    |   |  | $d = 20.8 \times 10^{-3} \text{ m}$<br>$S = 0.89 \times 10^{-3} \text{ m}$<br>$D = 8.75 \times 10^{-3} \text{ m}$<br>$P/d = 1.04$<br>$A = 52.4 \times 10^{-6} \text{ m}^2$  |                  |   |
|    |   |  | $d = 12 \times 10^{-3} \text{ m}$<br>$S = 6.3 \times 10^{-3} \text{ m}$<br>$D = 15.7 \times 10^{-3} \text{ m}$<br>$P/d = 1.17$<br>$A = 4.07 \times 10^{-4} \text{ m}^2$     |                  |   |

|    |   |   |   |               |                                   |
|----|---|---|---|---------------|-----------------------------------|
| 5. | Sadatomi et al. (2004), [Multichannel experiment S-S (1-1) and R-R (2-2) subchannel experiment] |  | $d=16\times 10^{-3}\text{m}$<br>$S=4\times 10^{-3}\text{m}$<br>$D=14.3\times 10^{-3}\text{m}$<br>$P/d=1.25$<br>$A=1.94\times 10^{-4}\text{m}^2$   | Water and air | 100 to 2000 (kg/m <sup>2</sup> s) |
|    |   |   | $d=16\times 10^{-3}\text{m}$<br>$S=4\times 10^{-3}\text{m}$<br>$D=11.2\times 10^{-3}\text{m}$<br>$P/d=1.25$<br>$A=1.38\times 10^{-4}\text{m}^2$   |               |                                   |
| 6. | Kawahara et al. (2006) [T-T subchannel experiment]  |  | $d=12\times 10^{-3}\text{m}$<br>$S=1.0\times 10^{-3}\text{m}$<br>$D=3.19\times 10^{-3}\text{m}$<br>$P/d=1.08$<br>$A=16.6\times 10^{-6}\text{m}^2$ | Water and air | 100 to 2000 (kg/m <sup>2</sup> s) |

These experiments provide important insights as given below:

- (a) The two phase turbulent mixing rate is sum of liquid phase turbulent mixing rate and gas phase turbulent mixing rate and it is strongly related to flow regimes. The liquid phase turbulent mixing rate starts at zero quality, which increases in bubbly flow reaches maximum value in slug churn and then decreases beyond churn-annular flow transition. The gas phase turbulent mixing rate starts near zero value of quality, reaches maximum in slug churn flow and then decreases with increase in quality. It is thus rational to consider the turbulent mixing separately in each flow pattern.
- (b) The magnitude of liquid phase turbulent mixing rate in two phase flow is quite higher as compared to gas phase turbulent mixing rate in two phase flow.

- (c) Two phase mixing rate depends on gap between the subchannels. On increasing the gap between the subchannels, mixing rate increases.
- (d) The two phase turbulent mixing rate increases with increase in mass flux.
- (e) The two phase turbulent mixing rate decreases with increase in pressure.

**(iv) Review of two phase turbulent mixing models.**

Initial attempts have been made for the prediction of liquid phase mixing rate and gas phase mixing rate in two phase flow by Bues (1972), Kazimi and Kelly (1983) and Carlucci et al. (2003). All these models consider all flow regimes as a single group. Only Kawahara et al. (2000) have made an attempt to consider the model separately for each flow regime.

Bues (1972) proposed a model which states that the total turbulent mixing rate is formulated for two regimes. A physical model is developed for the first region i.e. bubbly-slug region and it is combined with an empirical fit for the second region i.e. annular region. Kazimi and Kelly (1983) model is based on Bues (1972) model, which shows dependence of mixing rate on flow regimes. They proposed a correlation between the velocity fluctuation due to two phase turbulent mixing and the velocity fluctuation due to single phase turbulent mixing. Kawahara et al. (2000) model is for slug churn flow regime. In this model, the liquid phase turbulent mixing rate is the sum of three independent component mixing rate due to turbulent diffusion, convective transfer and pressure difference. Carlucci et al. (2003) model is based on the principle that the total phasic turbulent mixing rate is sum of homogenous turbulent mixing rate and incremental

turbulent mixing rate. Table 1.3 shows descriptions of two phase turbulent mixing models as follows

**Table 1.3** Description of two phase turbulent mixing models.

| S.no | Model                   | Equation derived for turbulent mixing rate  |
|------|-------------------------|---|
| 1    | Bues (1972)             | $W_l' = W_{l, sph}' + B_1 \left( \frac{AG}{D} \right) \frac{\rho_l}{\rho_g} \left( \frac{s-1}{s} \right) x$ $W_{II}' = W_{g, sph}' + (W_p' - W_{g, sph}') \left( \frac{1 - \left( \frac{x_0}{x_p} \right)}{\frac{x}{x_p} - \left( \frac{x_0}{x_p} \right)} \right)$ |
| 2    | Kazimi and Kelly (1983) | $W_q' = \rho_q \alpha_{gap, q} S \left( \frac{\varepsilon}{l} \right)_{tph},$ $\left( \frac{\varepsilon}{l} \right)_{tph} = \left( \frac{\varepsilon}{l} \right)_{sph} \theta$  |
| 3    | Carlucci et al. (2003)  | $W_l' = W_{l, hom}' + \Delta W_{l, tph}'$ $W_g' = W_{g, hom}' + \Delta W_{g, tph}'$   |
| 4    | Kawahara et al. (2000)  | $W_l' = W_{l, td}' + W_{l, ct}' + W_{l, pd}' ,$ $W_g' = \rho_g \left( \sum S \right) V_g$   |

The detailed description of these models are shown in Appendix 1

### **1.2.2 Void drift**

Void drift is due to redistribution of non-equilibrium flow to attain equilibrium flow or in other words we can say that non-equilibrium void fraction to attain equilibrium void fraction. Equilibrium void fraction means that the voids are constant in every subchannel and do not vary along the respective subchannel axis. This redistribution occurs in reactor rod bundle until it reaches to the state of equilibrium void fraction.

#### **(i) Review of void drift experiments**

The void fraction distribution is due to void drift has been observed in rod bundle experiments [Lahey and Schraub (1969), Lahey et al. (1972), Gonzalez-Santalo et al. (1972), Lahey (1986), Sato et al. (1987), Tapucu et al. (1988), Gencay et al. (2001), Sadatomi et al. (1994), Sadatomi et al. (2004)]. These experiments indicate that there is an observed tendency for the voids (i.e. vapour or gas) to move toward less obstructed regions.

Lahey and Schraub (1969) performed an experiment to simulate void drift in the subchannels of BWR bundle geometry. Water and air was used as working fluid. Isokinetic sampling technique was applied to obtain the average flow parameters in corner, wall and center subchannel, respectively. The mass flux for this experiment was  $1500 \text{ kg /m}^2\text{s}$ . They observed that the flow quality is much higher in the more open interior (centre) subchannels than in the corner and side subchannels of BWR bundle geometry. This indicates that the existence of a thick liquid film on the channel wall and an apparent affinity of the vapour or gas toward more open subchannels.

Lahey et al. (1972) performed an experiment to simulate void drift in the subchannels of BWR bundle geometry under diabatic condition with a steam-water mixture under typical BWR operating conditions. Isokinetic sampling technique was applied to obtain the average flow parameters in corner, wall and center subchannel, respectively. The mass fluxes for this experiment were  $450 \text{ kg /m}^2\text{s}$  and  $900 \text{ kg /m}^2\text{s}$ . A significant flow and enthalpy difference could be found in the different subchannel types. The corner subchannel shows quality and mass flux lower than the bundle average values despite its power-to-flow ratio was higher than the bundle average values. In contrast, the center subchannel has higher quality and mass flux than the bundle average values. This trend was in agreement with that observed by Lahey and Schraub (1969) in an adiabatic air-water two phase flow in a nine-rod bundle. It was concluded that this observed trend of gaseous phase accumulating in center subchannels is related to an affinity of the gaseous phase for less-obstructed high velocity regions, i.e. the center subchannels as in the case of the nine-rod bundle.

Gonzalez-Santalo et al. (1972) measured fully developed equilibrium flow distribution in a two-channel system simulating subchannels of a typical BWR fuel assembly with air-water system under atmospheric conditions. The mass fluxes for this experiment were  $500 \text{ kg /m}^2\text{s}$  and  $1000 \text{ kg /m}^2\text{s}$ . They observed void fraction distribution at equilibrium state, depends on test section geometry. In the case of test section consisting of two identical channels of the same dimension, the two-phase mixture was found equally distributed in the two channels at the equilibrium state.

Tapucu et al. (1988), measured mass exchange rate and pressure difference between two identical square channels (hydraulic diameter of 12.7 mm) laterally interconnected with a

gap of 1.5 mm clearance. Air-water two-phase mixture was used as working fluid. Inlet flows of the same mass flux but substantially different void fractions were introduced into the two subchannels. Due to the inlet void fraction difference, interchannel exchange through the gap occurs. Subchannel average void fractions along the test section were determined by measuring electrical conductivity variation between two thin plate electrodes applied on two opposite faces of each channels. Liquid phase exchange between the two channels was obtained by injecting a NaCl solution into the channel with higher inlet void fraction and measuring the salt concentration variation in both channels by sampling the liquid phase at various axial locations along the test section.

In order to know the effect of subchannel array on void drift, Gencay et al. (2001) conducted experiments having square duct channel and simulated subchannel geometry array. They observed that the diffusion coefficient which is a measure of void drift; increases with increasing average void fraction between adjacent subchannels. The turbulent void diffusion coefficient was found to be higher for subchannel geometry array as compared to square channel. Kawahara et al. (2006) conducted experiments having square-square and triangular-triangular subchannel array. They found that void diffusion coefficient due to void drift is smaller in triangular-triangular subchannel array as compared to square-square subchannel array.

In the past decades, a large amount of experimental investigations on two-phase interchannel mixing phenomena with air-water two-phase flow under atmospheric conditions were carried out in Kumamoto University, Japan [(Sato et al. 1987, Sadatomi et al. (1994), Sadatomi et al. (2004)] for investigations on interchannel mixing effect due to void drift. The applied geometrical models, as schematically varied from simple two-

channel systems to a  $2 \times 3$  multi-rod bundle. The covered flow regimes were mainly slug, churn and annular flow regime. Since test loop construction, experimental procedure and measurement techniques of the above mentioned investigations were quite similar, they are summarized here together.

All the test sections were made up of three parts: an entry section, a connection section and a discharge section. In the entry and discharge section, the gap between adjacent subchannels was completely blocked so that no inter-subchannel mixing exists, while in the connection section the blockage of the gap was removed so that inter-subchannel mixing through the gap can occur. The most important assumption made by the authors is that turbulent mixing (TM), which is the only active mixing effect at equilibrium state, induces neither net mass exchange nor net volume exchange between interacting subchannels. Furthermore, diversion cross flow was assumed by the authors to be prevented with the equal time-averaged mean pressure in each subchannels at both inlet and outlet of the connection section.

Under these conditions, the two-phase mixture at the end of the connection section was isokinetic split into individual subchannels and discharged. After passing the discharge section the two-phase mixture was finally separated and exit mass flow rates of each phases in individual subchannels were then measured due to void drift.

## (ii) Review of void drift models

Lahey and Moody (1993) proposed a model for void drift called as void settling model which has been widely used in two-subchannel system experiments by Sadatomi et al. (1994), Kawahara et al. (2006) and Kawahara et al. (2009); and for multi-subchannel system by Sadatomi et al. (2004). Net lateral mass flux of gas phase due to the void drift between subchannels  $G_{g,ij}$  is calculated from the equation as follows

$$G_{g,ij} = \rho_g D \left[ (\alpha_i - \alpha_j) - (\alpha_i - \alpha_j)_{eq} \right] / S_{ij} \quad (1.1)$$

where  $G_{g,ij}$  is net change in mass flux between adjacent subchannels (i.e. subchannel “i” and subchannel “j”) due to void drift,  $\rho_g$  is the density of gas,  $D$  is void diffusion coefficients,  $(\alpha_i - \alpha_j)$  is void fraction difference in non-equilibrium flow,  $(\alpha_i - \alpha_j)_{eq}$  is void fraction difference in equilibrium flow and  $S_{ij}$  is gap between the subchannels.

Lahey et al. (1972) derived a model based on Levy’s model (1963). They proposed a model for predicting equilibrium void fraction. It is based on the principle that ratio of void fraction difference to average void fraction is proportional to ratio of difference in mass flux to average mass flux. Rowe et al. (1990) derived a model for predicting equilibrium void fraction. It is based on the principle that the equilibrium void fraction is a function of average void fraction and average hydraulic diameter between adjacent subchannels. Carlucci et al. (2004) modified Rowe et al. (1990) model by including a constant  $K$  and the factor of mass-flux and pressure  $F_{G,p}$ . Lahey et al. (1972), Rowe et al. (1990) and Carlucci et al. (2003) proposed a model to evaluate the void fraction distribution in a hydraulically equilibrium flow as shown in Table 1.4.

**Table 1.4** Description of void drift models

| S.no | Model                  | Equation derived for turbulent mixing rate   |
|------|------------------------|--|
| 1    | Lahey et al. (1972)    | $\frac{(\alpha_i - \alpha_j)}{\alpha_{avg}} = \frac{(G_i - G_j)}{\tilde{G}_{avg}}$                               |
| 2    | Rowe et al. (1990)     | $\alpha_i = \alpha_{avg} + \alpha_{avg} (1 - \alpha_{avg}) \left(1 - \frac{D_{h,avg}}{D_{h,i}}\right)$           |
| 3    | Carlucci et al. (2004) | $\alpha_i = \alpha_{avg} + K \alpha_{avg} F_{G,p} (1 - \alpha_{avg}) \left(1 - \frac{D_{h,avg}}{D_{h,i}}\right)$ |

### 1.2.3 Diversion Cross flow

The third mechanism is diversion cross flow which occurs due to lateral pressure difference between adjacent subchannels. In this phenomenon, there is a net flow from one subchannel to the other subchannel at their common boundary. Lateral pressure difference can result from different subchannel hydraulic diameter, heat flux distribution; gradual or abrupt changes in flow area i.e. fuel rod bowing and spacer respectively.

#### (i) Review of diversion cross flow experiments

Diversions cross flow experiments were performed by (McNown (1954), Champman (1963), Dittrich and Graves (1956), Dittich (1958), Tappacu (1976), Kawahara (2006) and Iwamura (1986)). A survey of open literature on diversion cross-flow has shown that available experimental data are very limited. Early experiments on diversion cross-flow

were carried out on discrete blowing or sucking manifolds. In blowing manifolds, a large fluid stream is subdivided by a number of lateral discrete discharge ports, whereas in sucking manifolds a large stream is formed by the combination of smaller streams through the lateral ports. McNown (1954), using a 2-in. dia. pipe as the main channel, and 1-in. and ½-in. tubing as laterals, determined the changes in piezometric and total head of the main and lateral flow. Chapman (1963) conducted experiments in order to determine the effectiveness of cross-flow on pressure equalization between two parallel-flow channels coupled by holes. St. Pierre (1966) using the experimental data of McNown (1954) for discrete blowing manifolds, determined the values of the transverse resistance coefficient (K). Their study concluded that the transverse resistance coefficient decreases with the ratio of cross flow velocity to the average mean velocity between the subchannels.

In summary, very limited experimental data are available on transverse resistance coefficient in open literature. Most of the existing data were obtained on blowing or sucking manifolds, wall holes and short slots (McNown (1954), Champman (1963), Dittrich and Graves (1956), Dittich (1958). They are useful in giving an idea on the general behavior of the phenomenon, but are not applicable in nuclear reactor rod bundle sub-channel analysis. Only Tappacu (1976) and Kawahara (2006) have performed experiment using two subchannel systems. So there is need for more experimental data related to subchannel analysis.

## **(ii) Review of diversion cross flow models**

The cross-flow loss factor is denoted by the term 'transverse resistance coefficient. In computer predictions in codes such as COBRA, the transverse resistance coefficient is assumed to be constant all along the gap between the subchannels e.g. 0.15 [Rowe (1973)], 0.5 [Rowe (1973)], 1.0 [Tappacu (1988)], 2.5 [Shoukri, (1985)]. The experiment performed by Tapucu [1976] shows that cross flow resistance coefficient is not constant but it is a function of ratio of the lateral flow velocity to the donor channel axial velocity, the recipient channel axial velocity, and of the gap clearance and thickness of the slot.

Kim and Park (1975) proposed a correlation for predicting cross flow resistance as a function of ratio of the lateral flow velocity to the donor channel axial velocity, Reynolds number of recipient channel and ratio of pitch to diameter. Kawahara (2006) proposed a correlation for predicting cross flow resistance as a function of ratio of cross flow velocity to the average mean velocity between the subchannels. Iwamura (1986) proposed a correlation relating cross-flow resistance as proportional to void fraction and cross-flow Reynolds number.

## **1.3 Assessment of two phase turbulent mixing models**

As said before, there are a few turbulent mixing models available in literature like Bues (1972), Kazimi and Kelly (1983), Kawahara et al. (2000) and Carlucci et al. (2003), which are primarily developed from experimental data. In this work, an assessment of turbulent mixing models was performed against existing experimental data, which are presented in Figures 1.2, 1.3, 1.4 and 1.5.

In this section, we evaluate the turbulent mixing models against the data obtained from present experiments of two phase turbulent mixing as discussed above.

For evaluation, we have compared the measured (experimental) liquid and gas phase turbulent mixing rate in single phase flow  $W'_{exp}$  with predicted liquid and gas turbulent mixing rate in two phase flow  $W'_{cal}$ . The error analysis has been done to find out maximum, minimum and average error between measured and predicted value of single phase turbulent mixing rate. The error analysis shows how predicted value by turbulent mixing models differs from measured experimental values.

The maximum and minimum error is calculated as:

$$\text{Maximum Error (+ve deviation), } E_{\max} = \max \left( \frac{W'_{cal} - W'_{exp}}{W'_{exp}} \times 100 \right) \quad (1.2)$$

$$\text{Minimum Error (-ve deviation), } E_{\min} = \min \left( \frac{W'_{cal} - W'_{exp}}{W'_{exp}} \times 100 \right) \quad (1.3)$$

The average error is calculated as

$$\text{Average Error} = \frac{\sum_{i=1}^n E_i}{n} \% \quad (1.4)$$

where n= no. of data points and

$$E_i = \left( \frac{W'_{i,cal} - W'_{i,exp}}{W'_{i,exp}} \times 100 \right) \quad (1.5)$$

### (i) Evaluation of model of Bues (1972)

In Bues (1972) model, the calculated liquid phase turbulent mixing rate shows very large discrepancy against measured liquid phase mixing rate as shown in Figure 1.2 (a).

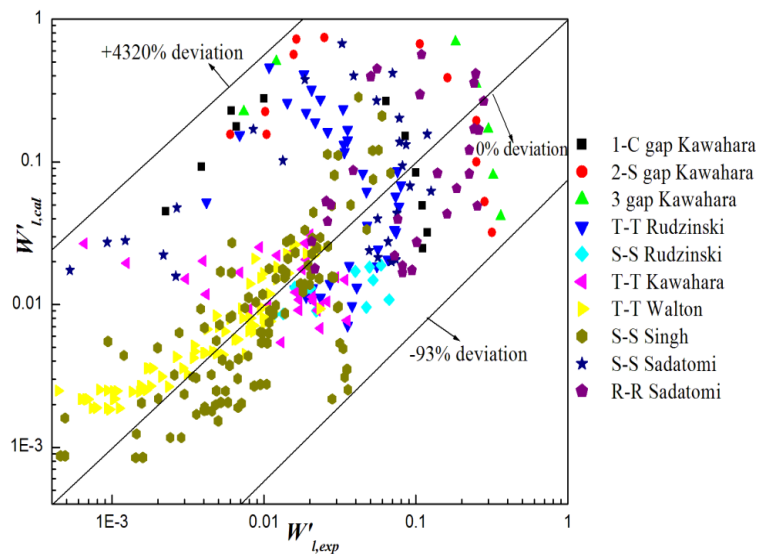


**Fig. 1.2 (a)** Comparison of the predictions of Bues (1972) model against subchannel experiments for liquid phase turbulent mixing rate in two phase flow.

For liquid phase, the calculated turbulent mixing rate differs from measured turbulent mixing rate by +4320% and -93% with an average error of +515.37%. Bues (1972) model is compared with liquid phase turbulent mixing experimental data for a gap width varies 1 mm to 4 mm. The prediction showed an average error of more than +700% for Kawahara et al. [1997b] and Sadatomi et al. [2004] subchannel experiment because the gap width is more than 2.1 mm and Bues (1972) model considers gap size less than equal to 2.1 mm.

The discrepancies between Bues (1972) model and experimental data for liquid phase in two phase flow have been compared for individual subchannel geometry, which are listed in Table 1.5.

**Table 1.5** Error analysis between calculated liquid phase turbulent mixing rate (Bues (1972) model) and measured liquid phase turbulent mixing rate in two phase flow.

| Subchannel geometry | +ve Error % | -ve Error % | Average Error % |
|---------------------|-------------|-------------|-----------------|
| 1-C gap Kawahara    | 3650        | 77.7        | +1210           |
| 2-S gap Kawahara    | 4320        | 89.9        | +1420           |
| 3 gap Kawahara      | 4100        | 88.5        | +1020           |
| T-T Rudzinski       | 4180        | 79.9        | +453            |
| S-S Rudzinski       | 47.2        | 83.8        | -37.7           |
| T-T Kawahara        | 3970        | 78.1        | +216            |
| T-T Walton          | 465         | 60          | +56.8           |
| S-S Singh           | 578         | 92.9        | +22.8           |
| S-S Sadatomi        | 3200        | 72.1        | +723            |
| R-R Sadatomi        | 709         | 81.5        | +60             |

The gas phase turbulent mixing rate data underpredicts measured gas phase turbulent mixing rate, as shown in Figure 1.2 (b).

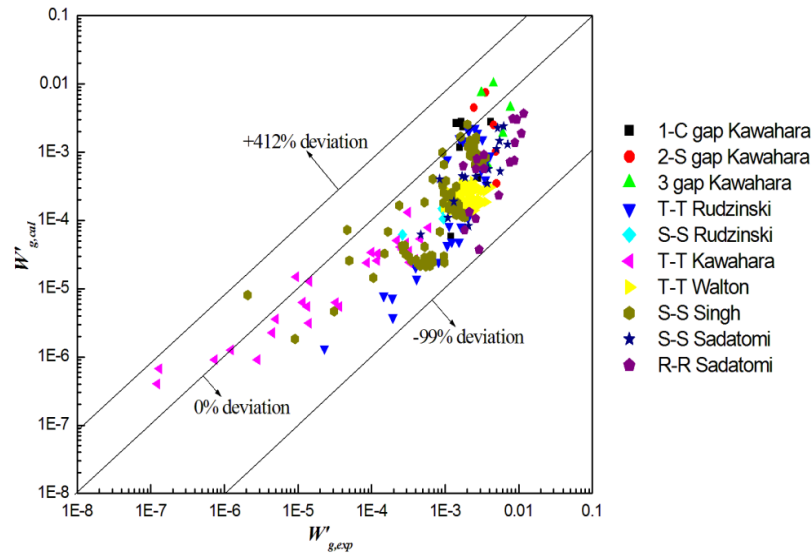


**Fig. 1.2 (b)** Comparison of the predictions of Bues (1972) model against subchannel experiments for gas phase turbulent mixing rate in two phase flow.

For gas phase, the calculated turbulent mixing rate differs from measured turbulent mixing rate by +412% and -99% with an average error of -52.13%. The discrepancies between Bues (1972) model and experimental data for gas phase in two phase flow have been compared for individual subchannel geometry, which are listed in Table 1.6.

**Table 1.6** Error analysis calculated gas phase turbulent mixing rate (Bues (1972) model) from measured gas phase turbulent mixing rate in two phase flow.

| Subchannel geometry | +ve Error % | -ve Error % | Average Error % |
|---------------------|-------------|-------------|-----------------|
| 1-C gap Kawahara    | 88.7        | 95.2        | -17.5           |
| 2-S gap Kawahara    | 109         | 93.1        | -5.39           |
| 3 gap Kawahara      | 138         | 83.4        | +13.8           |
| T-T Rudzinski       | 1.92        | 98.1        | -73.2           |
| S-S Rudzinski       | -           | 98.3        | -90.5           |
| T-T Kawahara        | 412         | 93.2        | -32.5           |
| T-T Walton          | -           | 94.9        | -87.6           |
| S-S Singh           | 290         | 97.5        | -67.0           |
| S-S Sadatomi        | -           | 96          | -79.3           |
| R-R Sadatomi        | -           | 98.7        | -82.2           |

**(ii) Evaluation of model of Kazimi and Kelly (1983)**

Kazimi and Kelly (1983) model shows that most of the calculated data overpredict the measured liquid phase turbulent mixing rate. The calculated liquid phase turbulent mixing rate differs from measured liquid phase turbulent mixing rate by +1480% and -86% with an average error of 153.24%, which is shown in Figure 1.3 (a).

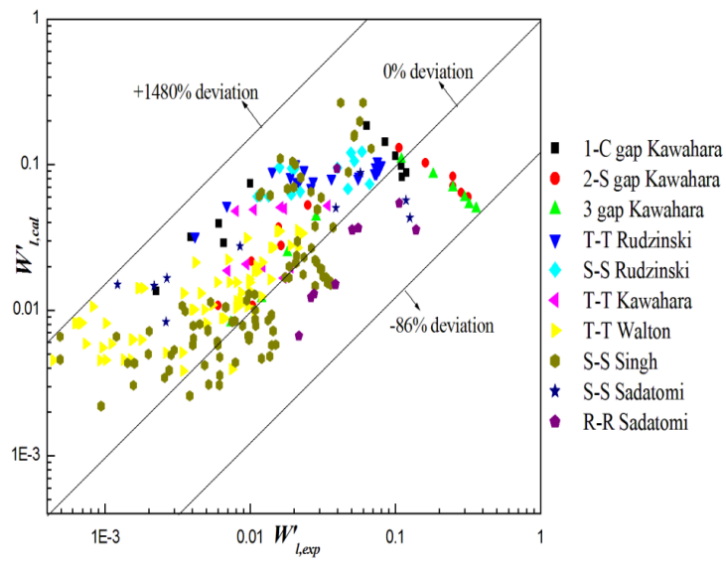


**Fig. 1.3 (a)** Comparison of the predictions of Kazimi and Kelly (1983) model against subchannel experiments for liquid phase turbulent mixing rate in two phase flow.

The discrepancies between Kazimi and Kelly (1983) model and experimental data for liquid phase in two phase flow have been compared for individual subchannel geometry, which are listed in Table 1.7.

**Table 1.7** Error analysis between calculated liquid phase turbulent mixing rate (Kazimi and Kelly (1983) model) and measured liquid phase turbulent mixing rate in two phase flow.

| Subchannel geometry | +ve Error % | -ve Error % | Average Error % |
|---------------------|-------------|-------------|-----------------|
| 1-C gap Kawahara    | 720         | 25.9        | + 270           |
| 2-S gap Kawahara    | 138         | 81          | + 17.1          |
| 3 gap Kawahara      | 53.9        | 86          | - 27.3          |
| T-T Rudzinski       | 1060        | 23.3        | + 218           |
| S-S Rudzinski       | 974         | -           | + 333           |
| T-T Kawahara        | 930         | 21          | + 142           |
| T-T Walton          | 1200        | 47.5        | + 289           |
| S-S Singh           | 1340        | 64.7        | + 134           |
| S-S Sadatomi        | 1480        | 65.6        | + 197           |
| R-R Sadatomi        | 139         | 78          | - 40.4          |

The calculated gas phase turbulent mixing rate underpredict the measured gas phase turbulent mixing rate. The calculated gas phase turbulent mixing differs from measured gas phase turbulent mixing rate by +2810% and -99% with an average error of -41.8%, which is shown in Figure 1.3 (b).

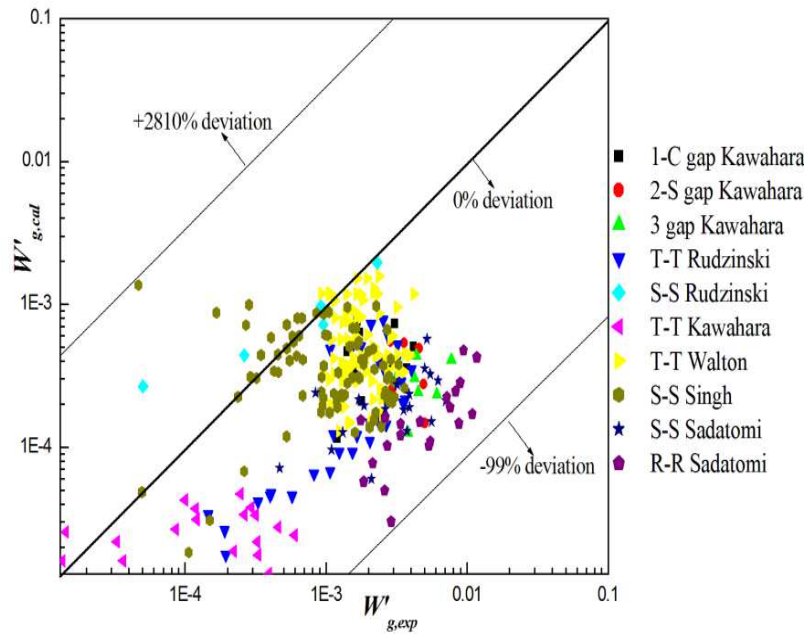


**Fig. 1.3 (b)** Comparison of the predictions of Kazimi and Kelly (1983) model against subchannel experiments for gas phase turbulent mixing rate in two phase flow.

Here, most of the calculated data overpredict the measured liquid phase turbulent mixing rate and underpredict measured gas phase turbulent mixing rate. The pattern of error is more or less same in comparison to Bues (1972) model. The discrepancies between Kazimi and Kelly (1983) model and experimental data for gas phase in two phase flow have been compared for individual subchannel geometry, which are listed in Table 1.8.

**Table 1.8** Error analysis between calculated gas phase turbulent mixing rate (Kazimi and Kelly (1983) model) from measured gas phase turbulent mixing rate in two phase flow.

| Subchannel geometry | +ve Error % | -ve Error % | Average Error % |
|---------------------|-------------|-------------|-----------------|
| 1-C gap Kawahara    | -           | 90.5        | -78.1           |
| 2-S gap Kawahara    | -           | 97          | -88.9           |
| 3 gap Kawahara      | -           | 96.7        | -93.6           |
| T-T Rudzinski       | -           | 94.6        | -85.2           |
| S-S Rudzinski       | 428         | 88.2        | +5.26           |
| T-T Kawahara        | 2480        | 96.7        | +152            |
| T-T Walton          | 27.7        | 93.3        | -67.4           |
| S-S Singh           | 2810        | 94.3        | +25.9           |
| S-S Sadatomi        | -           | 97.3        | -91.7           |
| R-R Sadatomi        | -           | 99          | -96.6           |

### (iii) Evaluation of model of Kawahara et al. (2000)

Kawahara et al. (2000) model is limited to slug churn flow regime only. This is not valid for other flow regimes like bubbly and annular flow regime. Validation of this model has been done for rectangular-rectangular subchannels (1-C, 2-S and 3 gaps) and square-square subchannels against Kawahara et al. (1997b) and Rudzinski (1970) experiment respectively. This model is not evaluated for other subchannel experiments. On evaluation of Kawahara et al. (2000) model against slug churn data obtained from subchannel experiments, it is found that most of the data for both calculated liquid and

gas phase turbulent mixing rate overpredict measured liquid and gas phase turbulent mixing rate which is shown in Figures 1.4 (a) and 1.4 (b).

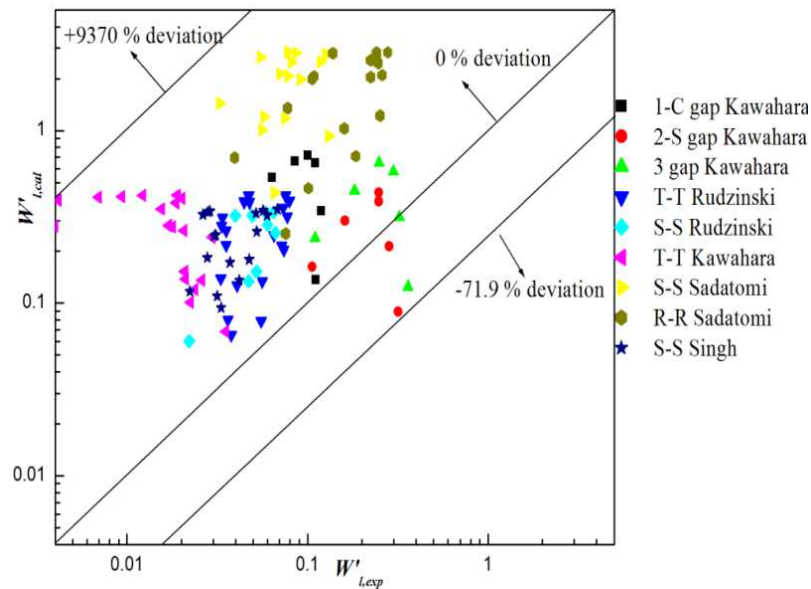


**Fig. 1.4 (a)** Comparison of the predictions of Kawahara et al. (2000) model against subchannel experiments for liquid phase turbulent mixing rate in two phase flow.

For liquid phase, the calculated turbulent mixing rate differs from measured turbulent mixing rate by +9370% and -71.9% with an average error of 1200%. The reason for showing large average error is that this model considers only rectangular-rectangular subchannels (1-C, 2-S and 3 gaps) having flow area more than other subchannel geometries. The discrepancies between Kawahara et al. (2000) model and experimental data for liquid phase in two phase flow have been compared for individual subchannel geometry, which are listed in Table 1.9.

**Table 1.9** Error analysis between calculated liquid phase turbulent mixing rate (Kawahara et al. (2000) model) and measured liquid phase turbulent mixing rate in two phase flow.

| Subchannel geometry | +ve Error % | -ve Error % | Average Error % |
|---------------------|-------------|-------------|-----------------|
| 1-C gap Kawahara    | 739         | -           | + 457           |
| 2-S gap Kawahara    | 87          | 71.9        | + 29.1          |
| 3 gap Kawahara      | 161         | 65.6        | +74.1           |
| T-T Rudzinski       | 823         | -           | + 405           |
| S-S Rudzinski       | 707         | -           | + 380           |
| T-T Kawahara        | 9370        | -           | + 2990          |
| S-S Sadatomi        | 4740        | -           | + 2450          |
| R-R Sadatomi        | 1930        | -           | +1000           |
| S-S Singh           | 1140        | -           | + 548           |

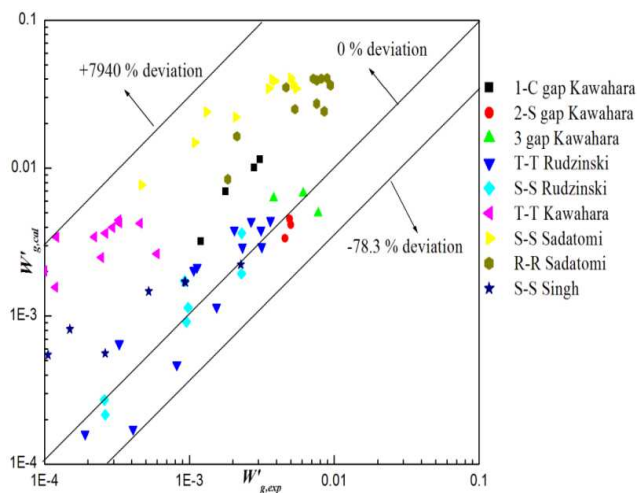


**Fig. 1.4 (b)** Comparison of the predictions of Kawahara et al. (2000) model against subchannel experiments for gas phase turbulent mixing rate in two phase flow.

For gas phase, the calculated turbulent mixing rate differs from measured turbulent mixing rate by +7940% and -78.3% with an average error of 637%. The reason for over prediction of calculated gas phase mixing rate is that it depends on liquid phase turbulent mixing rate which also overpredicts the measured liquid phase turbulent mixing rate. The discrepancies between Kawahara et al. (2000) model and experimental data for gas phase turbulent mixing rate have been compared for individual subchannel geometry, which are listed in Table 1.10.

**Table 1.10** Error analysis between calculated gas phase turbulent mixing rate (Kawahara et al. (2000) model) and measured gas phase turbulent mixing rate in two phase flow.

| Subchannel geometry | +ve Error % | -ve Error % | Average Error % |
|---------------------|-------------|-------------|-----------------|
| 1-C gap Kawahara    | 291         | -           | + 249           |
| 2-S gap Kawahara    | -           | 26.5        | -17.1           |
| 3 gap Kawahara      | 64.4        | 36          | +12.9           |
| T-T Rudzinski       | 98.2        | 78.3        | + 14.1          |
| S-S Rudzinski       | 84.9        | 18.3        | + 13.7          |
| T-T Kawahara        | 7940        | -           | + 1860          |
| S-S Sadatomi        | 1730        | -           | + 1010          |
| R-R Sadatomi        | 669         | -           | +401            |
| S-S Singh           | 626         | 1.47        | + 234           |

### (iii) Evaluation of model of Carlucci et al. (2003)

In Carlucci et al. (2003) model, the calculated liquid and gas turbulent mixing rate shows large discrepancy, when compared against measured liquid and gas phase turbulent mixing rate as seen in Figures 1.5 (a) and 1.5 (b) respectively.

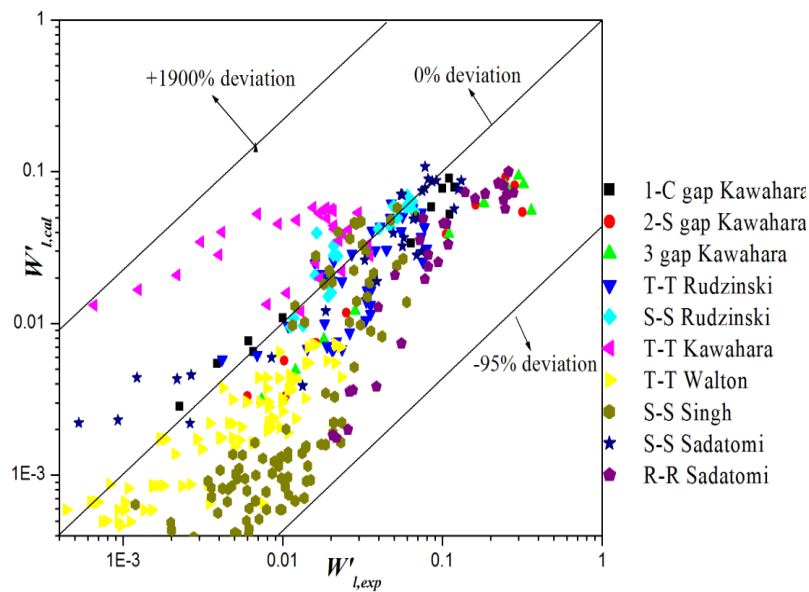


**Fig. 1.5 (a)** Comparison of the predictions of Carlucci et al. (2003) model against subchannel experiments for liquid phase turbulent mixing rate in two phase flow.

For liquid phase, the calculated turbulent mixing rate differs from measured turbulent mixing rate by +1900% and -95% with an average error of -15.6%. The discrepancies between Carlucci et al. (2003) model and experimental data for liquid phase in two phase flow have been compared for individual subchannel geometry, which are listed in Table 1.11.

**Table 1.11** Error analysis between calculated liquid phase turbulent mixing rate (Carlucci et al. (2003) model) and measured liquid phase turbulent mixing rate in two phase flow.

| Subchannel geometry | +ve Error % | -ve Error % | Average Error % |
|---------------------|-------------|-------------|-----------------|
| 1-C gap Kawahara    | 40.7        | 52.6        | -9.4            |
| 2-S gap Kawahara    | -           | 82.9        | -60.6           |
| 3 gap Kawahara      | -           | 84.6        | -65.6           |
| T-T Rudzinski       | 57.2        | 71.3        | -25.7           |
| S-S Rudzinski       | 143         | 28.1        | +10.7           |
| T-T Kawahara        | 1900        | 20.7        | +329            |
| T-T Walton          | 34          | 91.3        | -50.5           |
| S-S Singh           | 79.3        | 95          | -64.6           |
| S-S Sadatomi        | 321         | 70.8        | +13.1           |
| R-R Sadatomi        | -           | 92.2        | -69.6           |

For gas phase, the calculated turbulent mixing rate differs from measured turbulent mixing rate by +8910% and -96% with an average error of +104%. The discrepancies between Carlucci et al. (2003) model and experimental data for gas phase in two phase flow have been compared for individual subchannels geometry, which are listed in Table 1.12.

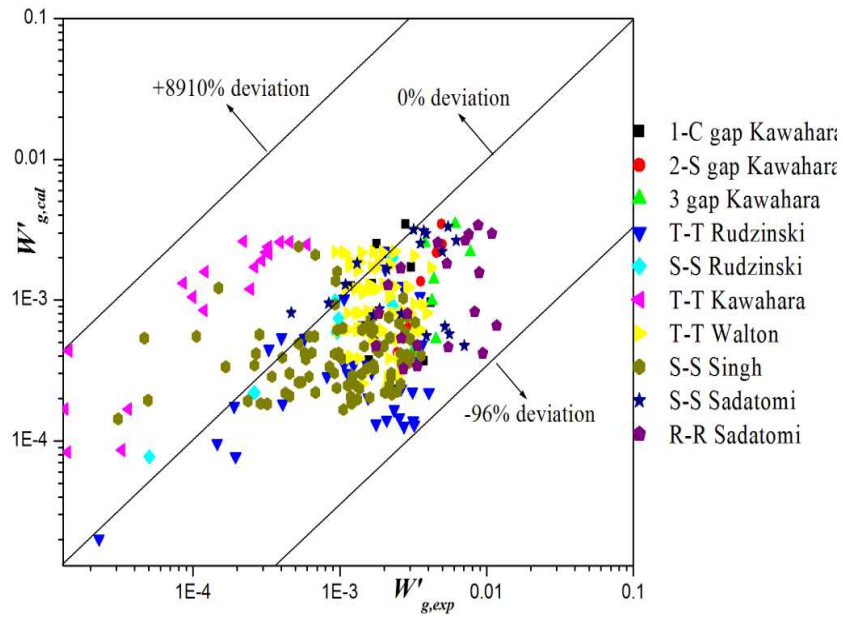


**Fig. 1.5 (b)** Comparison of the predictions of Carlucci et al. (2003) model against subchannel experiments for gas phase turbulent mixing rate in two phase flow.

**Table 1.12** Error analysis between calculated gas turbulent mixing rate Carlucci et al. (2003) model) and measured gas turbulent mixing rate in two phase flow.

| Subchannel Geometry | +ve Error % | -ve Error % | Average Error % |
|---------------------|-------------|-------------|-----------------|
| 1-C gap Kawahara    | 41.6        | 90.1        | -36.4           |
| 2-S gap Kawahara    | -           | 86.6        | -63.0           |
| 3 gap Kawahara      | -           | 88.4        | -66.9           |
| T-T Rudzinski       | 36.6        | 96          | -59.7           |
| S-S Rudzinski       | 53.2        | 59.8        | -14.2           |
| T-T Kawahara        | 8910        | -           | +1340           |
| T-T Walton          | 135         | 89          | -40.4           |
| S-S Singh           | 2350        | 90.9        | +28.8           |
| S-S Sadatomi        | 73.5        | 93.3        | -33.2           |
| R-R Sadatomi        | -           | 95.6        | -72.2           |

It may be noted that for triangular-triangular subchannels of Kawahara et al. (2006) experiment, the model predicts with an average error of +329% for liquid phase and +1340% of gas phase. The reason behind showing large average error is that the flow area of triangular-triangular subchannels is very less as compared to other subchannel geometry.

Evaluation of these models provide important shortcoming which are as follows.

(a) Array effect: In all these models except Kawahara et al (2000) model, the array effect like Square-Square, Rectangular- Rectangular, and Triangular-Triangular subchannel array has not been considered.

(b) Channel size effect: In Carlucci (2003) model, channel size effect is not properly modeled as shown by large error in Triangular-Triangular subchannel experiment of Kawahara (2006) where area of subchannel is very less ( $\sim 16.6 \text{ mm}^2$ ).

(c) Gap size effect: In Bues (1972), Kazimi and Kelly (1983) and Carlucci et al (2003), the gap between subchannels is not properly modeled which results a large error for gap more than 2.1 mm.

(d) Pressure effect: in Kawahara et al (2000) model, the effect of pressure has not been considered.

The major findings from the assessment of two phase turbulent mixing models are as follows.

1. There are large differences among the data of turbulent mixing rate from one subchannel array to another.
2. There are large differences among the models when it is compared with the same experimental data as shown in Table 1.13

**Table 1.13** Error analysis between calculated liquid turbulent mixing and measured liquid turbulent mixing rate in two phase flow.

| Model                  | Liquid mixing rate |                |                | Gas mixing rate |                |                |
|------------------------|--------------------|----------------|----------------|-----------------|----------------|----------------|
|                        | Maximum error%     | Minimum error% | Average error% | Maximum error%  | Minimum error% | Average error% |
| Bues (1972)            | +4320              | -93            | +515.4         | +412            | -93            | -52.1          |
| Kazimi and Kelly(1983) | +1480              | -86            | +153.2         | +2810           | -99            | -41.8          |
| Kawahara (2000)        | +9370              | -71.9          | +1200          | +7940           | -78.3          | +637           |
| Carlucci (2003)        | +1900              | -95            | -15.6          | +8910           | -96            | +104           |

The differences in results observed in the Figures can be due to differences in geometry and operating condition in the experimental set-up.

#### 1.4 Motivation for Ph.D work

Flow distribution within the rod bundle is very important for evaluation of thermal margin. For correct prediction of flow and enthalpy distribution, determination of inter-subchannel mixing phenomena like turbulent mixing, void drift and diversion cross flow is required. Our assessment of inter-subchannel models shows that there is large discrepancy between prediction by models and measured experimental data. This is because inter-subchannel mixing i.e. turbulent mixing, void drift and diversion cross flow are highly geometry and operating condition dependent. The literature also supports our assessment. The following points show how turbulent mixing, void drift and diversion cross flow are affected by subchannel array:

(i) Turbulent mixing: According to Lahey and Schraub (1969), subchannel array and size are important parameters which affect turbulent mixing rate. Rowe and Angle (1969) reported that turbulent mixing rate in square-square subchannel is lower than square-triangular subchannel array. Singh (1972) reported that turbulent mixing rate is dependent on subchannel array. The turbulent mixing rate was found to be the lowest in triangular-triangular array and increased for triangular-square and square-square array in ascending order while keeping gap spacing between subchannels constant. Sadatomi et al. (2004) performed experiment with multiple subchannels having square and rectangular subchannel array. They also reported that turbulent mixing rate in square-square and rectangular-rectangular is lower than square-rectangular subchannel array.

(ii) Void Drift: In order to know the effect of subchannel array on void drift, Gencay et al. (2001) conducted experiments having square duct channel and simulated subchannel geometry array. They observed that the diffusion coefficient which is a measure of void

drift; increases with increasing average void fraction between adjacent subchannels. The turbulent void diffusion coefficient was found to be higher for subchannel geometry array as compared to square channel. Kawahara et al. (2006) conducted experiments having square-square and triangular-triangular subchannel array. They found that void diffusion coefficient due to void drift is smaller in triangular-triangular subchannel array as compared to square-square subchannel array.

(iii) Diversion cross flow: The cross flow resistance in diversion cross flow is found to be dependent on subchannel array. Tappacu (1976) found that cross flow resistance for rod bundle geometry is different one to the other geometry.

In view of the above, it can be concluded that subchannel geometry has significant effect on inter-subchannel mixing phenomena.

It may be noted that, the subchannel geometry of AHWR rod bundle is different from conventional BWRs and ESBWR. The rods in AHWR bundle are arranged in circular subchannel array unlike conventional BWRs or ESBWR geometry in which rods are arranged in square-square, rectangular-rectangular and square-rectangular subchannel array as shown in Figure 1.6 (a) and 1.6 (b).

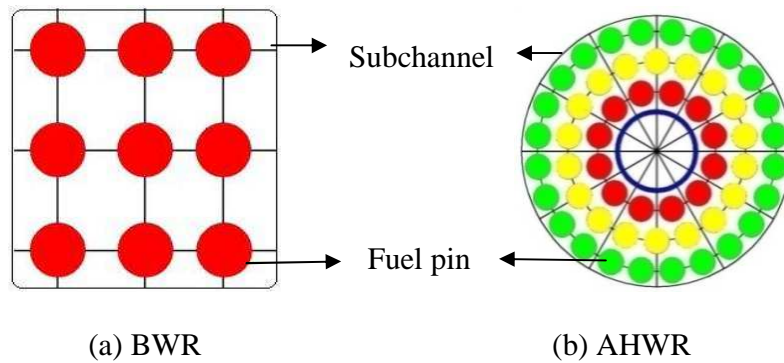


**Fig. 1.6** BWR and AHWR lattice

In the view of above, data obtained from conventional BWRs or ESBWR cannot be used for AHWR

In addition, AHWR being a natural circulation BWR, the mass flux condition in the subchannels can vary from close to zero to rated condition depending on the power, which is different from conventional BWRs wherein the mass flux in the subchannel is more or less constant irrespective of power. Effect of variation of mass flux in the subchannels on two phase mixing phenomena typical to AHWR specific geometry has never been investigated. The Steam generator heavy water reactor (SGHWR) bundle even though has similar geometry like AHWR rod bundle, however, there are almost no studies performed on inter-subchannel mixing studies for this reactor. The major thermal hydraulic parameter of AHWR and ESBWR is shown in Table 1.14

**Table 1.14.** Major thermal hydraulic parameter of AHWR and ESBWR

| Quantity       | AHWR                | ESBWR                |
|----------------|---------------------|----------------------|
| Thermal Power  | 920MW <sub>t</sub>  | 4500 MW <sub>t</sub> |
| Electric Power | 300 MW <sub>e</sub> | 1600 MW <sub>e</sub> |

|                          |             |             |
|--------------------------|-------------|-------------|
| Total number of channels | 452         | 1132        |
| Coolant                  | Light Water | Light Water |
| Moderator                | Heavy Water | Light Water |
| Total core flow rate     | 2237 kg/s   | 10,000 kg/s |
| Average Steam Quality    | 18.2 %      | 17 %        |
| Steam Drum Pressure      | 70 bar      | 71.1 bar    |

### 1.5 Objective and solution strategy

The objective of present work is to establish mixing in subchannels of AHWR rod bundle due to turbulent mixing, void drift and diversion cross flow.

The strategy for solving issues (indicated in section 1.4) in AHWR rod bundle is carried out in following steps

1. Carrying out experiments in 1:1 scaled test facility for each component of inter-subchannel mixing i.e. turbulent mixing, void drift and diversion cross flow applicable to AHWR rod bundle
2. Assessment of existing models against present experiment data for turbulent mixing, void drift and diversion cross flow applicable to AHWR rod bundle, and
3. Development of new models for turbulent mixing, void drift and diversion cross flow, if existing models cannot predict the measured values of present experiment applicable to AHWR rod bundle

### 1.6 Development of a new model for turbulent mixing in rod bundle.

Since previous models have large errors, there is a need to develop a new turbulent mixing model which can predict well for various subchannel geometries. A two phase turbulent mixing model is proposed in this thesis to predict liquid and gas phase mixing rate.

According to equi-volume model (Todreas and Kazimi (1976)), the turbulent mixing rate per unit length in single phase flow can be written as

$$W'_{ij} = \rho_i \left( \frac{\varepsilon}{Z_{ij}^T} \right) S \quad (1.6)$$

Where  $\rho$  is density,  $\varepsilon$  is eddy diffusivity,  $Z_{ij}^T$  is turbulent mixing length and  $S$  is gap spacing between subchannels.

Equation (1.6) can be further simplified as

$$W'_{ij} = \frac{\mu}{\nu} \left( \frac{\varepsilon}{Z_{ij}^T} \right) S \quad (1.7)$$

Where  $\mu$ = dynamic viscosity and  $\nu$ = kinematic viscosity.

Thus,

$$W'_{ij} = \mu \left( \frac{\varepsilon}{\nu} \right) \frac{S}{Z_{ij}^T} \quad (1.8)$$

or,

$$\frac{W'_{ij}}{\mu} = \left( \frac{\varepsilon}{\nu} \right) \frac{S}{Z'_{ij}} \quad (1.9)$$

The parameter  $\frac{\varepsilon}{\nu}$  is taken proportional to the Reynolds number

$$\frac{\varepsilon}{\nu} = K \text{Re}^a \quad (1.10)$$

To consider the effect of gap to centroidal distance ratio for different subchannel array as shown in Figure 1.7, the turbulent mixing length is modified according to (Todreas and Kazimi (1976)) as follows:

$$Z'_{ij} = K' \delta \left( \frac{S}{\delta} \right)^c \quad (1.11)$$

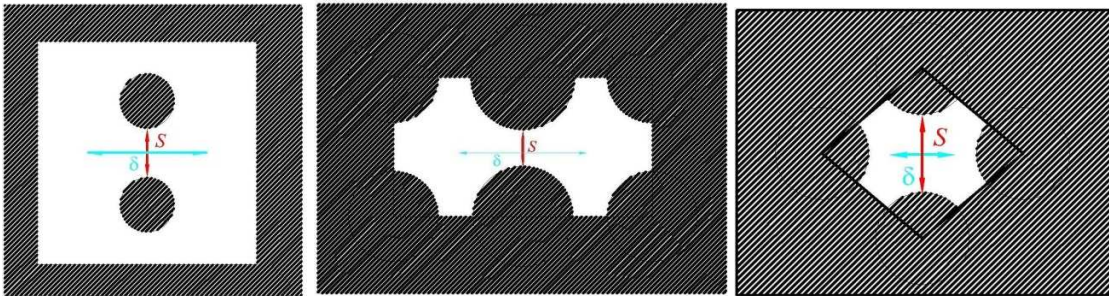


**Fig. 1.7** Representation of geometrical parameter in R-R, S-S and T-T subchannel array.

Substituting the results of equation (1.10) and (1.11) in equation (1.9), we get

$$\frac{W'_{ij}}{\mu} = \frac{K}{K'} \text{Re}^a \left( \frac{S}{\delta} \right)^{1-c} \quad (1.12)$$

Equation (1.12) is modified in terms of mixing number as follows

$$N_{mix} = C \text{Re}^a \left( \frac{S}{\delta} \right)^b \quad (1.13)$$

Where mixing number and Reynolds number can be represented by

$$N_{mix} = \frac{W_{ij}' \times D_h^2}{\mu \times A} \quad (1.14)$$

$$\text{Re} = \frac{\rho \times V \times D_h}{\mu} \quad (1.15)$$

$D_h$  is hydraulic diameter,  $A$  is flow area,  $V$  is velocity of fluid,  $S$  is gap between subchannels,  $\delta$  is centroidal distance between subchannels,  $C$  is coefficient and  $a$  and  $b$  are exponents.

Hence the model for single phase mixing rate is represented by Eq. (1.16) is as follows

$$N_{mix} = f(\text{Re}, S, \delta) \quad (1.16)$$

The model for two phase turbulent mixing rate is modified by replacing single phase flow properties with two phase flow properties. Thus liquid phase turbulent mixing number for two phase flow in subchannels is a function of mixture Reynolds number, gap and centroidal distance between subchannels. In addition, the volumetric fraction needs to be incorporated in the model.

The model can be represented as

$$N_{l,mix} = f(\text{Re}_{mix}, S, \delta, \beta) \quad (1.17)$$

The equation for liquid phase turbulent mixing in two phase flow can be written as follows

$$N_{l,mix} = C_l \times (\text{Re}_{mix})^{a_l} \quad (1.18)$$

$$\text{Where } N_{l,mix} = \left( \frac{W'_{l,mix} \times D^2}{A \times \mu_{\text{hom}}} \right) \quad (1.19)$$

$$\text{Re}_{mix} = \frac{G \times D}{\mu_{\text{hom}}} \quad (1.20)$$

$$\mu_{\text{hom}} = \left( \frac{x}{\mu_g} + \frac{1-x}{\mu_l} \right)^{-1} \quad (1.21)$$

The coefficient ( $C_l$ ) and exponent ( $a_l$ ) were obtained by fitting the test data plotted on dimensionless liquid phase turbulent mixing number against mixture Reynolds number as shown in Figure 1.8.

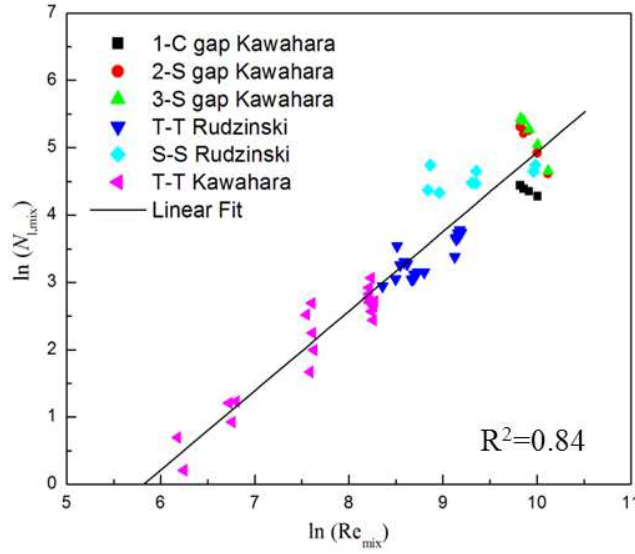


**Fig. 1.8** Liquid phase turbulent mixing rate.

The equation so obtained is given by relationship

$$W'_{l,mix} = \frac{0.00104 \times A \times \mu_{nom} \times (\text{Re}_{mix})^{1.80}}{D_h^2} \quad (1.22)$$

Similarly the gas phase turbulent mixing number for two phase flow in subchannels can be expressed as function of mixture Reynolds number, volumetric fraction, gap and centroidal distance between subchannels. The model can be represented as

$$N_{g,mix} = f(\text{Re}_{mix}, S, \delta, \beta) \quad (1.23)$$

The equation for gas phase turbulent mixing in two phase flow can be written as follows

$$N_{g,mix} = C_g \times (\beta_{gas} \times \ln(\text{Re}_{mix}))^{a_g} \quad (1.24)$$

$$\text{where } N_{g,mix} = \left( \frac{W'_{g,mix} \times D^2}{A \times \mu_{hom}} \right) \quad (1.25)$$

$$\text{Re}_{mix} = \frac{G \times D}{\mu_{hom}} \quad (1.26)$$

$$\beta_{gas} = \frac{J_g}{J_g + J_l} \quad (1.27)$$

The coefficient ( $C_g$ ) and exponent ( $a_g$ ) were obtained from the test data plotted on dimensionless gas phase turbulent mixing number against combined volumetric gas fraction and mixture Reynolds number as shown in Figure 1.9.

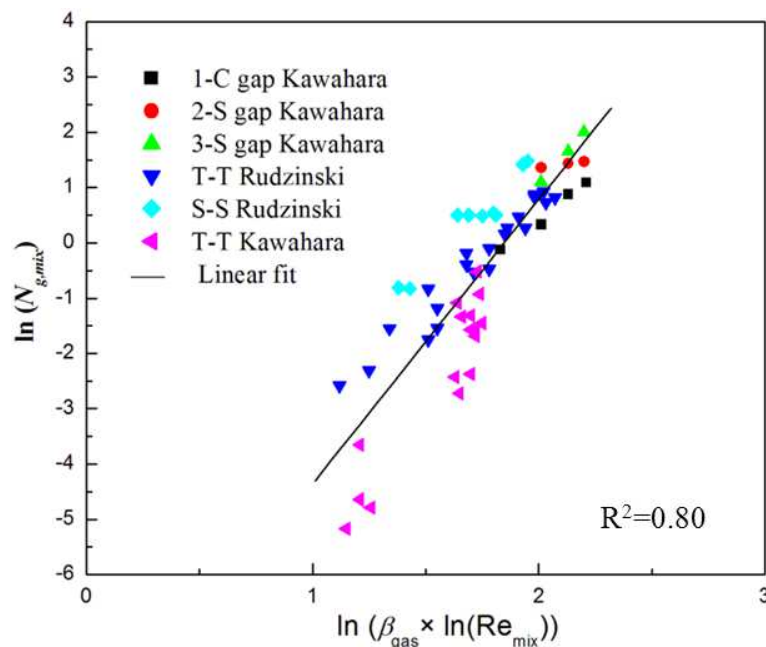


**Fig. 1.9** Gas phase turbulent mixing rate

The equation so obtained is given by relationship

$$W'_{g,mix} = \frac{0.0000749 \times A \times \mu_{hom} \times (\beta_{gas} \times \ln(\text{Re}_{mix}))^{5.1436}}{D^2} \quad (1.28)$$

The model described by equation (1.22) and (1.28) does not consider the subchannel geometry and pressure effect. To incorporate geometrical influence and pressure effect, the model has been modified as discussed below

**(a) Incorporation of gap and centroidal distance between subchannels:**

The two phase turbulent mixing is affected by various parameters such as subchannel geometry, spacer and gap spacing between subchannels.

The equation of gap to centroid factor for liquid phase turbulent mixing rate can be expressed as best fit by

$$F_{l,gc} = \left( \frac{N_{l,mix}}{K_l} \right) = C_1 \left[ (\beta_{liq}) \left( \frac{S}{\delta} \right) \right]^{a_1} \quad (1.29)$$

where

$$K_l = C_l \left[ \text{Re}_{mix} \right]^{a_l} \quad (1.30)$$

The coefficient ( $C_1$ ) and exponent ( $a_1$ ) were obtained using the test data of subchannel experiments of Rudzinski (1970), Kawahara et al. (1997(b)), and Kawahara et al. (2006) plotted on dimensionless gap to centroid factor against combined gap to centroidal

distance ratio and volumetric liquid fraction against combined gap to centroidal distance ratio and volumetric liquid fraction of individual subchannel geometries (R-R, T-T, and S-S) as shown in Figure 1.10 (a), 1.10 (b) and 1.10 (c).

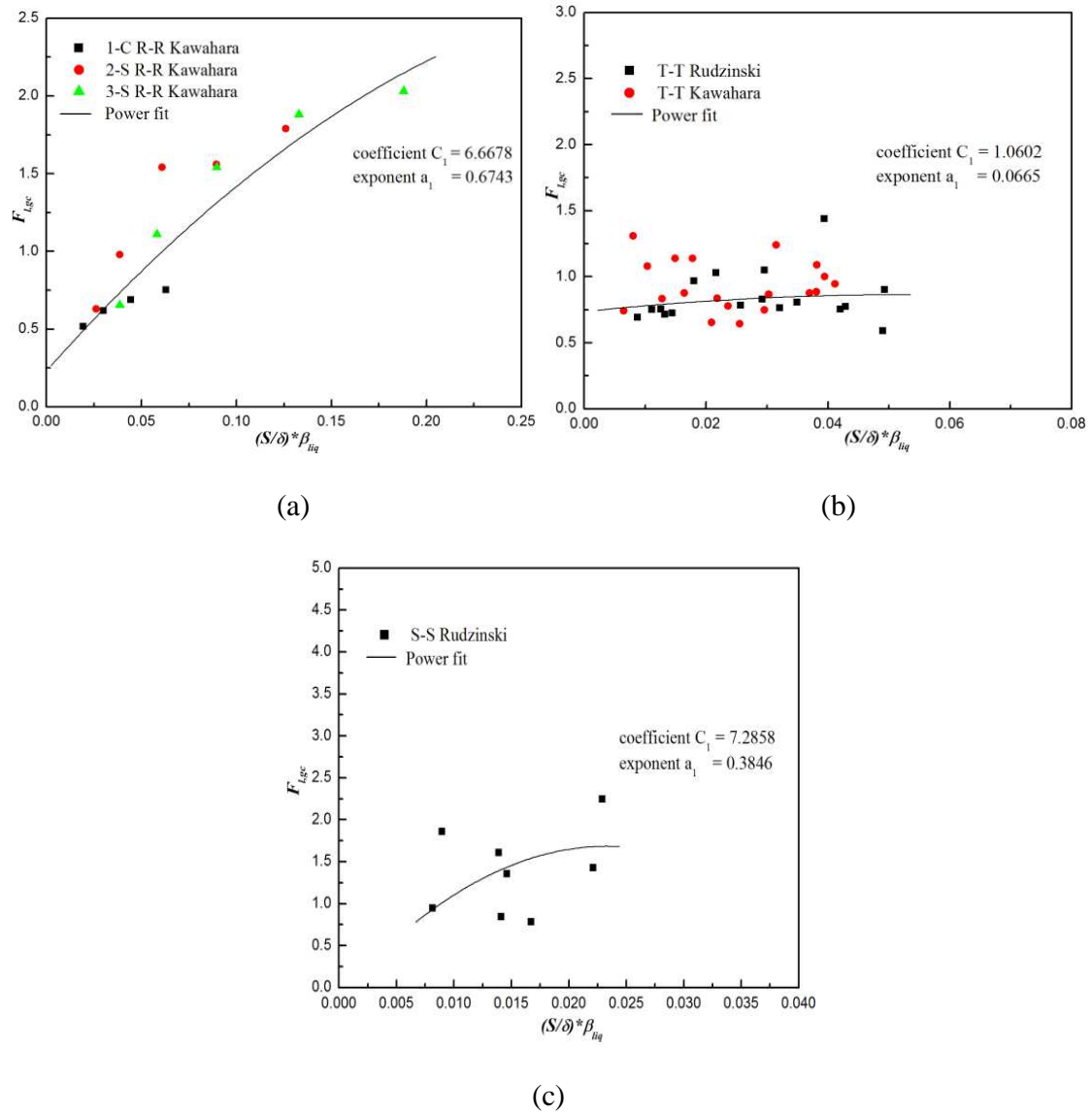


**Fig. 1.10** The coefficient  $C_1$  and exponent  $a_1$  for various subchannel geometry in liquid phase mixing rate

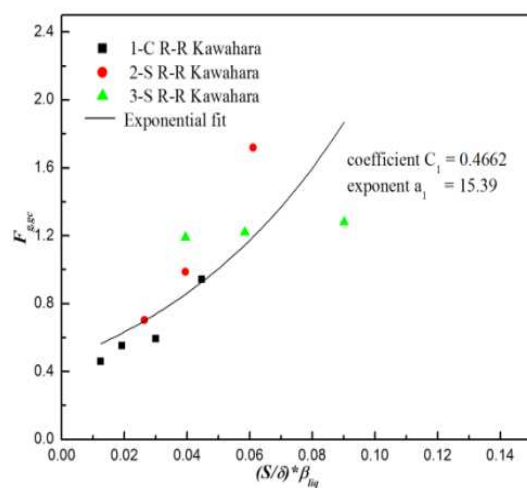
The equation of gap to centroid factor for gas phase turbulent mixing rate can be expressed as best fit by

$$F_{g,gc} = \left( \frac{N_{g,mix}}{K_g} \right) = C_1 \times e^{a_1 \times (\beta_{liq}) \left( \frac{S}{\delta} \right)} \quad (1.31)$$

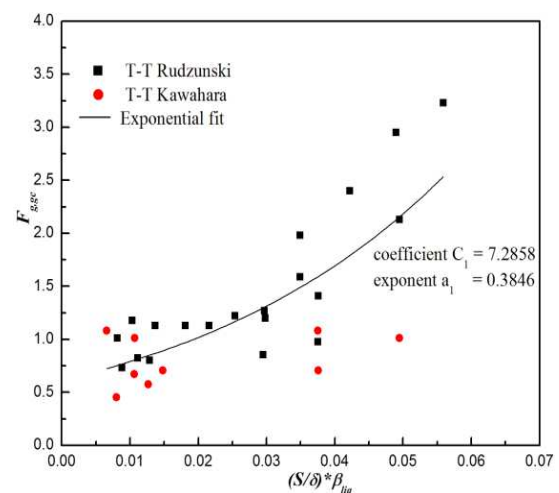
where

$$K_g = C_1 \left[ \beta_{gas} \times \ln(\text{Re}_{mix}) \right]^{a_1} \quad (1.32)$$

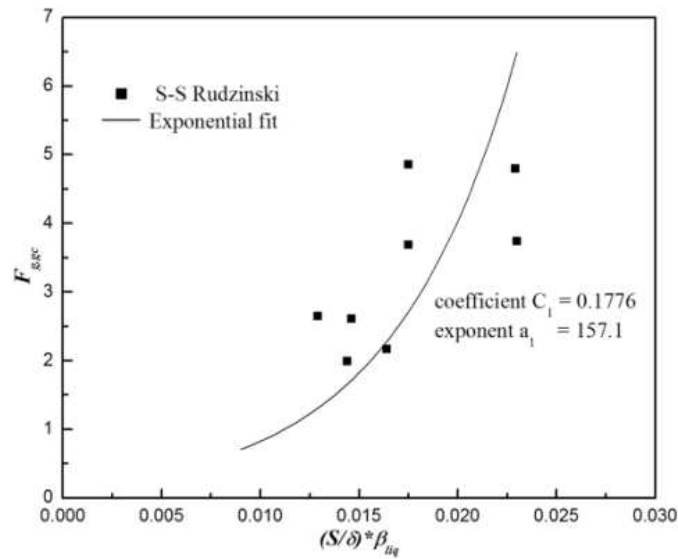
The coefficient ( $C_1$ ) and exponent ( $a_1$ ) were obtained using the test data of subchannel experiments of Rudzinski (1970), Kawahara et al. (1997(b)), and Kawahara et al. (2006) plotted on dimensionless gap to centroid factor against combined gap to centroidal distance ratio and volumetric liquid fraction of individual subchannel geometries (R-R, T-T, and S-S) as shown in Figure 1.11 (a), 1.11 (b), and 1.11 (c).



(a)



(b)



(c)

**Fig. 1.11** The coefficient  $C_1$  and exponent  $a_1$  for various subchannel geometry in gas phase turbulent mixing rate

### (ii) Modeling of pressure effect

Carlucci (2003) is the only model which considers pressure effect in terms of bubble diameter, which changes with change in pressure. However, bubble diameter is difficult to predict in two phase flow since the size of bubble does not have a single value for a particular operating condition. However the bubble diameter which has strong effect on void fraction depends on the surface tension of fluid. Hence, the present model considers the surface tension of fluid to model the effect of pressure. As surface tension of fluid is a function of temperature at corresponding pressure

Thus the effect of pressure is represented by the following expression

$$F_p = \left( \frac{\sigma_{H.T.}}{\sigma_{R.T.}} \right)^n \quad (1.33)$$

$\sigma_{H.T.}$  = surface tension at high temperature at a corresponding saturation pressure,

$\sigma_{R..T.}$  = surface tension at reference temperature i.e. ambient temperature at a corresponding saturation pressure

The correlation so obtained by equation (1.22) and equation (1.28) are modified by introducing gap to centroid factor ( $F_{gc}$ ) and pressure dependent factor ( $F_p$ ). The modified equation for liquid and gas phase are as follows

$$W'_{l,mix} = F_{l,gc} \times F_p \times \frac{0.00104 \times A \times \mu_{hom} \times (\text{Re}_{mix})^{1.80}}{D_h^2} \quad (1.34)$$

$$W'_{g,mix} = F_{g,gc} \times F_p \times \frac{0.0000749 \times A \times \mu_{hom} \times (\beta_{gas} \times \ln(\text{Re}_{mix}))^{5.1436}}{D_h^2} \quad (1.35)$$

The equations (1.34) and (1.35) for liquid phase and mixing rate is expressed in terms liquid phase and gas phase turbulent mixing number are as follows

$$N_{l,mix} = F_{l,gc} \times F_p \times 0.00104 \text{Re}_{mix}^{1.80} \quad (1.36)$$

$$N_{g,mix} = F_{g,gc} \times F_p \times 0.0000749 (\ln(\text{Re}_{mix} \times \beta))^{5.14} \quad (1.37)$$

The proposed model is evaluated by comparing the prediction from present model with experimental data in a two phase slug churn flow regime.

**(i) Test against low pressure and temperature (ambient) air-water experimental data**

Figure 1.12 shows comparison between calculated and measured liquid phase turbulent mixing rate in two phase flow.

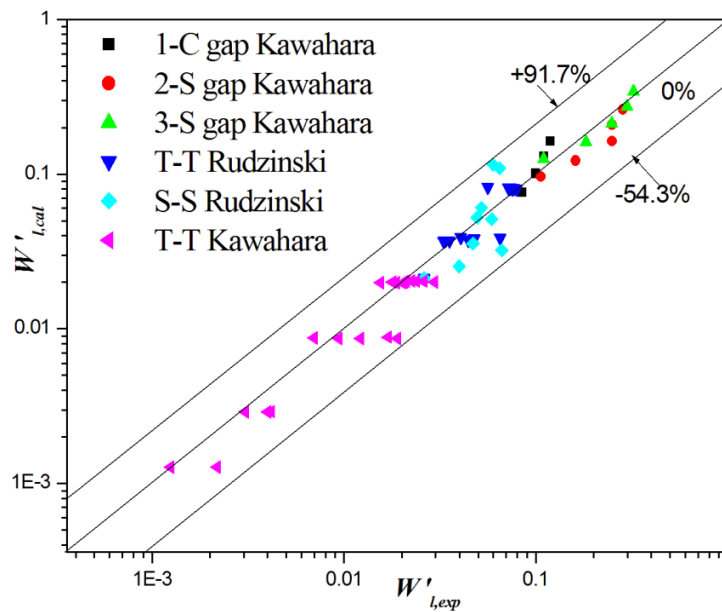


**Fig. 1.12** Comparison of the predictions of present model against subchannel experiments for liquid phase turbulent mixing rate in two phase flow.

An error analysis performed for liquid phase turbulent mixing rate and found that maximum error, minimum error and mean error for liquid phase mixing rate considering all subchannel geometry is about +91.7%, -54.3% and -4.27 % respectively. The error analysis for individual subchannel geometry, which are listed in Table 1.15.

**Table 1.15** Error analysis between calculated liquid phase turbulent mixing and measured liquid turbulent mixing rate in two phase flow

| Subchannels geometry | Max error | Min error | Average Error % |
|----------------------|-----------|-----------|-----------------|
| 1-C gap Kawahara     | +37       | -10.2     | +11.5           |
| 2-S gap Kawahara     | -8.01     | -34.5     | -18.5           |
| 3 gap Kawahara       | +13.6     | -14.9     | -3.05           |
| T-T Rudzinski        | +46.09    | -40.6     | +0.08           |
| S-S Rudzinski        | +91.7     | -51.4     | +4.35           |
| T-T Kawahara         | +28.4     | -54.3     | -12.3           |

Figure 1.13 shows comparison between calculated and measured gas phase turbulent mixing rate in two phase flow.

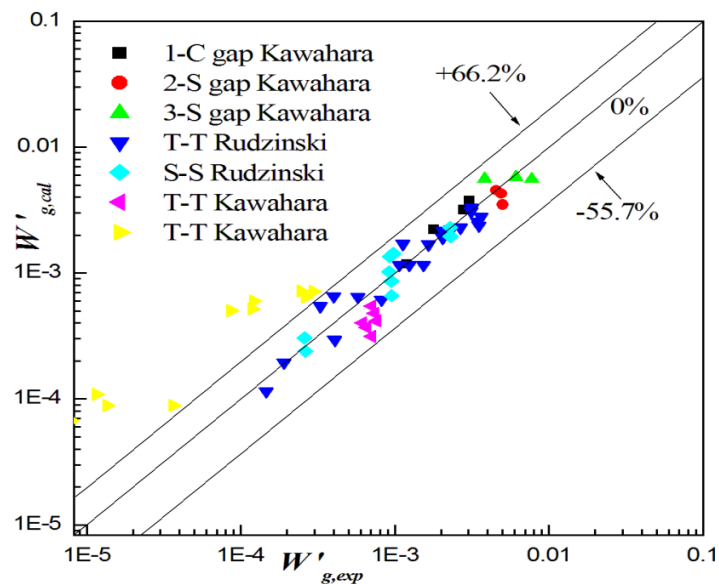


**Fig. 1.13** Comparison of the predictions of present model against subchannel experiment for gas phase turbulent mixing rate in two phase flow.

An error analysis performed for gas phase turbulent mixing rate and found maximum error, minimum error and mean error for gas phase mixing rate considering all subchannels geometry is about +66.2%, -55.7% and -3.29% respectively. The error analysis for individual subchannel geometry, which are listed in Table 1.16.

**Table 1.16** Error analysis between calculated gas turbulent mixing and measured gas turbulent mixing rate in two phase flow.

| Subchannels geometry | Max error | Min error | Average Error % |
|----------------------|-----------|-----------|-----------------|
| 1-C gap Kawahara     | +24.7     | -16.7     | +14.8           |
| 2-S gap Kawahara     | -65.8     | -30.5     | -14.9           |
| 3 gap Kawahara       | +46.3     | -28.2     | +4.08           |
| T-T Rudzinski        | +66.2     | -32.4     | +0.015          |
| S-S Rudzinski        | +45.8     | -30.9     | +6.24           |
| T-T Kawahara         | -22.7     | -55.7     | -39.6           |

(ii) Test against high pressure and temperature steam-water experimental data

**Figure 1.14** shows comparison between calculated and measured turbulent mixing rate in two phase flow.

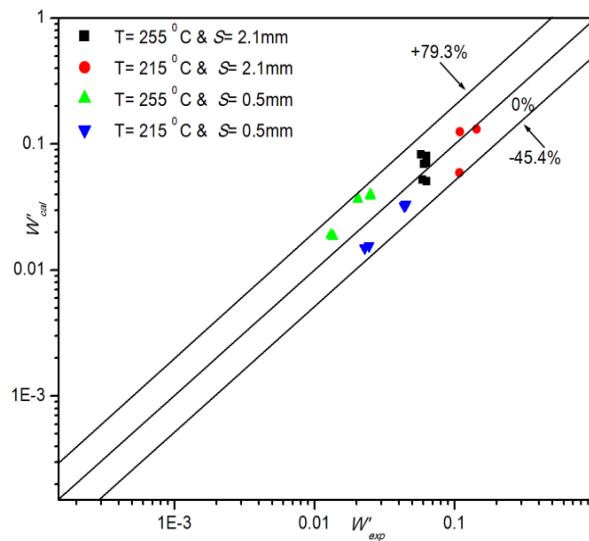


**Fig. 1.14.** Comparison of the predictions of present model against subchannel experiments for total turbulent mixing rate in two phase flow.

An error analysis performed against high pressure and temperature steam-water experiment (Rowe and angel (1969)) of 52 bar, 255<sup>0</sup>C and 28 bar, 215<sup>0</sup>C with mass flux 1356.8 and 2712.5 kg/m<sup>2</sup>-s for total turbulent mixing rate and found that maximum error, minimum error and mean error for total mixing rate considering square-square subchannel geometry ( $S=2.1$  mm and  $S=0.5$  mm) is about +79.3%, -45.4% and +9.94 %.

## 1.7 Organization of thesis

The dissertation of research work is organized in the following eight chapters of this thesis as follows:

Chapter 1 contributes introduction to different mixing phenomena in a rod bundle i.e. turbulent mixing, void drift and diversion cross flow; motivation and objective of research work. A detailed literature survey of each component of inter-subchannel mixing

has been presented. In this chapter, assessment of models against existing experimental data of BWRs geometry has been done. A new model has been developed from first principle for two phases turbulent mixing which correlates all the test data generated so far in literature with reasonable accuracy.

Chapter 2 describes the scaling methodology for experimental facility to simulate AHWR rod bundle and experimental flow conditions for turbulent mixing, void drift and diversion cross flow. In addition, mixing model for three subchannel system is proposed by solving tracer conservation equation to find turbulent mixing rate.

Chapter 3 gives details of test loop and associated equipment and experimental procedure for turbulent mixing, void drift and diversion cross flow in AHWR rod bundle.

Chapter 4 discusses results for single phase turbulent mixing in AHWR rod bundle. An assessment of existing models against our experimental data has been carried out and a new model for single phase turbulent mixing applicable to AHWR has been presented.

Chapter 5 discusses results for two phase turbulent mixing for AHWR rod bundle. In this chapter, an assessment of existing models against our experimental data has been carried out and new models for two phase turbulent mixing rate for different flow regimes applicable to AHWR has been presented.

Chapter 6 discusses results for void drift in AHWR rod bundle. In addition to this, an assessment of existing models against our experimental data has been presented.

Chapter 7 discusses results for diversion cross flow in AHWR rod bundle. An assessment of existing models against our experimental data has been carried out and a new model has been developed for diversion cross flow applicable to AHWR.

Chapter 8 gives important conclusions from this research and recommendation for future work.

### **1.8 Closure**

An assessment of turbulent mixing models against existing experimental data of BWRs geometry has been done and found that there are large errors between predicted and experimental data. Hence a new model has been developed from first principle for turbulent mixing which correlates all the test data generated so far in literature with reasonable accuracy.

## CHAPTER 2

# *SCALING OF TEST FACILITY TO SIMULATE MIXING PHENOMENA IN AHWR ROD BUNDLE*

---

---

### **2.1 Introduction**

The operating condition of nuclear reactor rod bundle is at high pressure and high temperature. The experiments for inter-subchannel mixing phenomena are very difficult and expensive under these operating conditions. In the view of this, the current experiments were performed at near atmospheric pressure and room temperature conditions with air and water as working fluids. For this, scaling methodology for experimental test facility has been presented in this chapter. An experimental flow conditions to simulate flow patterns for inter-subchannel mixing phenomena in AHWR rod bundle has been discussed. In addition to this mathematical equations for turbulent mixing rate are derived using tracer conservation equations.

## 2.2 Scaling of Test Facility

The fuel rods in AHWR rod bundle are arranged in the form of circular rings as shown Figure 2.1 (a) and 1/12<sup>th</sup> symmetric cross section of AHWR fuel rod bundle as shown in Figure 2.1 (b).

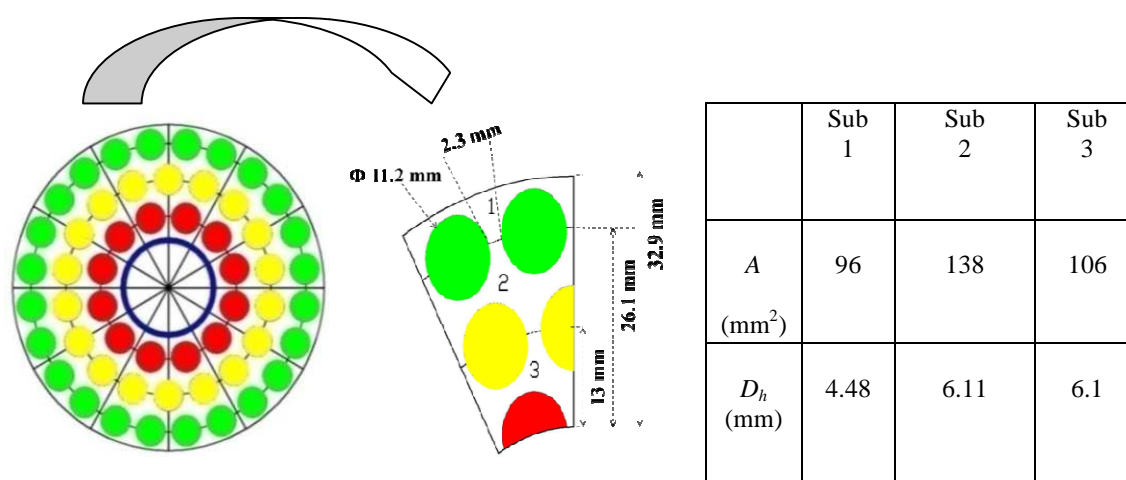


**Fig. 2.1 (a)** AHWR fuel rod bundle **Fig. 2.1 (b)** 1/12<sup>th</sup> segment of AHWR fuel rod bundle

To simulate mixing phenomena, a test facility has been designed. The rods used in the subchannel mixing studies have same size and pitch as that of actual rod bundle of AHWR. Three subchannels are considered in 1/12<sup>th</sup> symmetric cross section (Dasgupta et al. (2006)) of the actual rod bundle. The mass flow rate in actual rod bundle of AHWR varies from 0 to 4.7 kg/sec depending on operating condition. So if we consider three subchannels in 1/12 segment, the mass flow rate can vary in the range 0 to 0.12 kg/sec and correspondingly range of mean velocity is around 0 to 1.2 m/s. The void fraction in two phase flow is varied from 0 to 0.8 which is same as that of actual bundle (Chandraker (2012)). The mean superficial liquid velocity is varied from 0 to 1 m/s (Chandraker et al.

(2013)) and mean superficial gas velocity is varied from 0 to 1.3 m/s. Table 2.1 shows comparison of the dimensions of rod bundle between model and prototype.

**Table 2.1** Scaling of present experiment

| <b>Properties</b>                                     | <b>Prototype</b>    | <b>Model</b>        |
|---|---------------------|---------------------|
| Fluid   | Steam-water         | Air-water           |
| Fuel rod diameter                                     | 11.2 mm             | 11.2 mm             |
| Gap   | 2.3 mm              | 2.3 mm              |
| Height  | 3.5 m               | 3.5 m               |
| Subchannel Hydraulic diameter<br>(1/12 section)       | 5.9 mm              | 5.9 mm              |
| Flow Area (1/12 section)                              | 340 mm <sup>2</sup> | 340 mm <sup>2</sup> |
| liquid velocity in single phase<br>( $V_l$ )          | 0 to 1.2 m/s        | 0 to 1.2 m/s        |
| Superficial liquid velocity in two<br>phase ( $J_l$ ) | 0 to 1 m/s          | 0 to 1 m/s          |
| Superficial gas velocity in two<br>phase ( $J_g$ )    | -                   | 0 to 1.3 m/s        |
| Void fraction range                                   | 0 to 0.8            | 0 to 0.8            |

Conducting experiments to generate mixing parameters are very difficult and expensive for steam water system at higher elevated pressure and temperature. Therefore most of test so far are carried out with air-water system [Walton (1969), Rudzinski (1970), Singh K.S. (1972), Kawahara et al. (1997 (b)), Sadatomi et al. (2004) and Kawahara et al. (2006), Lahey and Schraub (1969), Lahey et al. (1972), Gonzalez-Santalo et al. (1972), Lahey (1986), Sato et al. (1987), Tapucu et al. (1988), Gencay et al. (2001), Sadatomi et al. (1994), Sadatomi et al. (2004) McNown (1954), Champman (1963), Dittrich and Graves (1956), Dittich (1958), Tappacu (1976), Kawahara (2006) and Iwamura (1986)]; which adequately simulate the mixing behavior in steam-water system. The current experiments were performed at near atmospheric pressure and room temperature conditions with air and water as working fluids.

However to take care of reactor operation condition, a correction factor ( $F_p$ ) which is function of surface tension of fluid has been proposed in the present thesis, which is agreed well with both air-water and steam-water condition. Hence, this correction factor can be used to evaluate mixing parameter in reactor operation condition.

### **2.3 Experimental flow condition**

To simulate the flow patterns in two phase bubbly, slug-churn and annular flow regime, superficial liquid and gas velocity are simulated in the experiment.

The transition criteria for bubbly-slug proposed by Griffith (1964) and slug-annular proposed by Wallis (1967) is used to simulate the flow patterns in two phase flow. It may be noted that the choice of these two criteria is according to rod bundle experiments by Walton (1969), Rudzinski (1970) and Singh K.S. (1972). These two criteria show good

agreement with their experiment. Hence these two correlations are used in present experiment.

### 2.3.1 Bubbly-Slug transition

For this, the model proposed by Griffith (1964) is used, as given by

$$\frac{J_g - 0.4}{J_l} < 1.1, \quad (2.1)$$

where  $J_g$  is gas superficial velocity and  $J_l$  as liquid superficial velocity.

### 2.3.2 Slug- Annular transition

For this, the model proposed by Wallis (1967) is used, as given by

$$J_g^* = 0.9 + 0.6J_l^*; \quad (J_l^* < 1) \quad (2.2)$$

$$J_g^* = \left[ 7 + 0.06 \left( \frac{\rho_l}{\rho_g} \right) \right] \left( \frac{\rho_l}{\rho_g} \right)^{1/2} J_l^*; \quad (J_l^* > 1) \quad (2.3)$$

where  $J_g^*$  is dimensionless gas superficial velocity and  $J_l^*$  is dimensionless liquid superficial velocity

$$J_g^* = (m_g / A) \rho_g^{-1/2} \left[ g D_h (\rho_l - \rho_g) \right]^{-1/2} \quad (2.4)$$

$$J_l^* = (m_l / A) \rho_l^{-1/2} \left[ g D_h (\rho_l - \rho_g) \right]^{-1/2} \quad (2.5)$$

For a fixed liquid superficial velocity ( $J_l$ ), the gas superficial velocity ( $J_g$ ) was varied to get void fraction ( $\alpha$ ) range. The void fraction is calculated by Chisom's correlation (1973).

$$\alpha_i = \frac{\beta_i}{\beta_i + \frac{1 - \beta_i}{\sqrt{1 - \beta_i \left( 1 - \frac{\rho_g}{\rho_l} \right)}}} \quad (2.6)$$

where  $\beta_i$  = gas volumetric fraction is given by  $\beta_i = \frac{J_g}{J_g + J_l}$  (2.7)

The correlation is valid for  $0 \leq \beta_i \leq 0.9$  provided that liquid is no more viscous than water (Chisholm (1973)). The correlation was compared with air-water flow experiment at atmospheric condition and found to be in good agreement with experiment in range  $\pm 6.02\%$  (Chisholm (1973)). The current experiments are performed at near atmospheric conditions with air and water as working fluids. The working range of  $\beta_i$  in present experiment varies from 0.2 to 0.9 which is well under the limit of correlation.

#### 2.4 Mixing model to evaluate turbulent mixing rate

Consider the turbulent flow of a fluid in three subchannels arrange in circular pitch (refer Figure 2.2). These subchannels are connected by a gap width  $S$  and length  $l$  through which turbulent transfer of liquid takes place. In one subchannel tracer is injected

upstream of mixing zone. The amount of liquid transferred from one subchannel to another is determined by employing a mass balance using measured tracer concentration in each channel.

The following basic assumptions are made in this analysis.

- (1) Subchannel axial pressure gradient are identical, thus eliminating radial pressure gradient and any net transfer of fluid from one subchannel to another.
- (2) Tracer concentration is small, hence the tracer has negligible effect on physical properties.
- (3) The fluid leaving one subchannel has the average properties (tracer concentration) of that channel.
- (4) After fluid has left donor subchannel it mixes immediately in the receiving subchannel.
- (5) There is no relative velocity between fluid and tracer.
- (6) The flow should be in hydrodynamic equilibrium. Here in the equilibrium flow, the flow rates of both phases in every subchannel do not vary along the channel axis i.e. radial pressure difference between the subchannels is zero.

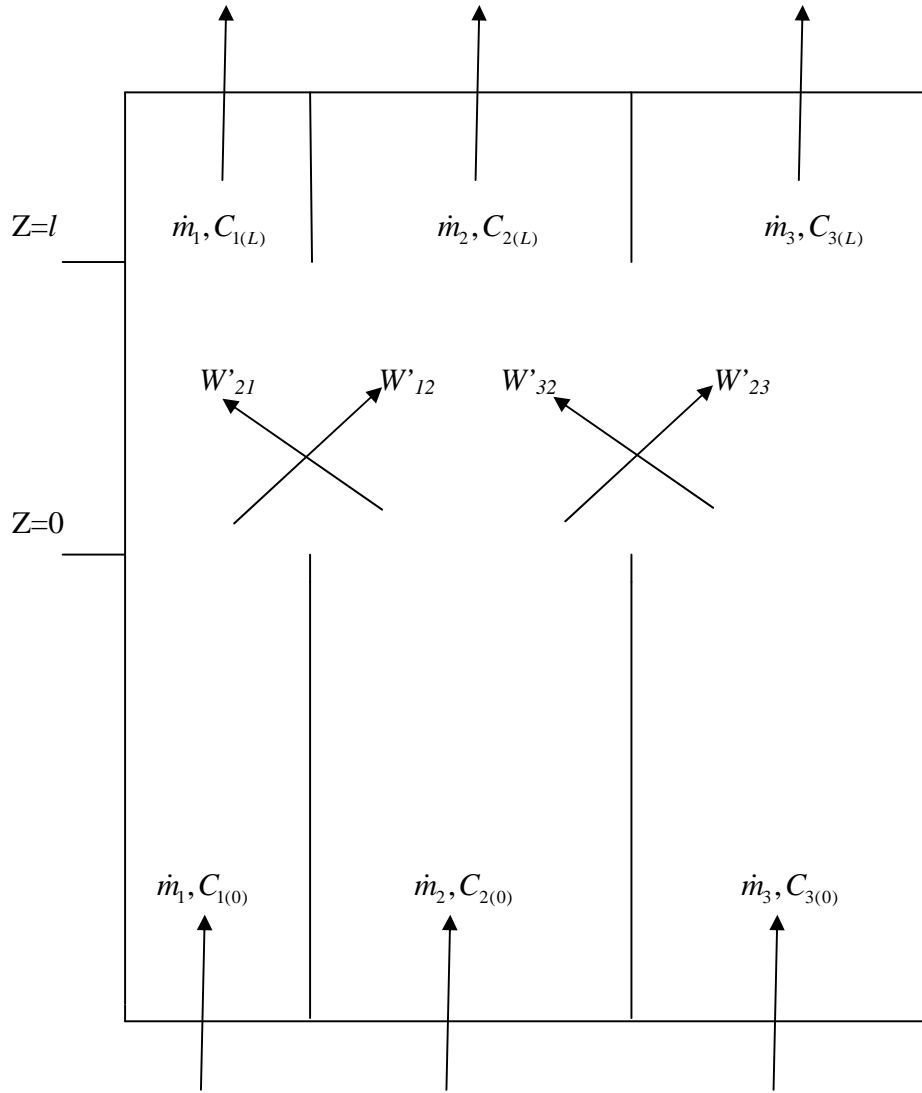


Fig 2.2 Mixing flow diagram

Consider a tracer mass balance, the equation are as follows

$$\frac{dC_1}{dZ} = -\frac{W'_{12}}{\dot{m}_1} (C_{1(z)} - C_{2(z)}) \quad (2.8)$$

$$\frac{dC_2}{dZ} = -\frac{W'_{21}}{\dot{m}_2} (C_{2(z)} - C_{1(z)}) - \frac{W'_{23}}{\dot{m}_2} (C_{2(z)} - C_{3(z)}) \quad (2.9)$$

$$\frac{dC_3}{dZ} = -\frac{W'_{32}}{\dot{m}_3} (C_{3(z)} - C_{2(z)}) \quad (2.10)$$

In turbulent mixing phenomena, there is neither mass transfer nor volume transfer between the subchannels. Hence  $W'_{12} = W'_{21}$  and  $W'_{32} = W'_{23}$

Simplifying eq. (2.8), (2.9) and (2.10), we get the equation is as follows

$$\frac{dC_2}{dZ} = -\frac{\dot{m}_1}{\dot{m}_2} \left( \frac{dC_1}{dZ} \right) - \frac{\dot{m}_3}{\dot{m}_2} \left( \frac{dC_3}{dZ} \right) \quad (2.11)$$

The equation (2.11) can be written mathematically as follows

$$dC_{2(z)} = -a_1 dC_{1(z)} - a_2 dC_{3(z)} \quad (2.12)$$

Where  $a_1 = \frac{\dot{m}_1}{\dot{m}_2}$  and  $a_2 = \frac{\dot{m}_3}{\dot{m}_2}$ . Since change in concentration  $C_1$  and  $C_3$  are independent.

Therefore we can simplify equation (2.12) is as follows.

$$\frac{\partial C_{2(z)}}{\partial C_{1(z)}} = -a_1 \text{ and } \frac{\partial C_{2(z)}}{\partial C_{3(z)}} = -a_2 \quad (2.13)$$

$$\frac{\partial C_{3(z)}}{\partial C_{1(z)}} = \frac{a_1}{a_2} \quad (2.14)$$

On integrating above equation (2.14), we get equation is as follows

$$C_{3(z)} = \frac{a_1}{a_2} C_{1(z)} + C^* \quad (2.15)$$

The initial condition for untraced subchannels as follows

$$\text{At } Z = 0, C_{1(z=0)} = C_{3(z=0)} = 0$$

$$\therefore C_{3(z)} = \frac{a_1}{a_2} C_{1(z)} \quad (2.16)$$

$$\text{or } C_{3(z)} = \frac{\dot{m}_1}{\dot{m}_3} C_{1(z)} \quad (2.17)$$

For subchannel 1-2:

$$\frac{dC_1}{dZ} = -\frac{W'_{12}}{\dot{m}_1} (C_{1(z)} - C_{2(z)}) \quad (2.18)$$

$$\frac{dC_2}{dZ} = -\frac{W'_{21}}{\dot{m}_2} (C_{2(z)} - C_{1(z)}) - \frac{W'_{23}}{\dot{m}_2} (C_{2(z)} - C_{3(z)}) \quad (2.19)$$

For three subchannels case, the equation can be written as follows

$$\dot{m}_2 C_{2(z)} = \dot{m}_2 C_{2(0)} - \dot{m}_1 C_{1(z)} - \dot{m}_3 C_{3(z)} \quad (2.20)$$

Using eq. (2.17), substitute value of  $C_{3(z)}$  in terms of  $C_{1(z)}$  in eq. (2.20), we get equation is as follows

$$C_{2(z)} = C_{2(0)} - \frac{\dot{m}_1}{\dot{m}_2} C_{1(z)} - \frac{\dot{m}_1}{\dot{m}_2} C_{1(z)} \quad (2.21)$$

$$C_{2(z)} = C_{2(0)} - 2 \frac{\dot{m}_1}{\dot{m}_2} C_{1(z)} \quad (2.22)$$

Substituting eq. (2.22) in eq. (2.18), we get equation is as follows

$$\frac{dC_{1,z}}{dZ} = -\frac{W'_{12}}{\dot{m}_1} \left[ C_{1,z} - \left( C_{2(0)} - 2 \frac{\dot{m}_1}{\dot{m}_2} C_{1(z)} \right) \right] \quad (2.23)$$

$$\frac{dC_{1,z}}{dZ} = -\frac{W'_{12}}{\dot{m}_1} \left[ C_{1,z} - C_{2(0)} + 2 \frac{\dot{m}_1}{\dot{m}_2} C_{1(z)} \right] \quad (2.24)$$

$$\frac{dC_1}{dZ} = -W'_{12} \left( C_{1,z} \left( \frac{1}{\dot{m}_1} + \frac{2}{\dot{m}_2} \right) - C_{2(0)} \right) \quad (2.25)$$

$$C_{1(z)} = \frac{C_{2(0)}}{2} + \frac{k}{2} \exp \left[ - \left( \frac{1}{\dot{m}_1} + \frac{2}{\dot{m}_2} \right) W'_{12} Z \right] \quad (2.26)$$

The initial condition for untraced subchannel no. 1 as follows

$$\text{At } Z = 0, C_{1(z=0)} = C_{3(z=0)} = 0$$

$$C_{1(z)} = \frac{C_0}{2} - \frac{C_0}{2} \exp \left[ - \left( \frac{1}{\dot{m}_1} + \frac{2}{\dot{m}_2} \right) W'_{12} Z \right] \quad (2.27)$$

$$C_{1(z)} = \frac{C_0}{2} \left[ 1 - \exp \left[ - \left( \frac{1}{\dot{m}_1} + \frac{2}{\dot{m}_2} \right) W'_{12} Z \right] \right] \quad (2.28)$$

$$\frac{2C_{1(z)}}{C_0} = \left[ 1 - \exp \left[ - \left( \frac{1}{\dot{m}_1} + \frac{2}{\dot{m}_2} \right) W'_{12} Z \right] \right] \quad (2.29)$$

$$1 - \frac{2C_{1(z)}}{C_0} = \exp \left[ - \left( \frac{1}{\dot{m}_1} + \frac{2}{\dot{m}_2} \right) W'_{12} Z \right] \quad (2.30)$$

$$\ln \left( 1 - \frac{2C_{1(z)}}{C_0} \right) = \left[ - \left( \frac{1}{\dot{m}_1} + \frac{2}{\dot{m}_2} \right) W'_{12} Z \right] \quad (2.31)$$

On rearranging eq. (2.31), the equation for turbulent mixing rate between subchannel 1-2 obtained as follows

$$W'_{12} = -\frac{1}{\left(\frac{1}{\dot{m}_1} + \frac{2}{\dot{m}_2}\right)Z} \ln\left(1 - \frac{2C_{1(z)}}{C_0}\right) \quad (2.32)$$

Similarly for subchannel 3-2:

The equation for turbulent mixing rate between subchannel 3-2 is as follows

$$W'_{32} = -\frac{1}{\left(\frac{1}{\dot{m}_3} + \frac{2}{\dot{m}_2}\right)Z} \ln\left(1 - \frac{2C_{3(z)}}{C_0}\right) \quad (2.33)$$

#### 2.4.1 Selection of tracer

As per literature review, it is suggested that methane and potassium nitrate are good tracers for estimating turbulent mixing rate because of following reasons:

- (1) Measurability: The requirement of experiment is such that tracer concentration is so small so that it has negligible effect on physical properties on working fluid. Both can be detected at very low ppm about 1 ppm as compared to other tracer.
- (2) Non- reactivity: Both the tracer does not react chemically or physically with each other or with any part of system under study.

(3) Safety: The presence of tracer does not pose hazard to people, material or activity in and out around the test area, which are as follows.

1. We are using Methane + balance Nitrogen canister 0.05% (by volume). This is well below LFL and UFL (a LFL of 5% (by volume) and UFL of 15% (by volume)). It means if the atmosphere has less than 5% methane, an explosion cannot occur even if a source of ignition is present

2. According to dental care safe limit of potassium nitrate in tooth paste is 5 % and we are using potassium nitrate diluted in water which has 0.01% and it will again reduce to 0.001 % when it mixes with flowing water and then it goes to drain completely.

## **2.5 Closure**

In this chapter, scaling methodology for experimental test facility has been presented. An experimental flow conditions to simulate flow patterns for turbulent mixing, void drift and diversion cross flow in AHWR rod bundle has been presented. In addition to this, mathematical equation for turbulent mixing rate is derived using tracer conservation equations.

## CHAPTER 3

# *EXPERIMENTAL TEST FACILITY AND EXPERIMENTAL PROCEDURE*

---

---

### **3.1 Introduction**

This chapter provides detailed description of experimental test facility and associated equipment used to investigate turbulent mixing, void drift and diversion cross flow in simulated subchannels of AHWR rod bundle. It also gives detailed description of experimental procedure for each component of inter-subchannel mixing phenomena i.e. turbulent mixing, void drift and diversion cross flow that are pertinent to the results presented in chapters 4, 5, 6 and 7.

### **3.2 Experimental Test Facility**

The air-water loop and associated equipment used in this study were located in the Reactor Engineering Division, Bhabha Atomic Research Centre, Mumbai, India. The loop was designed and built for inter-subchannel mixing experiments employing air-water flows. The facility has already been installed in order to determine turbulent mixing rate, void drift and diversion cross flow in a simulated subchannels of AHWR fuel bundle

(1/12<sup>th</sup> segment) which contain two half and three full rod. This segment is divided three subchannels as shown in Figure 3.1.

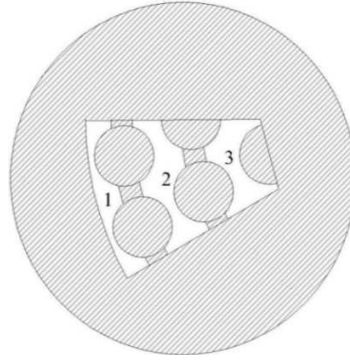


**Fig 3.1** AHWR fuel rod bundle (1/12<sup>th</sup> segment)

The facility consists of a test section along with air-water mixer and separator, which is shown Figure 3.2. There are six rotameters, used to measure air flow rate, six rotameters are used to measure water flow rate and two rotameters are used to measure tracer flow rate. There are four Differential pressure transducers (DPT), used to measure radial pressure difference between subchannels.

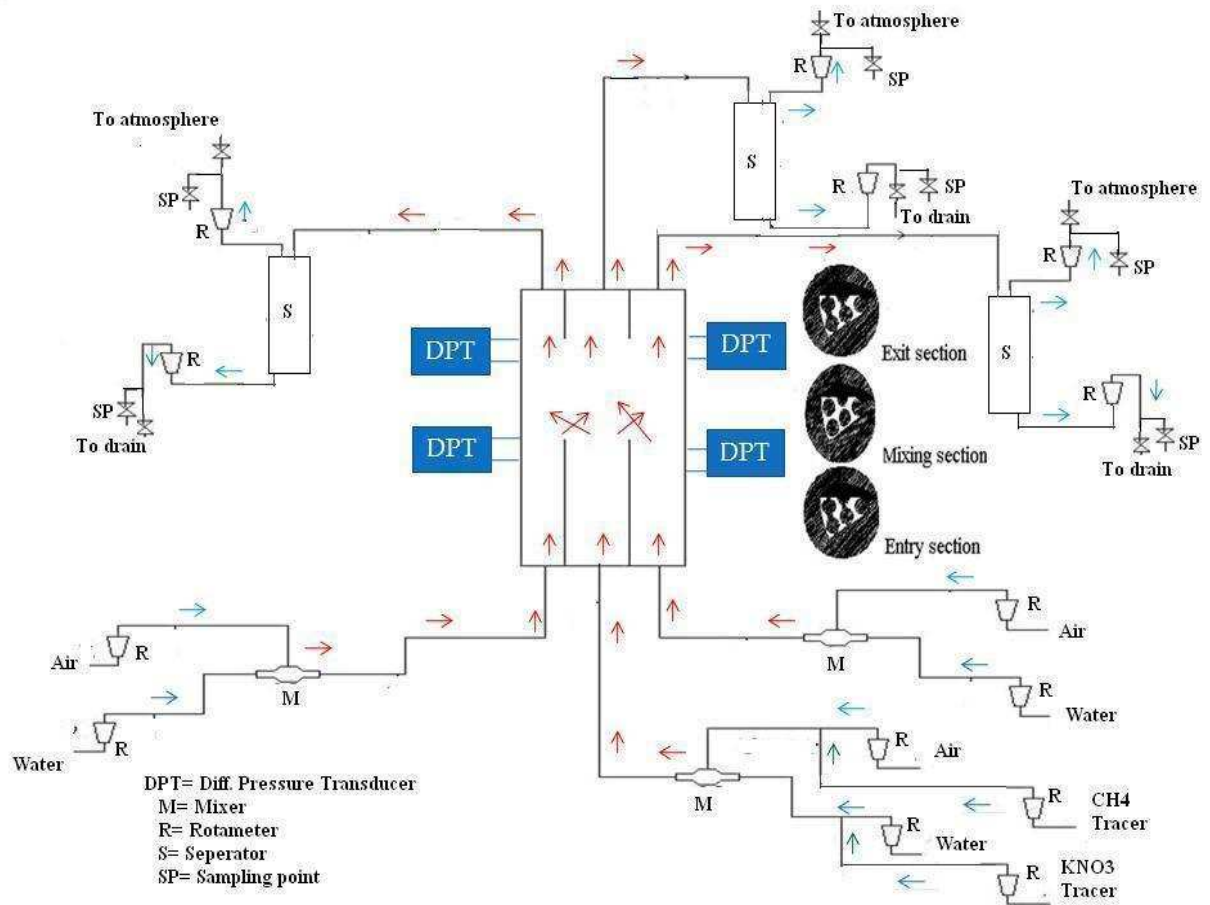


**Fig. 3.2** Test rig schematic

Air from air service line splits into three separate streams and metered separately using matched rotameters. Similarly water from water service line also splits into three separate streams and metered separately using matched rotameters. The air-water mixture flows from mixer, in which measured air passes through holes of tube and mixes with metered water to develop two phase flow. This mixture, then passes through the test section and finally to the separator where air and water, gets separated due to density difference. The air moving upward vents to atmosphere and water flows down to drain through respective rotameters.

### 3.2.1 Test section

The test section is shown in Fig 3.3.

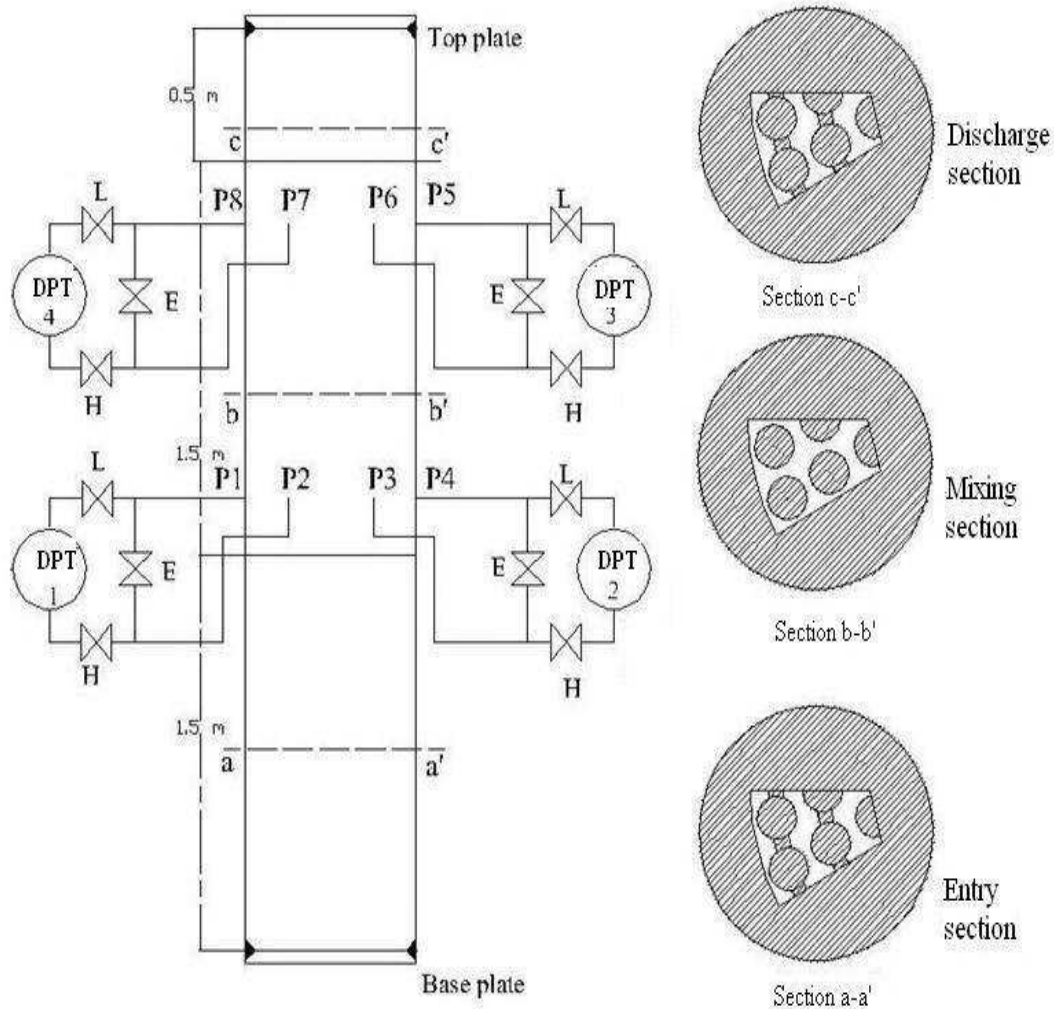


**Fig 3.3** Schematic of test section

The vertical test channel of 3.5 m long is divided into three sections; entry section (1.5 m), mixing section (1.5 m) and discharge section (0.5 m) from bottom to the top of channel. In entry section and exit section, subchannels are completely separated by a 4 mm partition and in mixing section; subchannels are completely free from partition to allow mixing between subchannels. This test section is made of SS316 material, 65 mm

OD size. The length of entry, mixing and exit section is chosen according to literature (Walton (1969), Rudzinski (1970), Singh K.S. (1972), Kawahara et al. (1997 (b)), Sadatomi et al. (2004), Kawahara et al. (2006)) such that entry length should be enough for flow to be developed along the axis; mixing length should be enough to accommodate mixing between subchannels and exit section should be enough for separation of flow. The fully developed flow in each subchannel is achieved by keeping the entry length more than 127 times hydraulic diameter (Walton (1969)). According to Peterniuk (1968), the mixing length should be more than 13 times hydraulic diameter to avoid any entrance effect. The entry and mixing length used here is more than 330 times hydraulic diameter. These lengths are considered to be sufficient in respect of fully developed flow and entrance effect

### **3.2.2 Mixer**

The air-water mixture is shown in Figure 3.4.

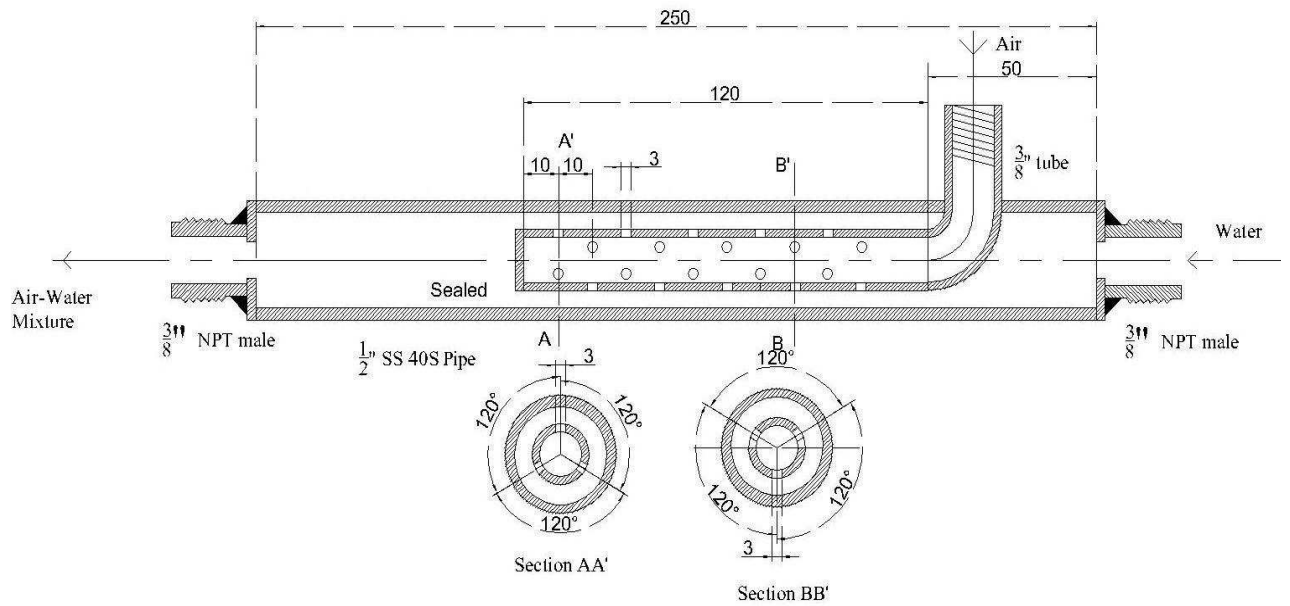


**Fig 3.4** Schematic of mixer.

The air-water mixer consists of 1/2" pipe of 250 mm length and 3/8" tube of 120 mm length having holes of diameter 3 mm. The measured air passes through 3mm holes in 3/8" tube, mixes with metered water which flows through 1/2" pipe to develop the two phase flow.

### 3.2.3 Separator

The air-water separator is shown in Figure. 3.5

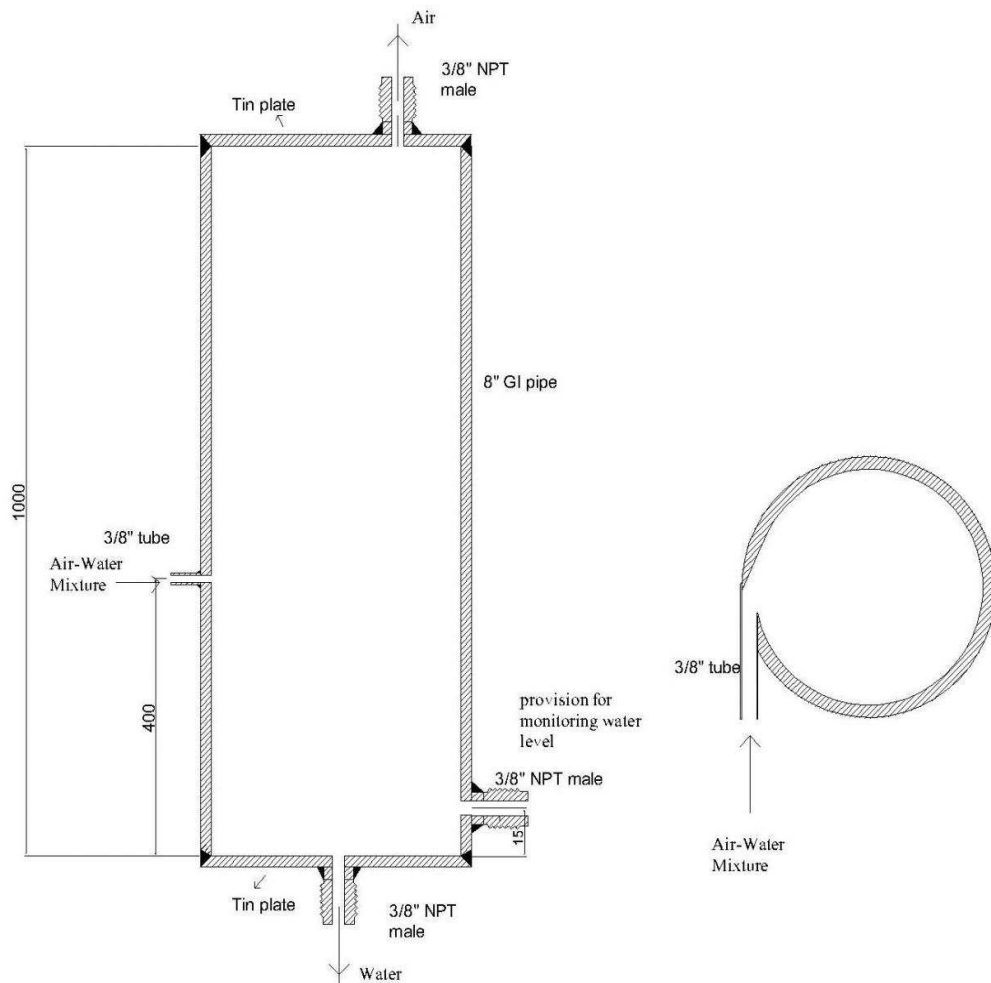


**Fig 3.5** Schematic of separator

The air-water separator consists of 8” GI pipe of 1000 mm length and having 3/8” tube. The air-water mixture flows tangentially through 3/8” tube from the outlet of subchannel to the separator where air and water get separated due to density difference. The air moves upward and vents to atmosphere and water flows down to drain by gravity and measured through respective rotameters.

### **3.2.4 Tubes and fitting.**

The test facility consists of tubes of size 3/8" OD and is made of SS-316. Fittings like union, Tee and NPT compression type fitting are used for piping connections, designed for pressure of 200 bar and temperature of 100 deg C.

### **3.2.5 Needle valve**

Needle valves used in facility are of size 3/8" tube end connection. The body material of needle valve is SS316 with nut and ferrule, designed for pressure of 40 bar and temperature of 100 deg C.

### **3.2.6 Rotameter**

The flow rate of water is measured by rotameter in the range 0 to 20 lpm. This can withstand pressure of 15 bar. The flow rate of air is measured by rotameter having range 0 to 10 lpm. This can withstand pressure of 10 bar. The flow rate of methane gas tracer is measured by rotameter having range 0 to 0.1 lpm. This can withstand pressure of 10 bar. The flow rate of potassium nitrate is measured by rotameter having range of 0 to 0.6 lpm. This can withstand pressure of 15 bar.

## **3.3 Measurement of experimental variable**

### **(i) Air flow**

The inlet air flow is measured using rotameter installed after PRV at the inlet air line before air-water mixer. The air flow is measured in three lines. The flow range is 0-10 lpm and the outlet air flow is measured using rotameter installed at the outlet air line after

air-water separator. The air flow is measured in three lines. The flow range is 0-10 lpm. The accuracy of air rotameter is  $\pm 1\%$  over the full span of 10 lpm.

**(ii) Water flow**

The inlet water flow is measured using rotameter installed at the inlet water line before air-water mixer. The inlet water flow is measured in three lines. The flow range is 0-20 lpm and the outlet water flow is measured using rotameter installed at the outlet water line after air-water separator. The water flow is measured in three lines. The flow range is 0-20 lpm. The accuracy of water rotameter is  $\pm 2\%$  over the full span of 20 lpm

**(iii) Tracer flow**

The methane tracer is added to individual subchannel by mixing with air lines through the tracer line addition system. The inlet methane flow rate is measured with rotameter. The flow range of rotameter is 0-1 lpm. The accuracy of methane gas tracer rotameter is  $\pm 1\%$  over the full span of 1 lpm

The potassium nitrate tracer is added to individual subchannel by mixing with water lines through the tracer line addition system. The potassium nitrate flow rate is measured with rotameter. The flow range of rotameter is 0-0.6 lpm. The accuracy of potassium nitrate tracer rotameter is  $\pm 2\%$  over the full span of 0.6 lpm

**(iv) Radial pressure measurement**

Four differential pressure transmitters (DPT 1 to DPT 4) are provided to measure radial pressure difference between the subchannels shown in Figure 3.6.

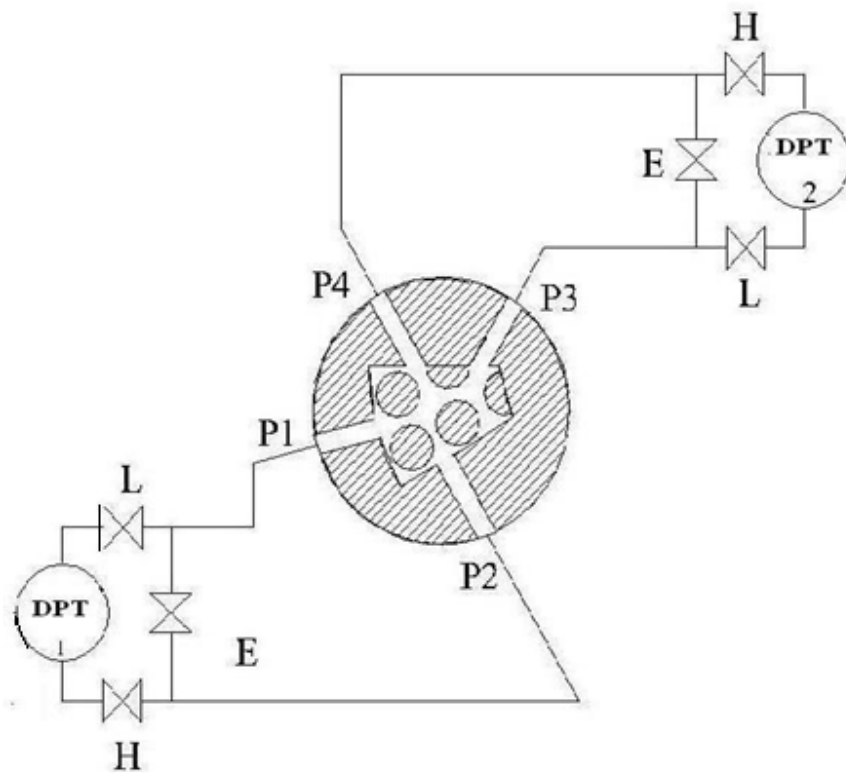


**Fig 3.6** Radial pressure difference measurement of subchannels

The radial pressure drop between subchannels is measured with the help of smart differential pressure transmitters. The range of measurement is -300 to 300 mm WC. All these transmitters output (4-20 mA) are connected to recorder. The process variable data are displayed on the monitor as well as stored in the hard disc of recorder for further analysis and hard copy generation. The radial pressure drop has to be maintained at 0 mm by adjusting inlet air and water flows to obtain proper turbulent mixing during experimentation.

**(v) Tracer concentration measurement**

To study the mixing behavior, tracers like potassium nitrate and methane are added with water and air respectively. The concentration of methane tracer for air of 515 ppm and balance is nitrogen and dil. potassium nitrate tracer for water which has concentration of 100 ppm and rest is water.

It may be noted that the percentage of nitrogen in air 78 %. We are using Methane + balance Nitrogen canister 0.05% (by volume) which is just like air. Hence there is no relative velocity between tracer and air. Similarly, we are using potassium nitrate diluted in water which has 0.01% (by mass) which is just like water. Hence there is no relative velocity between tracer and water

The samples of tracers are collected from different sample collection points. The tracer concentration of potassium nitrate and methane is measured by offline lab analysis using spectrophotometer and gas chromatograph respectively. The spectrophotometer and gas chromatograph are calibrated to  $\pm 1\%$ . The inlet flow rates of tracers are measured with rotameters.

**3.4 Experimental procedure for inter-subchannel mixing phenomena.**

**(i) Single phase turbulent mixing**

Single phase water was introduced into all three subchannels. Potassium nitrate tracer is added to subchannel 2 by tracer line injection system. The tracer is mixed with water before entering to the inlet of subchannel. The radial pressure difference across these three subchannels is minimized by controlling the opening of respective valve in discharge line. At outlet of the discharge section, samples from respective subchannel lines were extracted. The concentration of tracer in each subchannel was obtained by

analysis through an absorption spectrophotometer. For each test, the experiments were repeated three times and error found among them was within  $\pm 2\%$ . The turbulent mixing rate was determined by solving tracer conservation equation. The detailed mathematical steps involved in the process are shown chapter 2. The experimental test matrix for single phase turbulent mixing is given in Table 3.1.

**Table 3.1** Experimental test matrix for single phase turbulent mixing

| S. No | Velocity in subchannel 3<br>m/s | Velocity in subchannel 2<br>m/s | Velocity in subchannel 1<br>m/s |
|-------|---------------------------------|---------------------------------|---------------------------------|
| 1     | 0.39                            | 0.33                            | 0.44                            |
| 2     | 0.49                            | 0.42                            | 0.57                            |
| 3     | 0.58                            | 0.47                            | 0.62                            |
| 4     | 0.60                            | 0.50                            | 0.65                            |
| 5     | 0.63                            | 0.53                            | 0.70                            |
| 6     | 0.68                            | 0.56                            | 0.75                            |
| 7     | 0.76                            | 0.65                            | 0.84                            |
| 8     | 0.8                             | 0.67                            | 0.88                            |
| 9     | 0.95                            | 0.78                            | 1.02                            |
| 10    | 1.05                            | 0.88                            | 1.20                            |
| 11    | 1.16                            | 0.96                            | 1.33                            |
| 12    | 1.33                            | 1.10                            | 1.47                            |

**(ii) Two phase turbulent mixing**

Two phase air-water mixture was introduced into all three subchannels. A tracer is added to subchannel 2 by tracer line injection system. Potassium nitrate used as a tracer for water and methane gas is used as a tracer for air. The tracer is mixed with fluid before entering to the inlet of subchannel. The radial pressure difference across these three subchannels is minimized by controlling the opening of respective valve in air discharge line which is connected with three separators. At outlet of the separator, samples from respective subchannel lines were extracted. The concentration of tracer in each subchannel was obtained by analysis through an absorption spectrophotometer. For each test, the experiments were repeated three times and error found among them was within  $\pm 3\%$ . The turbulent mixing rate was determined by solving tracer conservation equation shown in chapter 2.

The experimental test matrix for two phase turbulent mixing is given in Table 3.2

**Table 3.2** Experimental test matrix for two phase turbulent mixing.

| S. no | Superficial Liquid velocity<br>$J_l$ in sub 3 | Superficial gas velocity<br>$J_g$ in sub 3 | Superficial Liquid velocity<br>$J_l$ in sub 2 | Superficial gas velocity<br>$J_g$ in sub 2 | Superficial Liquid velocity<br>$J_l$ in sub 1 | Superficial gas velocity<br>$J_g$ in sub 1 |
|-------|---|--|---|--|---|--|
| 1     | 0.13  | 0.63 to 1.06                               | 0.10  | 0.73 to 1.38                               | 0.14  | 0.66 to 1.14                               |
| 2     | 0.19  | 0.63 to 1.16                               | 0.15  | 0.73 to 1.22                               | 0.20  | 0.66 to 1.26                               |
| 3     | 0.27  | 0.01 to 0.64                               | 0.21  | 0.01 to 0.69                               | 0.28  | 0.01 to 0.64                               |
| 4     | 0.32  | 0.01 to 0.64                               | 0.25  | 0.01 to 0.69                               | 0.33  | 0.01 to 0.64                               |

|   |      |              |      |              |      |              |
|---|------|--------------|------|--------------|------|--------------|
| 5 | 0.34 | 0.01 to 0.64 | 0.28 | 0.01 to 0.69 | 0.36 | 0.01 to 0.64 |
| 6 | 0.41 | 0.01 to 0.44 | 0.32 | 0.01 to 0.49 | 0.43 | 0.01 to 0.44 |
| 7 | 0.47 | 0.01 to 0.20 | 0.37 | 0.01 to 0.23 | 0.49 | 0.01 to 0.20 |

**(iii) Void drift**

The necessary condition for void drift to occur is that, at both the inlet and the outlet ends of the mixing section, the time-averaged radial pressures difference between subchannels has to be zero i.e.  $\Delta P_{1-2} = \Delta P_{3-2} = 0$ . The measured inlet water and air flow rate from respective subchannel line passes through mixer to form two phase flow. This two phase air-water mixture was introduced into all three subchannels such that difference in radial pressure between the subchannels is minimum. This was achieved by throttling the air discharge line valve after the air-water separator. Under this condition, flow rate of each phase at outlet of the separators were again measured through respective subchannel lines rotameters. The experiments were repeated three times and error found was within  $\pm 1\%$ . This difference in flow rate at inlet (non-equilibrium flow) and outlet (equilibrium flow) of individual subchannel of test section gives net change in flow rate due to void drift. The experimental test matrix for void drift is given in Table 3.3

**Table 3.3** Experimental test matrix for void drift

| S. no | Superficial Liquid velocity<br>$J_l$ in sub 3 | Superficial gas velocity<br>$J_g$ in sub 3 | Superficial Liquid velocity<br>$J_l$ in sub 2 | Superficial gas velocity<br>$J_g$ in sub 2 | Superficial Liquid velocity<br>$J_l$ in sub 1 | Superficial gas velocity<br>$J_g$ in sub 1 |
|-------|---|--|---|--|---|--|
| 1     | 0.12  | 0.73 to 1.32                               | 0.11  | 0.58 to 1.02                               | 0.13  | 0.77 to 1.38                               |
| 2     | 0.19  | 0.73 to 1.32                               | 0.16  | 0.58 to 1.02                               | 0.19  | 0.77 to 1.38                               |
| 3     | 0.26  | 0.07 to 0.71                               | 0.22  | 0.06 to 0.56                               | 0.26  | 0.08 to 0.75                               |
| 4     | 0.34  | 0.07 to 0.71                               | 0.29  | 0.06 to 0.56                               | 0.35  | 0.08 to 0.75                               |
| 5     | 0.40  | 0.23 to 0.71                               | 0.34  | 0.18 to 0.56                               | 0.42  | 0.25 to 0.75                               |
| 6     | 0.46  | 0.08 to 0.14                               | 0.38  | 0.06 to 0.11                               | 0.48  | 0.08 to 0.15                               |

**(iv) Single phase diversion cross flow**

The necessary condition for diversion cross flow to occur is that, at the inlet of the mixing section, the time-averaged radial pressures difference between the subchannels is not zero i.e.  $\Delta P_{1-2} = \Delta P_{3-2} \neq 0$ . The measured inlet water flow rate was introduced into all three subchannels such that difference in radial pressure between the subchannels should exist. Under this condition, flow rate of each phase at outlet of the separators were again measured through respective subchannel lines rotameters. The experiments were repeated three times and error found was within  $\pm 1$  %. This difference in flow rate at inlet and outlet of individual subchannel of test section will give net change in flow rate due to

diversion cross flow. The experimental test matrix for single phase diversion cross flow is given in Table 3.4.

**Table 3.4** Experimental test matrix for single phase diversion cross flow

| S. no | Velocity in subchannel 3<br>m/s | Velocity in subchannel 2<br>m/s | Velocity in subchannel 1<br>m/s |
|-------|---------------------------------|---------------------------------|---------------------------------|
| 1     | 0.08                            | 0.18                            | 0.09                            |
| 2     | 0.11                            | 0.26                            | 0.12                            |
| 3     | 0.16                            | 0.36                            | 0.17                            |
| 4     | 0.2                             | 0.47                            | 0.22                            |
| 5     | 0.28                            | 0.64                            | 0.3                             |
| 6     | 0.38                            | 0.87                            | 0.42                            |
| 7     | 0.47                            | 1.1                             | 0.52                            |

**(v) Two phase diversion cross flow**

The measured inlet water and air flow rate from respective subchannel line passes through mixer to form two phase flow. This two phase air-water mixture was introduced into all three subchannels such that difference in radial pressure between subchannel should exist. Under this condition, flow rate of each phase at outlet of the separators were again measured through respective subchannel lines rotameters. The experiments repeated three times and error found was within  $\pm 1\%$ . This difference in flow rate at inlet and outlet of individual subchannel of test section gives net change in flow rate due

to diversion cross flow. The experimental test matrix for two phase diversion cross flow is given in Table 3.5

**Table 3.5** Experimental test matrix for two phase diversion cross flow

| S. no | Superficial<br>Liquid<br>velocity<br>$J_l$ in sub 3 | Superficial<br>gas<br>velocity<br>$J_g$ in sub 3 | Superficial<br>Liquid<br>velocity<br>$J_l$ in sub 2 | Superficial<br>gas<br>velocity<br>$J_g$ in sub 2 | Superficial<br>Liquid<br>velocity<br>$J_l$ in sub 1 | Superficial<br>gas<br>velocity<br>$J_g$ in sub 1 |
|-------|---|--|---|--|---|--|
| 1     | 0.08  | 0.44 to 0.78                                     | 0.17  | 1.00 to 1.8                                      | 0.09  | 0.48 to 0.86                                     |
| 2     | 0.11  | 0.44 to 0.78                                     | 0.26  | 1.00 to 1.8                                      | 0.12  | 0.48 to 0.86                                     |
| 3     | 0.16  | 0.04 to 0.40                                     | 0.36  | 0.10 to 0.97                                     | 0.17  | 0.05 to 0.48                                     |
| 4     | 0.20  | 0.04 to 0.40                                     | 0.47  | 0.10 to 0.97                                     | 0.22  | 0.05 to 0.48                                     |
| 5     | 0.27  | 0.04 to 0.40                                     | 0.64  | 0.10 to 0.97                                     | 0.30  | 0.05 to 0.48                                     |

### 3.5 Closure

This chapter gives detailed description of test loop and associated equipment like test section, air-water mixer and air-water separator. A detailed experimental procedure has been given for turbulent mixing, void drift and diversion cross flow in AHWR rod bundle. The parameter variations for inter-subchannel mixing phenomena are based on experimental flow condition and are according to existing literature as discussed in chapter 1.

## CHAPTER 4

### *STUDY OF SINGLE PHASE TURBULENT MIXING RATE IN AHWR ROD BUNDLE*

---

---

#### **4.1 Introduction**

In this chapter, results of single phase turbulent mixing rate for AHWR rod bundle are discussed. For determination of turbulent mixing rate in single phase flow condition, water was introduced into all three subchannels. A potassium nitrate tracer is added to subchannel 2 (refer fig 2.1) by tracer line injection system. The tracer is mixed with water before entering to the inlet of subchannel. The radial pressure difference across these three subchannels is minimized by controlling the opening of respective valve in discharge line. At outlet of the discharge section, samples from respective subchannel lines were extracted. The concentration of tracer in each subchannel was obtained by analysis through an absorption spectrophotometer. The single phase turbulent mixing rate was calculated by substituting tracer concentration at inlet and outlet of subchannels in equation derived mathematically in section 2.3 which are as follows.

$$W'_{12} = -\frac{1}{\left(\frac{1}{\dot{m}_1} + \frac{2}{\dot{m}_2}\right)Z} \ln\left(1 - \frac{2C_{1(z)}}{C_0}\right) \quad (4.1)$$

$$W'_{32} = -\frac{1}{\left(\frac{1}{\dot{m}_3} + \frac{2}{\dot{m}_2}\right)Z} \ln\left(1 - \frac{2C_{3(z)}}{C_0}\right) \quad (4.2)$$

In addition to above, an assessment of existing models against measured turbulent mixing rate has been carried out and a new model for single phase turbulent mixing rate applicable to AHWR has been presented

#### 4.2 Experiments conducted

Experiments were carried out to determine single phase turbulent mixing rate among the subchannels of AHWR rod bundle. The single phase turbulent mixing rate is measured for different liquid flow rate ranging from 0 to 0.12 kg/s corresponding mean liquid velocity 0 to 1.2 m/s. These velocities are same as that in actual reactor. The liquid flow rate of each subchannels was measured by respective rotameter. Table 4.1 shows the experimental test matrix for single phase turbulent mixing rate

**Table 4.1** Experimental test matrix for single phase turbulent mixing

| S. No | Velocity in subchannel 3<br>m/s | Velocity in subchannel 2<br>m/s | Velocity in subchannel 1<br>m/s |
|-------|---------------------------------|---------------------------------|---------------------------------|
| 1     | 0.39                            | 0.33                            | 0.44                            |
| 2     | 0.49                            | 0.42                            | 0.57                            |
| 3     | 0.58                            | 0.47                            | 0.62                            |
| 4     | 0.60                            | 0.50                            | 0.65                            |
| 5     | 0.63                            | 0.53                            | 0.70                            |
| 6     | 0.68                            | 0.56                            | 0.75                            |

|    |      |      |      |
|----|------|------|------|
| 7  | 0.76 | 0.65 | 0.84 |
| 8  | 0.8  | 0.67 | 0.88 |
| 9  | 0.95 | 0.78 | 1.02 |
| 10 | 1.05 | 0.88 | 1.20 |
| 11 | 1.16 | 0.96 | 1.33 |
| 12 | 1.33 | 1.10 | 1.47 |

A potassium nitrate tracer having concentration of 100 ppm is added to water flowing in subchannel 2. After mixing of tracer with water, the samples of respective subchannels were extracted at inlet and outlet of the test section. The concentration of tracer in each subchannel at inlet and outlet of test section was obtained by analysis through an absorption spectrophotometer. For each test, the experiments were repeated three times and error found among them was within  $\pm 2\%$ .

The single phase turbulent mixing rate for subchannel 1-2 (i.e.  $W'_{12}$ ) and subchannel 3-2 (i.e.  $W'_{32}$ ) was calculated by using equations (4.1) and (4.2) respectively with the mass flow rate of respective subchannels, mixing length (i.e.  $Z = 1.5$  m) and tracer concentrations at inlet and outlet of subchannels.

The Reynolds number for each subchannel was calculated by substituting liquid velocity of respective subchannels (refer Table 4.1.) in equation as follows

$$\text{Re} = \frac{\rho \times V \times D_h}{\mu} \quad (4.3)$$

### 4.3 Results and discussion

The single phase turbulent mixing rate for subchannel 1-2 (i.e.  $W'_{12}$ ) and subchannel 3-2 (i.e.  $W'_{32}$ ) is measured by varying mean liquid velocity 0 to 1.2 m/s. The corresponding average Reynolds number was varied from 0 to 6425.

It may be noted that during cold start-up condition, the flow remains in single phase condition at 70 bar and 285 °C, then transition takes place from single phase to two phase flow condition in reactor rod bundle with increase in power. In cold start-up condition, the mass flow rate in the rod bundle is close to 1 kg/s at 2 % of full power. So if we consider three subchannels in 1/12 segment, correspondingly range of average Reynolds number in the subchannels of reactor rod bundle varies 0 to 6500. In the present experiment, Reynolds number in single phase flow varies 0 to 6424. The flow conditions were closer to the actual reactor condition during start-up condition. In addition, AHWR being a natural circulation BWR, the mass flux condition in the subchannels can vary from close to zero to rated condition depending on the power. Hence flow starts laminar to transition and transition to turbulent flow.

It is well known that the laminar flow occurs in circular pipe when  $Re < 2100$  and turbulent flow occurs when  $Re > 4000$ . In between this range transition region occurs. However it is not true for rod bundle case where pitch to diameter ratio is different from circular pipe ( $p/d=1$ ). According to Kawahara (2006), Reynolds number at which the laminar-to-transition and the transition-to-turbulent occur very early in case of rod bundle. Corresponding to AHWR rod bundle ( $p/d=1.2$ ), the onset of laminar-transition occurs at  $Re=300$  and onset of turbulent-transition occurs at  $Re=1250$

The average Reynolds number for subchannel 1-2 and subchannel 3-2 is calculated by equations as follows

$$Re_{avg,12} = \frac{Re_1 + Re_2}{2} \quad (4.4 (a))$$

$$Re_{avg,32} = \frac{Re_3 + Re_2}{2} \quad (4.4 (b))$$

Figure 4.1 shows variation of measured mixing rate with average Reynolds number for subchannel 1-2 and subchannel 3-2 is given by equation (1.8).

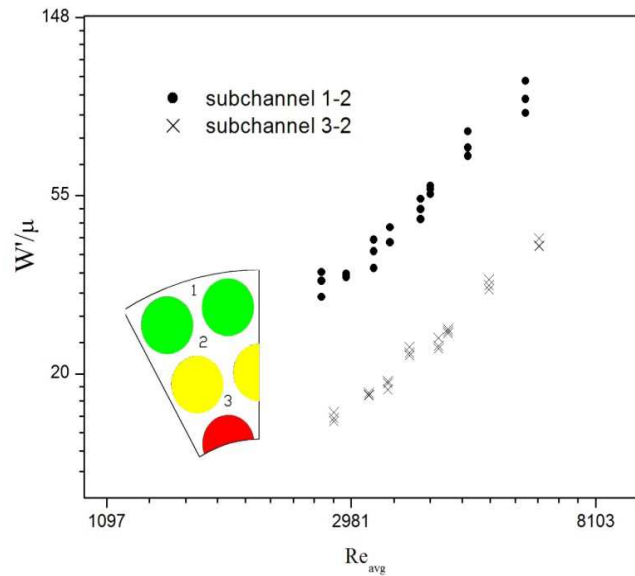


**Fig. 4.1** Comparison of  $W'/\mu$  against  $Re_{avg}$ .

The main findings are as follows

1. The turbulent mixing rate increases with increase in average Reynolds number.
2. It also indicates that the turbulent mixing rate between subchannel 1-2 i.e.  $W'_{12}$  is higher as compared to subchannel 3-2 i.e.  $W'_{32}$  because subchannel 1-2 has higher gap to centroidal ratio ( $S/\delta=0.43$ ) as compared to subchannel 3-2 ( $S/\delta=0.26$ ).

#### 4.4 Assessment of existing model to simulate single phase turbulent mixing rate

An attempt has been made to study the capability of existing models like Roger and Tahir (1975), Peterniuk (1968), Galibert and Knudsen (1971), Kelly and Todreas (1977), Rowe and Angel (1969), Rehme (1992) and Seale (1979) to predict the measured single phase turbulent mixing rate. These models have been proposed to predict single phase turbulent mixing rate.

In this section, we evaluate the turbulent mixing models against the data obtained from present experiments of single phase turbulent mixing as discussed above.

For evaluation, we have compared the measured (experimental) liquid phase turbulent mixing rate in single phase flow  $W'_{exp}$  with predicted turbulent mixing rate in single phase flow  $W'_{cal}$ . The error analysis has been done to find out maximum, minimum and average error between measured and predicted value of single phase turbulent mixing rate. The error analysis shows how predicted value by turbulent mixing models differs from measured experimental values.

The maximum and minimum error is calculated as:

$$\text{Maximum Error (+ve deviation), } E_{\max} = \max \left( \frac{W'_{cal} - W'_{exp}}{W'_{exp}} \times 100 \right) \quad (4.5)$$

$$\text{Minimum Error (-ve deviation), } E_{\min} = \min \left( \frac{W'_{cal} - W'_{exp}}{W'_{exp}} \times 100 \right) \quad (4.6)$$

The average error is calculated as

$$\text{Average Error} = \frac{\sum_{i=1}^n E_i}{n} \% \quad (4.7)$$

where n= no. of data points and

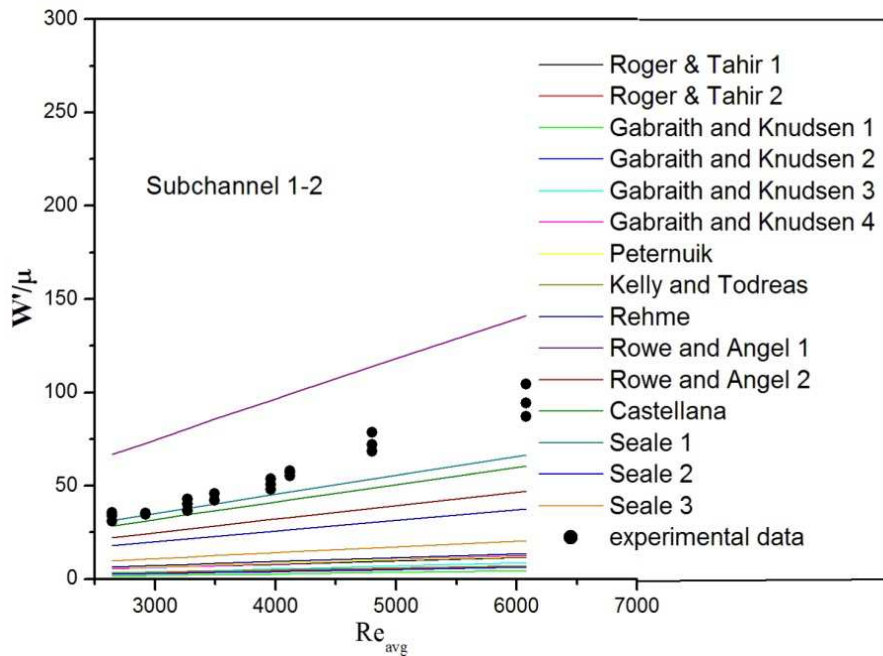
$$E_i = \left( \frac{W'_{i,cal} - W'_{i,exp}}{W'_{i,exp}} \times 100 \right) \quad (4.8)$$

The error analysis for existing correlations against present experimental data is shown in Table 4.2.

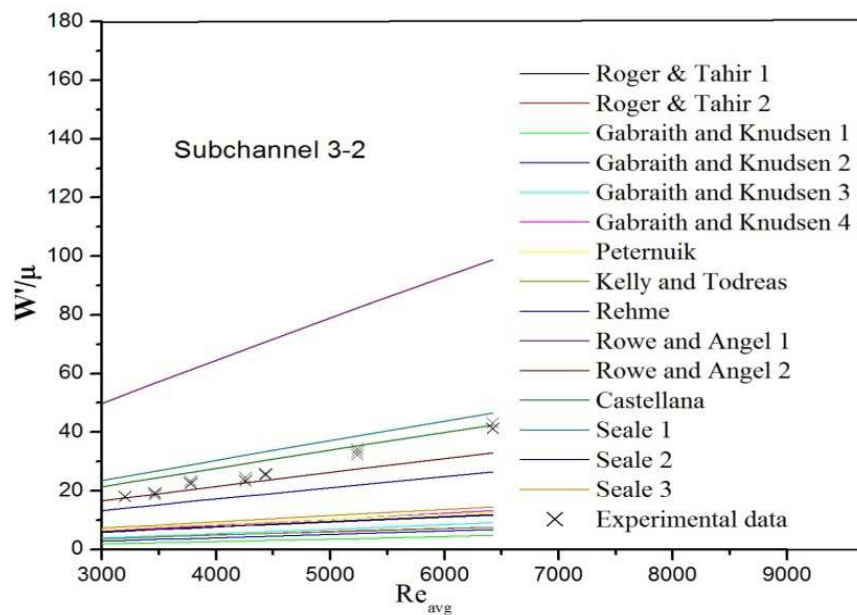
**Table 4.2** Error analysis for various correlations for single phase mixing rate

| Authors                       | $W'_{12}/\mu$ |           |               | $W'_{32}/\mu$ |           |               |
|-------------------------------|---------------|-----------|---------------|---------------|-----------|---------------|
|                               | Max Error     | Min Error | Average error | Max Error     | Min Error | Average error |
| Roger and Tahir 1 (1975)      | -65           | -83       | -77           | -24           | -64       | -59           |
| Roger and Tahir 2 (1975)      | -80           | -91       | -87           | -51           | -71       | -66           |
| Peternuik (1968)              | -64           | -82       | -75           | -19           | -59       | -43           |
| Galibert and Knudsen 1 (1971) | -86           | -95       | -92           | -69           | -89       | -81           |
| Galibert and Knudsen 2 (1971) | -81           | -92       | -88           | -56           | -83       | -73           |
| Galibert and Knudsen 3(1971)  | -74           | -90       | -84           | -41           | -77       | -63           |
| Galibert and Knudsen 4 (1971) | -62           | -84       | -76           | -15           | -63       | -44           |
| Kelly and Todreas (1977)      | -78           | -90       | -85           | -51           | -77       | -67           |
| Rowe and Angel 1(1969)        | +315          | +95       | +177          | +528          | +195      | +327          |
| Rowe and Angel 2 (1969)       | +38           | -34       | -7            | +109          | -1.5      | +42           |
| Castellana (1974)             | +78           | -16       | 19            | +169          | +26       | +83           |
| Rehme (1992)                  | -59           | -80       | -72           | -24           | -64       | -48           |
| Seale 1 (1979)                | +95           | -7        | +30           | +196          | +39       | +101          |
| Seale 2 (1979)                | +10           | -47       | -25           | +67           | -21       | +14           |
| Seale 3 (1979)                | -39           | -71       | -59           | -7            | -56       | -37           |

Figures 4.2 (a) and 4.2 (b) shows comparison of existing models with present experimental data of single phase turbulent mixing rate.



(a)



(b)

**Fig. 4.2** Comparison of existing models against present experimental data

Results show that none of these correlations are able to predict measured turbulent mixing rate in AHWR accurately. Only Castellana (1974) and Seale (1979) correlations were found to predict  $W'_{12}/\mu$  up to  $Re=4200$  with reasonable accuracy. Similarly Rowe and Angel (1969) were found predict  $W'_{32}/\mu$  up to  $Re=4500$  and Castellana (1974) correlation predicts  $W'_{32}/\mu$  up to  $Re>4500$  with reasonable accuracy. Hence these correlations are not reliable considering AHWR geometrical array.

#### 4.5 Model development

In order to develop a new model applicable for AHWR geometry, the model presented earlier in equation (1.8) was used as follows

$$N_{mix} = \frac{K}{K'} Re_{avg}^a \left( \frac{S}{\delta} \right)^b \quad (4.9)$$

where

$$N_{mix} = \frac{W'_{ij} \times D_h^2}{\mu \times A} \quad \text{and} \quad Re_{avg} = \frac{Re_i + Re_j}{2} \quad (4.10)$$

Thus liquid turbulent mixing number for single phase flow in subchannels can be expressed as

$$N_{mix} = K Re_{avg}^a \quad (4.11)$$

The coefficient  $K$  and exponent  $a$  were obtained by fitting the experimental test data plotted on dimensionless liquid mixing number against mixture Reynolds number as shown in Figure 4.3.

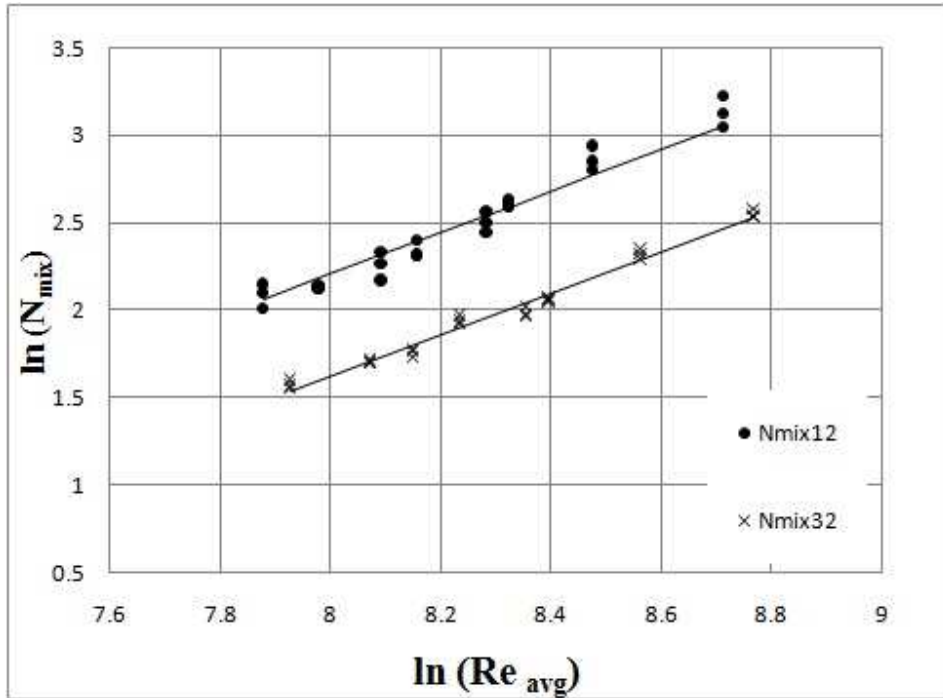


**Fig 4.3.**  $\ln(N_{mix})$  vs  $\ln(Re_{avg})$

The equations so obtained for subchannel 1-2 and subchannel 3-2 respectively are as follows

$$N_{mix,12} = 0.000694 Re_{avg}^{1.185} \quad \text{and} \quad N_{mix,32} = 0.000385 Re_{avg}^{1.185} \quad (4.12)$$

The final coefficient and exponent were obtained by fitting the experimental test data plotted on dimensionless liquid mixing number against combined Reynolds number and gap to centroidal ratio as shown in Figure 4.4.

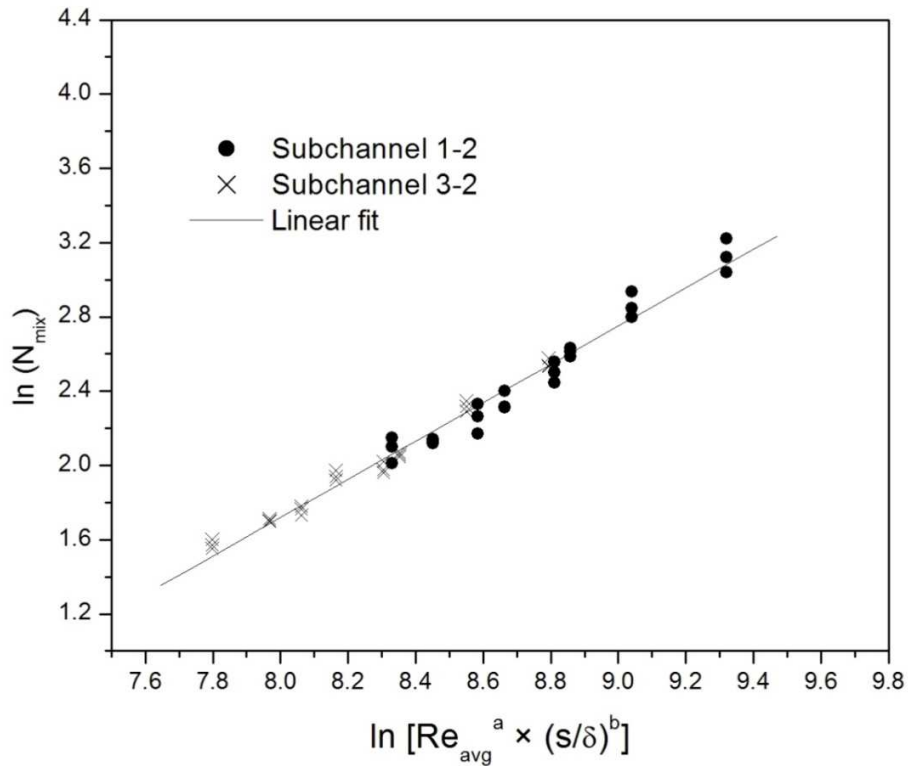


**Fig. 4.4.**  $\ln (N_{mix})$  vs  $\ln (Re_{avg} \times (S/\delta))$

The final equation so obtained considering geometrical parameter is as follows

$$N_{mix} = 0.001446 Re_{avg}^{1.223} \left( \frac{S}{\delta} \right)^{1.23} \quad (4.13)$$

The present model applicable to AHWR rod bundle having pitch to diameter ratio is 1.2.

The model is valid for Reynolds number varies from 0 to 6424.

Figure 4.5 shows the comparison between calculated and measured turbulent mixing number.

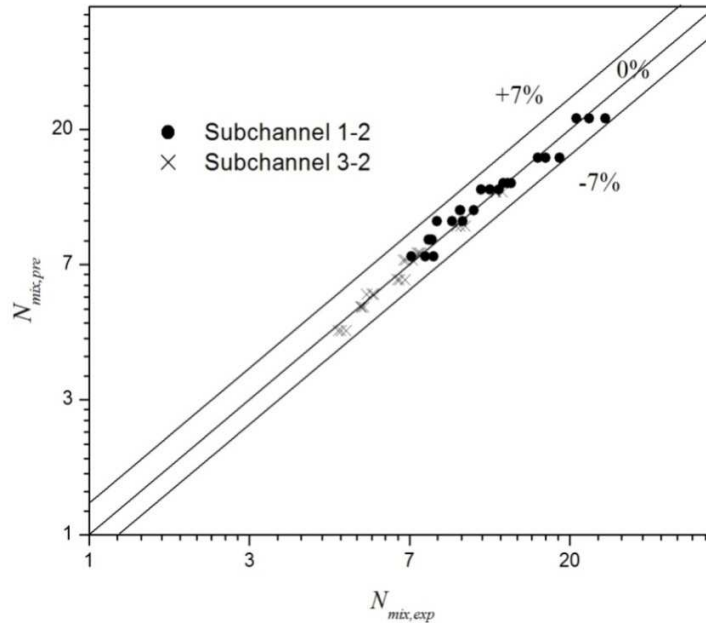


**Fig. 4.5** Comparison of the predictions of model against experiment for liquid phase turbulent mixing rate.

The model can predict measured turbulent mixing number within  $\pm 7\%$

#### 4.6 Closure

The single phase turbulent mixing rate among the subchannels of AHWR rod bundle is measured for different liquid flow rate and found that it increases with increase in average Reynolds number. An assessment of existing models against our experimental data has been carried out and found that none of these models predict measured turbulent mixing rate for AHWR rod bundle. Hence a new model applicable to AHWR has been presented which predicts turbulent mixing rate quite accurately.

## CHAPTER 5

### *STUDY OF TWO PHASE TURBULENT MIXING RATE IN AHWR ROD BUNDLE*

---

---

#### **5.1 Introduction**

In this chapter, results of two phase turbulent mixing rate for AHWR rod bundle are discussed. For determination of mixing rate in two phase flow condition, air-water mixture was introduced into all three subchannels. A tracer is added to subchannel 2 (refer fig 2.1) by tracer line injection system. Potassium nitrate used as a tracer for water and methane gas is used as a tracer for air. The tracer is mixed with fluid before entering to the inlet of subchannel. The radial pressure difference across these three subchannels is minimized by controlling the opening of respective valve in air discharge line which is connected with three separators. At outlet of the separator, samples from respective subchannel lines were extracted. The concentration of tracer i.e. potassium nitrate and methane in each subchannel was obtained by analysis through an absorption spectrophotometer and gas chromatograph respectively.

The liquid and gas phase turbulent mixing rate was calculated by substituting tracer concentration at inlet and outlet of subchannels in equation derived mathematically in section 2.3 which are as follows

$$W'_{12} = -\frac{1}{\left(\frac{1}{\dot{m}_1} + \frac{2}{\dot{m}_2}\right)Z} \ln\left(1 - \frac{2C_{1(z)}}{C_0}\right) \quad (5.1)$$

$$W'_{32} = -\frac{1}{\left(\frac{1}{\dot{m}_3} + \frac{2}{\dot{m}_2}\right)Z} \ln\left(1 - \frac{2C_{3(z)}}{C_0}\right) \quad (5.2)$$

The turbulent mixing rate was determined for each phase i.e. liquid and gas in two phase flow by varying void fraction under various ranges of superficial liquid velocity. The void fraction in two phase flow condition is calculated by Chisom's correlation (1973) as given by

$$\alpha_i = \frac{\beta_i}{\beta_i + \frac{1 - \beta_i}{\sqrt{1 - \beta_i \left(1 - \frac{\rho_g}{\rho_l}\right)}}} \quad (5.3)$$

Where  $\beta_i$  = gas volumetric fraction is given by  $\beta_i = \frac{J_g}{J_g + J_l}$  (5.4)

$J_l$  is superficial liquid velocity and  $J_g$  is superficial gas velocity in two phase flow.

The correlation is valid for  $0 \leq \beta_i \leq 0.9$  provided that liquid is no more viscous than water (Chisholm (1973)). The correlation was compared with air-water flow experiment at atmospheric condition and found to be in good agreement with experiment in range  $\pm$

6.02% (Chisholm (1973)). The current experiments are performed at near atmospheric conditions with air and water as working fluids. The working range of  $\beta_i$  in present experiment varies from 0.2 to 0.9 which is well under the limit of correlation.

In addition to above, an assessment of existing models against measured turbulent mixing rate has been carried out and a new model for liquid and gas phase turbulent mixing rate in two phase flow applicable to AHWR has been presented

## 5.2 Experiments conducted

Experiments were carried out to determine two phase turbulent mixing rate among the subchannels of AHWR rod bundle. The turbulent mixing rate in two phase flow is sum of liquid and gas phase turbulent mixing rate in two phase flow. The two phase turbulent mixing rate among the subchannels of AHWR rod bundle was measured under varying void fraction ranging from 0 to 0.8 which is same as that in prototype. The mean superficial liquid velocity varies from 0 to 0.42 m/s and mean superficial gas velocity varies from 0 to 1.3 m/s. The liquid and gas flow rate of each subchannels was measured by respective liquid and gas rotameter.

The experimental test matrix for two phase turbulent mixing is given in Table 5.1

**Table 5.1** Experimental test matrix for two phase turbulent mixing.

| S. no | Superficial Liquid velocity<br>$J_l$ in sub 3 | Superficial gas velocity<br>$J_g$ in sub 3 | Superficial Liquid velocity<br>$J_l$ in sub 2 | Superficial gas velocity<br>$J_g$ in sub 2 | Superficial Liquid velocity<br>$J_l$ in sub 1 | Superficial gas velocity<br>$J_g$ in sub 1 |
|-------|---|--|---|--|---|--|
| 1     | 0.13  | 0.63 to 1.06                               | 0.10  | 0.73 to 1.38                               | 0.14  | 0.66 to 1.14                               |
| 2     | 0.19  | 0.63 to 1.16                               | 0.15  | 0.73 to 1.22                               | 0.20  | 0.66 to 1.26                               |
| 3     | 0.27  | 0.01 to 0.64                               | 0.21  | 0.01 to 0.69                               | 0.28  | 0.01 to 0.64                               |
| 4     | 0.32  | 0.01 to 0.64                               | 0.25  | 0.01 to 0.69                               | 0.33  | 0.01 to 0.64                               |
| 5     | 0.34  | 0.01 to 0.64                               | 0.28  | 0.01 to 0.69                               | 0.36  | 0.01 to 0.64                               |
| 6     | 0.41  | 0.01 to 0.44                               | 0.32  | 0.01 to 0.49                               | 0.43  | 0.01 to 0.44                               |
| 7     | 0.47  | 0.01 to 0.20                               | 0.37  | 0.01 to 0.23                               | 0.49  | 0.01 to 0.20                               |

A potassium nitrate tracer having concentration of 100 ppm is added to water and methane tracer having concentration of 515 ppm is added to air flowing in subchannel 2. After mixing of potassium nitrate tracer with water and methane tracer with air, the samples of respective subchannels were extracted at inlet and outlet of the test section. The concentration of tracer in each subchannel at inlet and outlet of test section was obtained by analysis through an absorption spectrophotometer and gas chromatograph. For each test, the experiments were repeated three times and error found among them was within  $\pm 3\%$ .

The liquid and gas phase turbulent mixing rate in two phase flow for subchannel 1-2 (i.e.  $W'_{12}$ ) and subchannel 3-2 (i.e.  $W'_{32}$ ) is calculated by using equations (5.1) and (5.2) with

the mass flow rate of respective subchannels, mixing length (i.e.  $Z = 1.5$  m) and tracer concentrations at inlet and outlet of subchannels.

The void fraction for each subchannel is calculated by substituting superficial liquid velocity and superficial gas velocity of respective subchannels (refer Table 5.1.) given in equation (5.3).

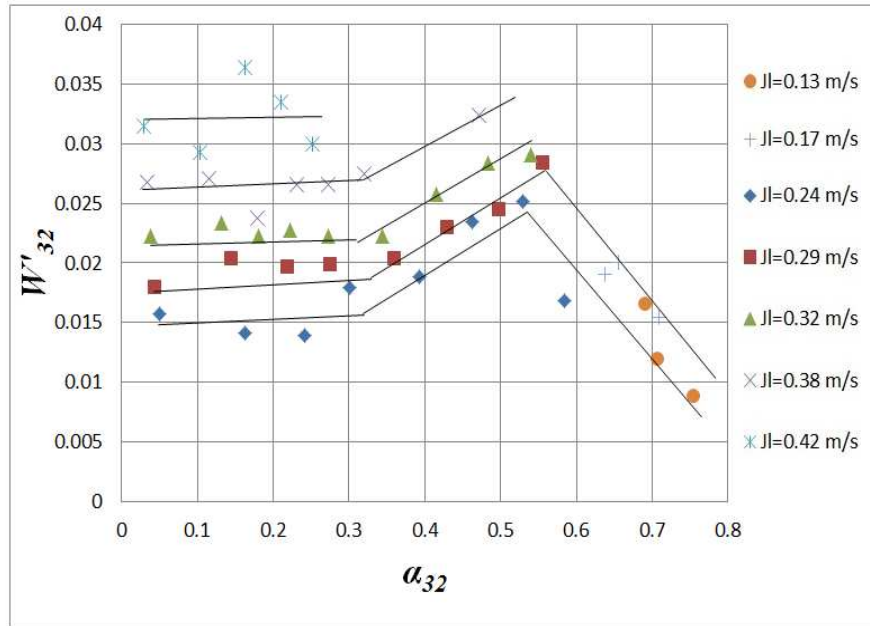
### 5.3 Results and discussion

The liquid and gas phase turbulent mixing rate in subchannel 1-2 and subchannel 3-2 is measured for average void fraction ranging from 0 to 0.8 by varying superficial liquid velocity from 0 to 0.42 m/s.

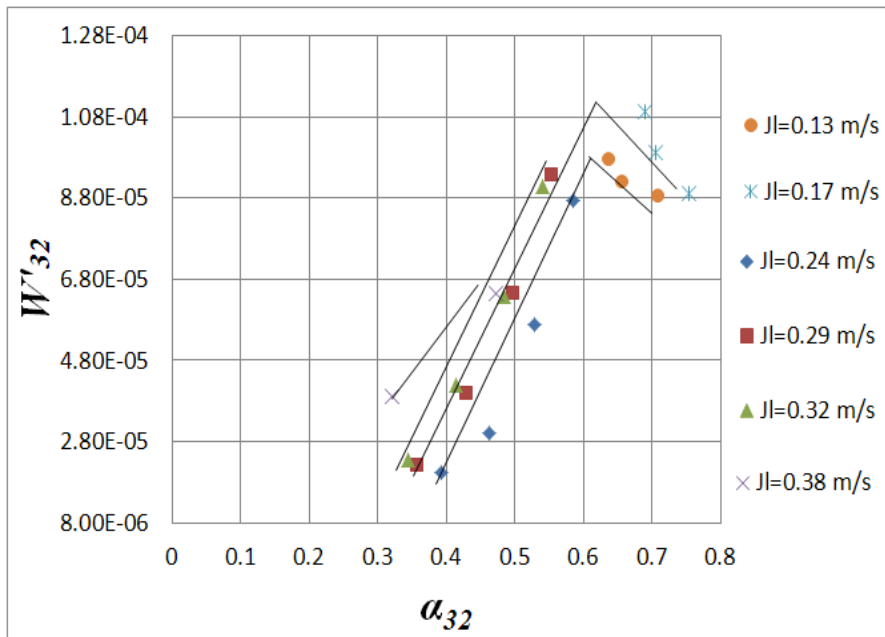
The average void fraction for subchannel 1-2 and subchannel 3-2 was calculated by substituting void fraction from equation (5.3) into equation as follows

$$\alpha_{avg,12} = \frac{\alpha_1 + \alpha_2}{2} \text{ and } \alpha_{avg,32} = \frac{\alpha_3 + \alpha_2}{2} \quad (5.5)$$

Figure 5.1 shows variation of mixing rate against average void fraction between the subchannel 3 and subchannel 2 of AHWR rod bundle



(a) Liquid phase



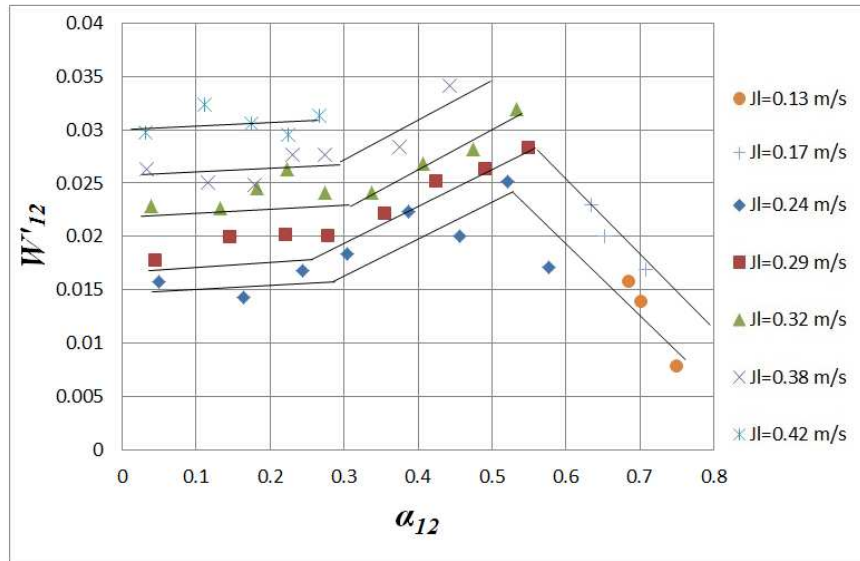
(b) Gas phase

Fig. 5.1. Turbulent mixing rate vs average void fraction between subchannel 3-2

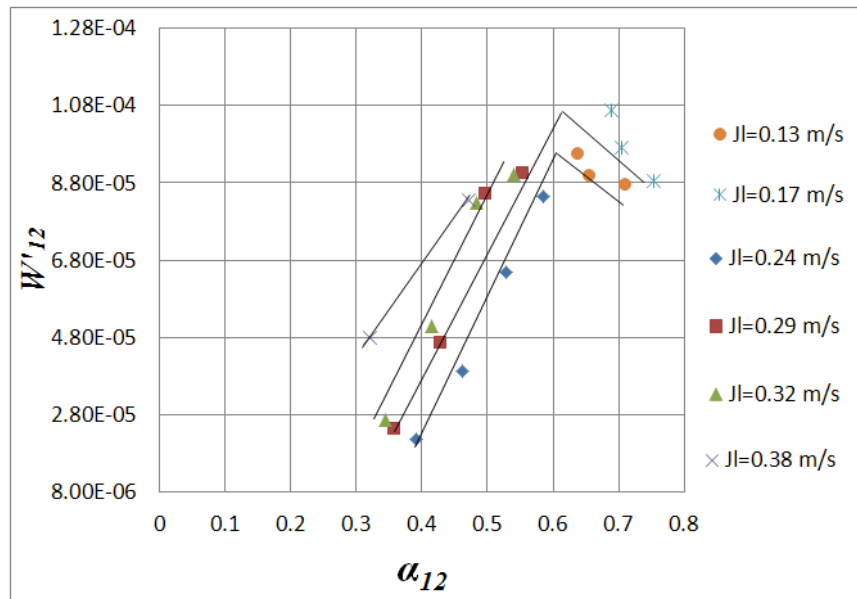
The main findings of these experiments are as follows

1. The liquid phase turbulent mixing rate is more or less constant up to average void fraction of 0.3 which is in bubbly flow regime, and then increases and reaches to a maximum at void fraction equal to 0.55 afterwards it decreases till it reaches void fraction equal to 0.8 which is in slug-churn flow regime. The criteria used to defined for bubbly and slug churn flow regime is discussed earlier in section 2.3
2. The gas phase turbulent mixing rate increases with increase in average void fraction and reaches maximum at void fraction equal to 0.65. Afterwards, it decreases till it reaches void fraction equal to 0.8. However the gas phase turbulent mixing is difficult to measure in bubbly flow due to low air flow (void fraction equal to 0.3)
3. The results indicate that turbulent mixing rate increases with increase in superficial liquid velocity.
4. These trends are agreement with the findings of Walton (1969), Rudzinski (1970), Singh K.S. (1972), Kawahara et al. (1997 (b)), Sadatomi et al. (2004) and Kawahara et al. (2006).
5. The magnitude of turbulent mixing rate between the subchannels of AHWR rod bundle (varies in range of  $10^{-2}$  to  $10^{-1}$ ) is relatively larger as compared to subchannels of conventional BWRs (varies in range of  $10^{-3}$  to  $10^{-2}$ ) for the same liquid superficial velocity (Walton (1969), Rudzinski (1970), Singh K.S. (1972), Kawahara et al. (1997 (b)), Sadatomi et al. (2004) and Kawahara et al. (2006)).

Figure 5.2 shows variation of mixing rate against average void fraction between the subchannel 1 and subchannel 2 of AHWR rod bundle



(a) Liquid phase



(b) Gas phase

Fig. 5.2 Turbulent mixing rate vs average void fraction between subchannel 1-2.

Figure 5.2 indicates that the turbulent mixing rate in two phase flow between subchannel 1-2 i.e.  $W'_{12}$  is nearly same as subchannel 3-2 i.e.  $W'_{32}$ , while in case of single phase turbulent mixing rate between subchannel 1-2 i.e.  $W'_{12}$  found to be higher as compared to subchannel 3-2 i.e.  $W'_{32}$  (seen earlier in chapter 4). The reason behind this is that the two phase fluctuation is more as compared to single phase flow due to bubble induced turbulence which homogenizes mixing in subchannels 3-2 and subchannels 1-2 of rod bundle.

The liquid and gas phase turbulent mixing rate in subchannel 1-2 and subchannel 3-2 is measured for void fraction ranging from 0 to 0.8 by varying superficial liquid velocity. It was difficult to measure turbulent mixing rate accurately beyond void fraction of  $\alpha=0.55$  at superficial liquid velocity equal to 0.2. This is because above this limit, the two phase air-water mixture is found to be unstable and difficult to quantify the mixing rate in the test.

#### **5.4 Assessment of existing model to simulate two phase turbulent mixing rate**

An attempt has been made to study the capability of existing to predict the measured two phase turbulent mixing rate. These models have been proposed to predict two phase turbulent mixing rate are shown in Appendix 1.

In this section, we evaluate the turbulent mixing models against the data obtained from present experiments of two phase turbulent mixing as discussed above. For evaluation, we have compared the measured (experimental) turbulent mixing rate in two phase flow  $W'_{exp}$  with predicted liquid phase turbulent mixing rate in two phase flow  $W'_{cal}$ . The error analysis has been done to find out maximum, minimum and average error between

measured and predicted value of two phase turbulent mixing rate. The error analysis shows how predicted value by turbulent mixing models differs from measured experimental values.

The maximum and minimum error is calculated as:

$$\text{Maximum Error (+ve deviation), } E_{\max} = \max \left( \frac{W'_{cal} - W'_{exp}}{W'_{exp}} \times 100 \right) \quad (5.6)$$

$$\text{Minimum Error (-ve deviation), } E_{\min} = \min \left( \frac{W'_{cal} - W'_{exp}}{W'_{exp}} \times 100 \right) \quad (5.7)$$

The average error is calculated as

$$\text{Average Error} = \frac{\sum_{i=1}^n E_i}{n} \% \quad (5.8)$$

where n= no. of data points and

$$E_i = \left( \frac{W'_{i,cal} - W'_{i,exp}}{W'_{i,exp}} \times 100 \right) \quad (5.9)$$

Figures 5.3 (a), (b) and (c) show comparison of existing model with present experimental data

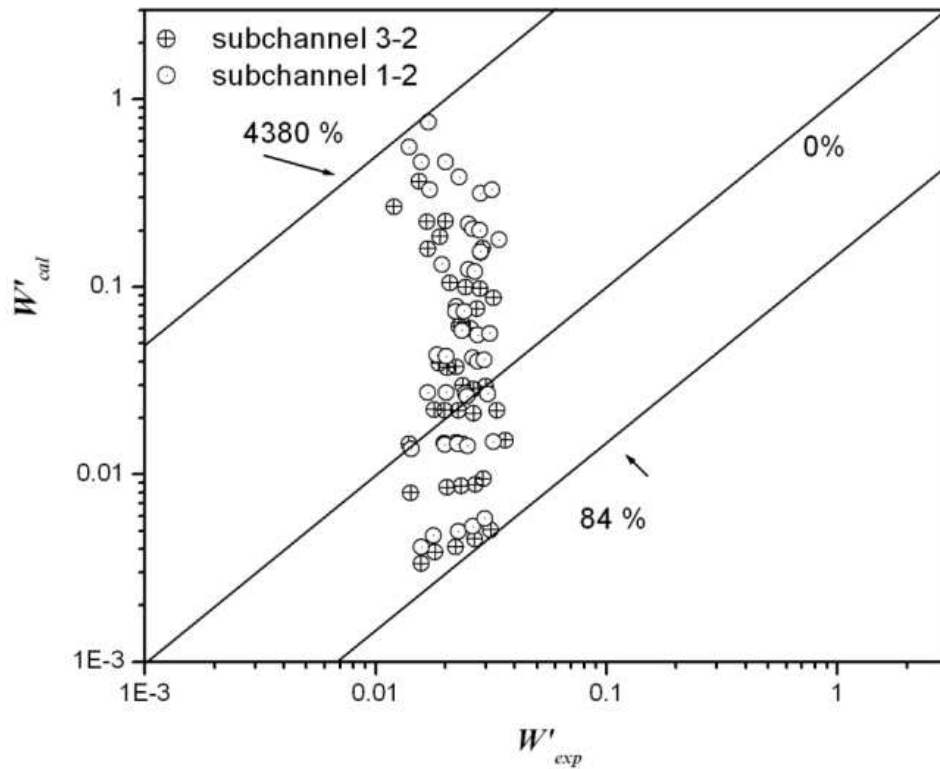


**Fig.5.3 (a).** Comparison of the predictions of Bues model (1972) against subchannel experiments for turbulent mixing rate in two phase flow

The calculated two phase turbulent mixing rate by Bues model (1972) shows large discrepancy, when compared against measured two phase turbulent mixing rate as seen in Fig. 5.3 (a). The calculated turbulent mixing rate for subchannel 3-2 differs from measured turbulent mixing rate by maximum error of +2270%, minimum error of -84% and an average error of +249 %. Similarly the calculated turbulent mixing rate for subchannel 1-2 differs from measured turbulent mixing rate by maximum error of +4380%, minimum error of -80% and an average error of + 567%.

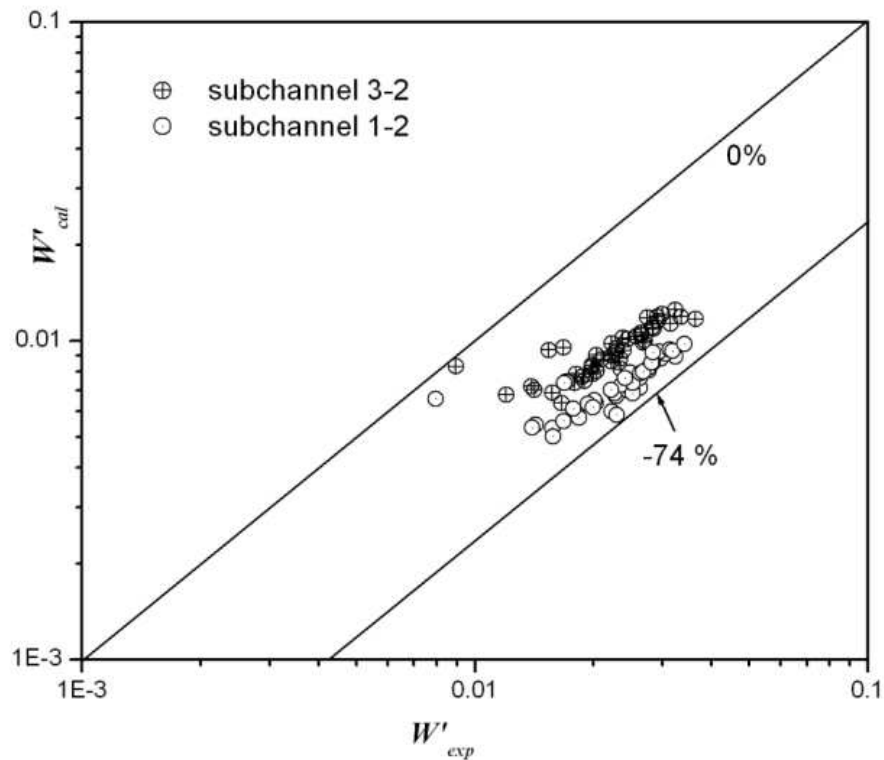


**Fig. 5.3 (b).** Comparison of the predictions of Kazimi and Kelly's (1983) against subchannel experiments for turbulent mixing rate in two phase flow.

The calculated two phase turbulent mixing rate by Kazimi and Kelly model (1983) shows large discrepancy, when compared against measured two phase turbulent mixing rate as seen in Fig. 5.3 (b). The calculated turbulent mixing rate for subchannel 3-2 differs from measured turbulent mixing rate by maximum error of -7 %, minimum error of -68% and an average error of -57.2 %. Similarly the calculated turbulent mixing rate for subchannel 1-2 differs from measured turbulent mixing rate by maximum error of -17 %, minimum error of -74 % and an average error of -67.6 %.

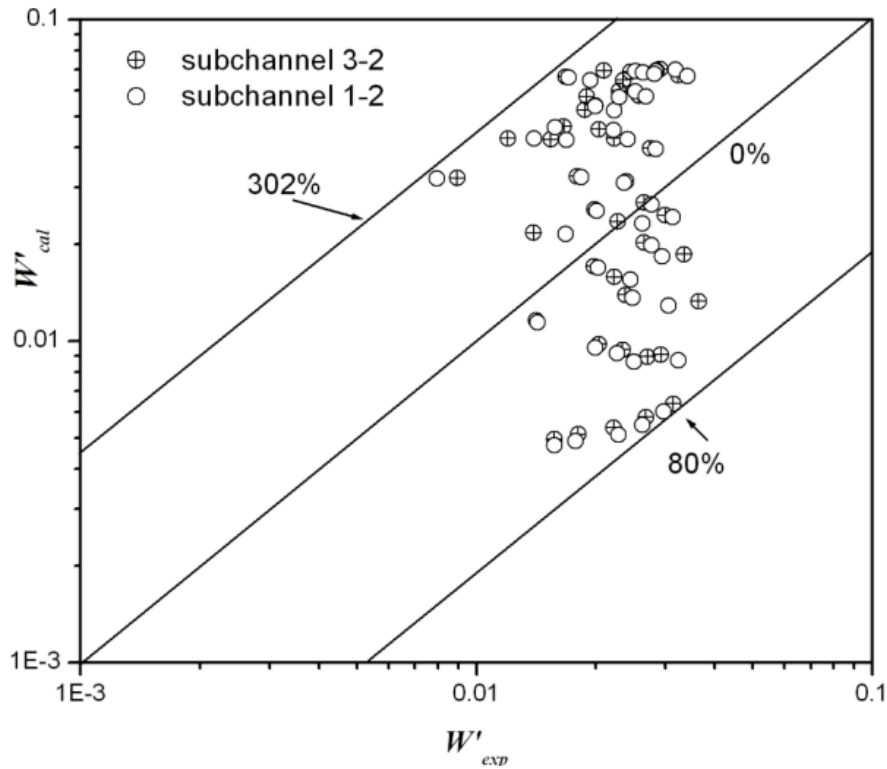


**Fig. 5.3 (c).** Comparison of the predictions of Carlucci et al. (2003) against subchannel experiments for turbulent mixing rate in two phase flow.

The calculated two phase turbulent mixing rate by Carlucci et al. model (2003) shows large discrepancy, when compared against measured two phase turbulent mixing rate as seen in Fig. 5.3 (c). The calculated turbulent mixing rate for subchannel 3-2 differs from measured turbulent mixing rate by maximum error of +295%, minimum error of -80% and an average error of +63 %. Similarly the calculated turbulent mixing rate for subchannel 1-2 differs from measured turbulent mixing rate by maximum error of +302%, minimum error of -80% and an average error of +55.1%.

## 5.5 Model development

Because of large difference in models prediction and present test data, it is important to develop AHWR specific models. As we have seen in Figures 5.1 and 5.2, the characteristics of liquid and gas phase turbulent mixing rate in two phase flow changes with void fraction ranging from 0 to 0.8. This is because turbulent mixing rate is flow regime dependent (i.e. for liquid phase void fraction ranges from  $0 \leq \alpha \leq 0.3$ ,  $0.3 \leq \alpha \leq 0.55$  and  $0.55 \leq \alpha \leq 0.8$  and for gas phase  $0.3 \leq \alpha \leq 0.65$  and  $0.65 \leq \alpha \leq 0.8$ ). So in order to develop a flow regime based model applicable for AHWR geometry, the model presented earlier in equation (1.31) and (1.32) was used for liquid and gas phase turbulent mixing rate respectively and modified for different flow regimes.

The equation of liquid phase turbulent mixing number is as follows

$$N_{l,mix} = F_{l,gc} \times F_p \times C_l \text{Re}_{mix}^{a_l} \quad (5.10)$$

where gap to centroid factor ( $F_{l,gc}$ ) and pressure factor ( $F_p$ ) are as follows

$$F_{l,gc} = C_1 \left[ (\beta_{liq}) \left( \frac{S}{\delta} \right) \right]^{a_1} \text{ and } F_p = \left( \frac{\sigma_{H.T.}}{\sigma_{R.T.}} \right)^n \quad (5.11)$$

The equation of gas phase turbulent mixing number is as follows

$$N_{g,mix} = F_{g,gc} \times F_p \times C_g (\ln(\text{Re}_{mix} \times \beta))^{a_g} \quad (5.12)$$

where gap to centroid factor ( $F_{l,gc}$ ) and pressure factor ( $F_p$ ) are as follows

$$F_{g,gc} = C_1 \times e^{a_1 \times (\beta_{liq}) \left(\frac{S}{\delta}\right)} \quad \text{and} \quad F_p = \left(\frac{\sigma_{H.T.}}{\sigma_{R.T.}}\right)^n \quad (5.13)$$

These coefficients and exponents for liquid and gas phase mixing rate are determined in following section 5.4.1 and 5.4.2

### 5.5.1 Liquid phase turbulent mixing rate

#### (a) Liquid phase turbulent mixing model for void fraction ranges from $0 \leq \alpha \leq 0.3$ .

Figure 5.4 (a) shows the test data plotted on dimensionless liquid mixing number against mixture Reynolds number for void fraction ranges from  $0 \leq \alpha \leq 0.3$

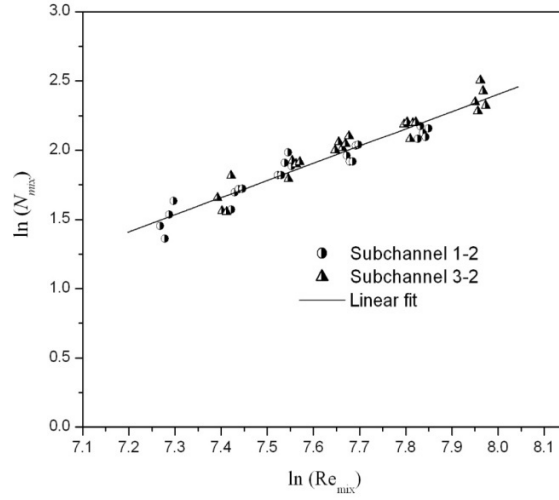


Fig. 5.4 (a) Liquid phase mixing rate ( $0 \leq \alpha \leq 0.3$ )

The final equations so obtained for liquid phase mixing number considering geometrical and pressure parameter are as follows.

$$N_{l,mix} = F_{l,gc} \times F_p \times 0.00053 \text{Re}_{mix}^{1.2} \quad (5.14)$$

or

$$W'_{l,mix} = F_{l,gc} \times F_p \times \frac{0.00053 \times A \times \mu_{hom} \times (\text{Re}_{mix})^{1.2}}{D_h^2} \quad (5.15)$$

**(b) Liquid phase turbulent mixing model for void fraction ranges from  $0.3 \leq \alpha \leq 0.55$ .**

Figure 5.4 (b) shows the test data plotted on dimensionless liquid mixing number against mixture Reynolds number for void fraction ranges from  $0.3 \leq \alpha \leq 0.55$

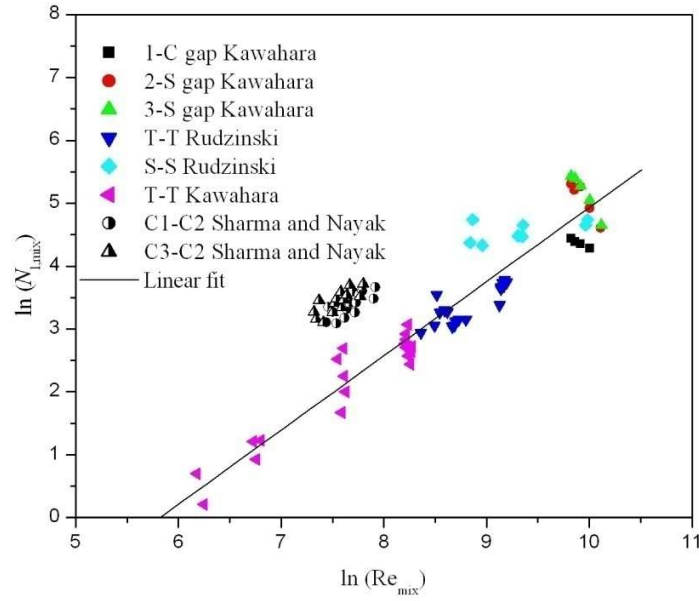


**Fig 5.4 (b)** Liquid phase mixing rate ( $0.3 \leq \alpha \leq 0.55$ ).

The equations so obtained for liquid phase mixing rate considering geometrical and pressure factor are as follows

$$N_{l,mix} = F_{l,gc} \times F_p \times 0.00104 Re_{mix}^{1.80} \tag{5.16}$$

or

$$W'_{l,mix} = F_{l,gc} \times F_p \times \frac{0.00104 \times A \times \mu_{hom} \times (Re_{mix})^{1.80}}{D_h^2} \tag{5.17}$$

**(c) Liquid phase turbulent mixing model for void fraction ranges from  $0.55 \leq \alpha \leq 0.8$**

Figure 5.4 (c) shows the test data plotted on dimensionless liquid mixing number against mixture Reynolds number for void fraction ranges from  $0.55 \leq \alpha \leq 0.8$

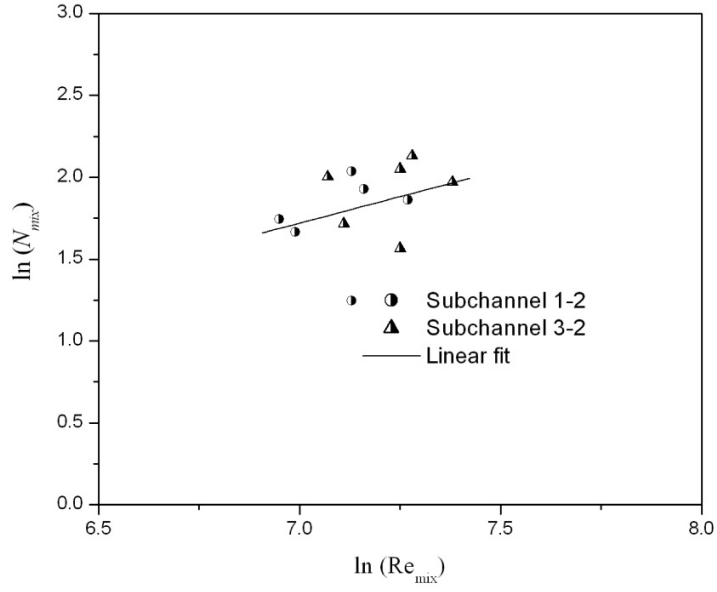


Fig 5.4 (c) Liquid phase mixing rate ( $0.55 \leq \alpha \leq 0.8$ ).

The equations so obtained for liquid phase mixing rate considering geometrical and pressure factor are as follows

$$N_{l,mix} = F_{l,gc} \times F_p \times 0.06 \text{Re}^{0.64} \quad (5.18)$$

or

$$W'_{l,mix} = F_{l,gc} \times F_p \times \frac{0.06 \times A \times \mu_{hom} \times (\text{Re}_{mix})^{0.64}}{D_h^2} \quad (5.19)$$

The details of gap to centroid factor ( $F_{l,gc}$ ) and pressure factor ( $F_p$ ) is given in Appendix 2

### 5.5.2 Gas phase turbulent mixing rate

#### (a) Gas phase turbulent mixing model for void fraction ranges from $0.3 \leq \alpha \leq 0.65$

Figure 5.5 (a) shows the test data plotted on dimensionless gas mixing number against combined volumetric gas fraction and mixture Reynolds number for void fraction ranges from  $0.3 \leq \alpha \leq 0.65$ .

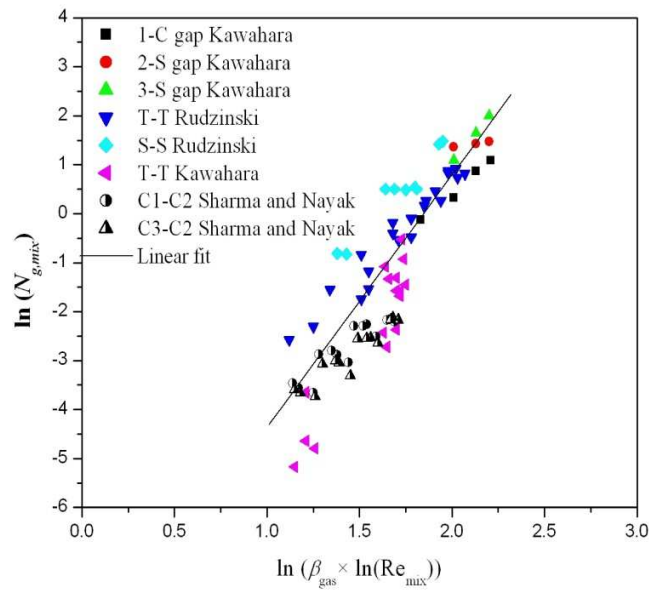


**Fig 5.5 (a)** Gas phase mixing rate ( $0.3 \leq \alpha \leq 0.65$ )

The equations so obtained for gas phase mixing rate considering geometrical and pressure factor are as follows

$$N_{g,mix} = F_{g,gc} \times F_p \times 0.0000749 \left( \ln(\text{Re}_{mix} \times \beta_g) \right)^{5.14} \quad (5.20)$$

or

$$W'_{l,mix} = F_{g,gc} \times F_p \times \frac{0.0000749 \times A \times \mu_{hom} \times (\ln(\text{Re}_{mix} \times \beta_g))^{5.14}}{D_h^2} \quad (5.21)$$

**(b) Two phase turbulent mixing model for void fraction ranges from  $0.65 \leq \alpha \leq 0.8$**

Figure 5.5 (b) shows the test data plotted on dimensionless gas mixing number against combined volumetric gas fraction and mixture Reynolds number for void fraction ranges from  $0.65 \leq \alpha \leq 0.8$

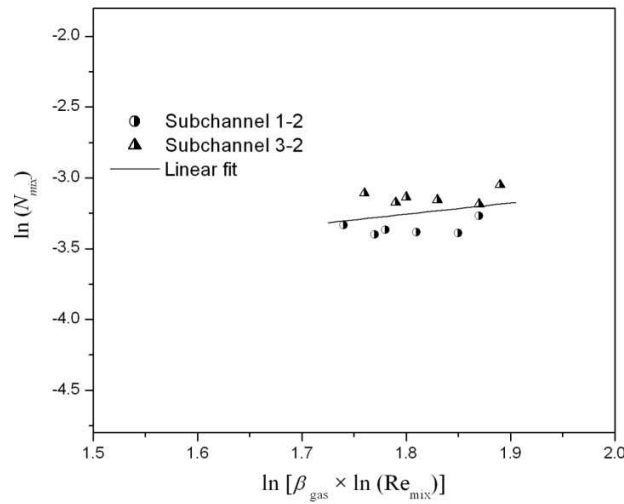


**Fig 5.5 (b)** Gas phase mixing rate ( $0.65 \leq \alpha \leq 0.8$ )

The equations so obtained for gas phase mixing rate considering geometrical and pressure factor are as follows

$$N_{g,mix} = F_{g,gc} \times F_p \times 0.009 (\ln(\text{Re}_{mix} \times \beta))^{0.79} \quad (5.22)$$

Or

$$W'_{l,mix} = F_{g,gc} \times F_p \times \frac{0.009 \times A \times \mu_{hom} \times (\ln(\text{Re}_{mix} \times \beta_g))^{0.79}}{D_h^2} \quad (5.23)$$

The details of gap to centroid factor ( $F_{g,gc}$ ) and pressure factor ( $F_p$ ) is given in Appendix2.

It may be noted that the present model applicable to AHWR rod bundle having pitch to diameter ratio is 1.2. The present model is valid for void fraction varies from  $0 \leq \alpha \leq 0.8$ . The validity of this model is checked against present experimental data as shown in Figure 5.6.

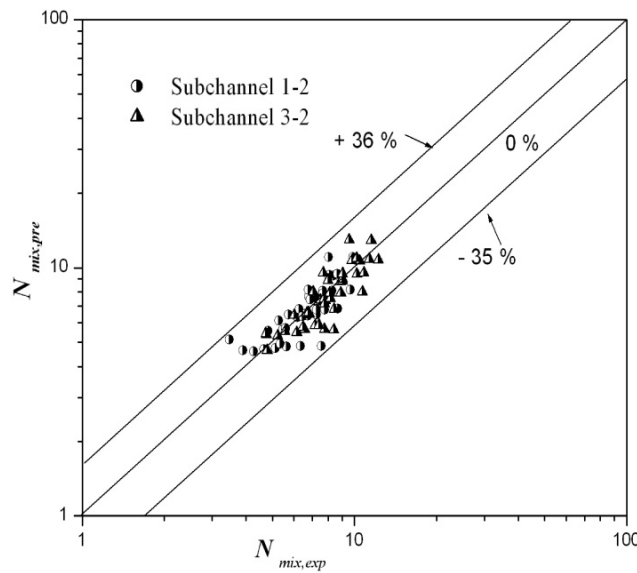


**Fig. 5.6.** Comparison of the predictions of present model against subchannel experiments for turbulent mixing rate in two phase flow.

The calculated mixing number for subchannel 3-2 differs from measured mixing number by maximum error of +36 %, minimum error of -34 % and an average error of -2 % whereas calculated mixing number for subchannel 1-2 differs from measured mixing

number by maximum error of +20 %, minimum error of -35 % and an average error of +1.6 %. These errors are significantly less than that predicted by previous models.

## 5.6 Closure

The two phase turbulent mixing rate among the subchannels of AHWR rod bundle is measured by varying void fraction for different superficial liquid velocity and found that turbulent mixing rate is flow regimes dependent. The magnitude of turbulent mixing rate is found to increase with increase in superficial liquid velocity. An assessment of existing models against present experimental data has been carried out and found that none of these models predict measured turbulent mixing rate for AHWR rod bundle. In the view of this, a new model applicable to AHWR has been presented which predicts turbulent mixing rate quite accurately.

## CHAPTER 6

### *STUDY OF VOID DRIFT IN AHWR ROD BUNDLE*

---

---

#### **6.1 Introduction**

In this chapter, results of void drift for AHWR rod bundle are discussed. The necessary condition for void drift to occur is that, at both the inlet and the outlet ends of the mixing section, the time-averaged radial pressures difference between subchannels has to be zero i.e.  $\Delta P_{1-2} = \Delta P_{3-2} = 0$ . The measured inlet water and air flow rate from respective subchannel line passes through mixer to form two phase flow. This two phase air-water mixture was introduced into all three subchannels such that difference in radial pressure between the subchannels is minimum. This was achieved by throttling the air discharge line valve after the air-water separator. Under this condition, flow rate of each phase at outlet of the separators were again measured through respective subchannel lines rotameters. This difference in flow rate at inlet (non-equilibrium flow) and outlet (equilibrium flow) of individual subchannel of test section gives net change in flow rate due to void drift.

The net change in gas mass flux between the subchannels due to void drift can be expressed by (Lahey and Moody (1993))

$$G_{g,ij} = \rho_g D [(\alpha_i - \alpha_j) - (\alpha_i - \alpha_j)_{eq}] / S_{ij} \quad (6.1)$$

where  $G_{g,ij}$  is net change in mass flux between adjacent subchannel due to void drift,  $\rho_g$  is the density of gas,  $D$  is void diffusion coefficients,  $(\alpha_i - \alpha_j)$  is void fraction difference in non-equilibrium flow,  $(\alpha_i - \alpha_j)_{eq}$  is void fraction difference in equilibrium flow and  $S_{ij}$  is gap between the subchannels.

There are two known parameters ( $\rho_g$  and  $S_{ij}$ ) and three unknown parameters ( $G_{g,ij}$ ,  $(\alpha_i - \alpha_j)$  in equilibrium and non equilibrium condition and  $D$ ) in equation (6.1). To determine these parameters, the following steps have been taken:

**Step 1:** For gas mass flux, the mass flux in respective subchannel was calculated by substituting measured volumetric flow rate ( $Q_g$ ) by gas rotameter into following equation

$$G_{g,i} = \frac{\rho_g \times Q_{g,i}}{A_i} \quad (6.2)$$

The net change in gas mass flux between subchannels is given by

$$G_{g,ij} = G_{g,i,in} - G_{g,i,out} \quad (6.3)$$

where  $G_{g,in}$  and  $G_{g,out}$  is the gas mass flux at inlet and outlet of the subchannel and is calculated by equation (6.2)

**Step 2:** For void fraction difference in equilibrium and non-equilibrium flow, the void fraction in each subchannel, i.e. subchannels 1, 2 and 3 is calculated by following steps

- (a) Superficial velocity of both the phases in all three subchannels i.e. subchannel no. 1, 2 and 3 were calculated by

$$J_{g,i} = Q_{g,i}/A_i \text{ and } J_{l,i} = Q_{l,i}/A_i \quad (6.4)$$

where  $J_g$  is gas superficial velocity,  $J_l$  is liquid superficial velocity,  $Q_g$  is volumetric flow rate of gas,  $Q_l$  is volumetric flow rate of liquid and  $A$  is flow area of subchannel.

- (b) The equilibrium and non-equilibrium void fraction is evaluated by substituting respective gas volumetric fraction into Chisom correlation (1973) as follows

$$\alpha_i = \frac{\beta_i}{\beta_i + \frac{1 - \beta_i}{\sqrt{1 - \beta_i \left( 1 - \frac{\rho_g}{\rho_l} \right)}}} \quad (6.5)$$

Where  $\beta_i$  = gas volumetric fraction is given by  $\beta_i = \frac{J_g}{J_g + J_l}$  (6.6)

The correlation is valid for  $0 \leq \beta_i \leq 0.9$  provided that liquid is no more viscous than water (Chisholm (1973)). The correlation was compared with air-water flow experiment at atmospheric condition and found to be in good agreement with experiment in range  $\pm 6.02\%$  (Chisholm (1973)). The current experiments are performed at near atmospheric conditions with air and water as working fluids. The working range of  $\beta_i$  in present experiment varies from 0.2 to 0.9 which is well under the limit of correlation.

**Step 3:** The void diffusion coefficient ( $D$ ) is determined by substituting void fraction difference in equilibrium and non-equilibrium condition and net gas mass flux due to void drift in void settling model given in equation (6.1).

In addition to above, an assessment of existing models for prediction of equilibrium void fraction against our experimental data has been carried out.

## 6.2 Experiments conducted

Experiments were carried out to determine void drift among the subchannels of AHWR rod bundle. The flow redistribution due to void drift among the subchannels of AHWR rod bundle was measured by varying superficial liquid velocity in non-equilibrium flow condition at inlet ranging from 0 to 0.48 m/s and superficial gas velocity ( $J_g$ ) ranging from 0 to 1.38 m/s corresponding void fraction ranging from 0 to 0.8 which is same as that in prototype.

The experiments were repeated three times and error found was within  $\pm 1$  %. The liquid and gas flow rate of each subchannels was measured by respective liquid and gas rotameter.

The experimental test matrix for void drift is given in Table 6.1

**Table 6.1** Experimental test matrix for void drift

| S. no | Superficial Liquid velocity<br>$J_l$ in sub 3 | Superficial gas velocity<br>$J_g$ in sub 3 | Superficial Liquid velocity<br>$J_l$ in sub 2 | Superficial gas velocity<br>$J_g$ in sub 2 | Superficial Liquid velocity<br>$J_l$ in sub 1 | Superficial gas velocity<br>$J_g$ in sub 1 |
|-------|---|--|---|--|---|--|
| 1     | 0.12  | 0.73 to 1.32                               | 0.11  | 0.58 to 1.02                               | 0.13  | 0.77 to 1.38                               |
| 2     | 0.19  | 0.73 to 1.32                               | 0.16  | 0.58 to 1.02                               | 0.19  | 0.77 to 1.38                               |
| 3     | 0.26  | 0.07 to 0.71                               | 0.22  | 0.06 to 0.56                               | 0.26  | 0.08 to 0.75                               |
| 4     | 0.34  | 0.07 to 0.71                               | 0.29  | 0.06 to 0.56                               | 0.35  | 0.08 to 0.75                               |
| 5     | 0.40  | 0.23 to 0.71                               | 0.34  | 0.18 to 0.56                               | 0.42  | 0.25 to 0.75                               |
| 6     | 0.46  | 0.08 to 0.14                               | 0.38  | 0.06 to 0.11                               | 0.48  | 0.08 to 0.15                               |

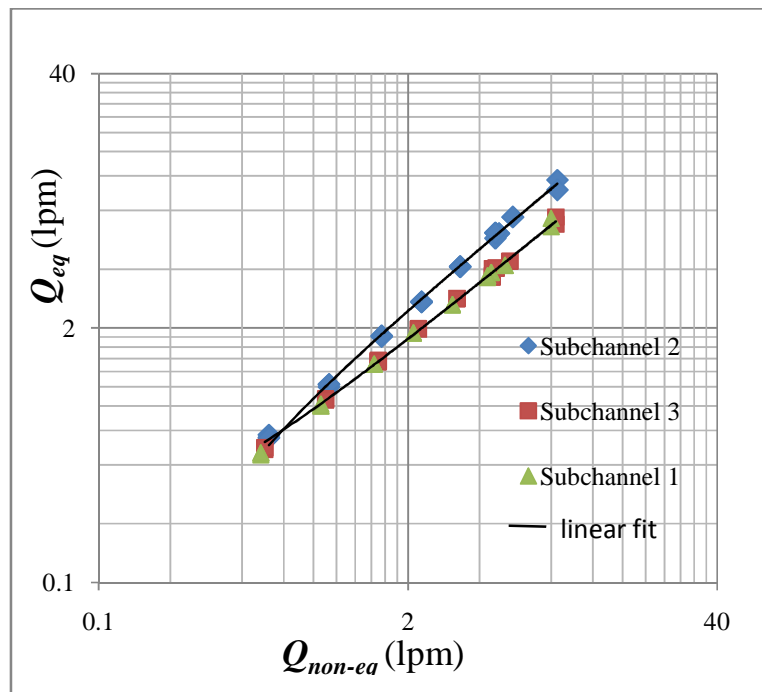
The void fraction for each subchannel is calculated by using equation (6.5) with the superficial liquid velocity and superficial gas velocity of respective subchannels in equilibrium and non-equilibrium flow condition. The net change in mass flux between adjacent subchannels is calculated by using equation (6.3). Afterward, the void diffusion coefficient ( $D$ ) is determined by using equation (6.1) with the void fraction difference in

equilibrium and non-equilibrium condition and net gas mass flux due to void drift in void settling model given in equation (6.1).

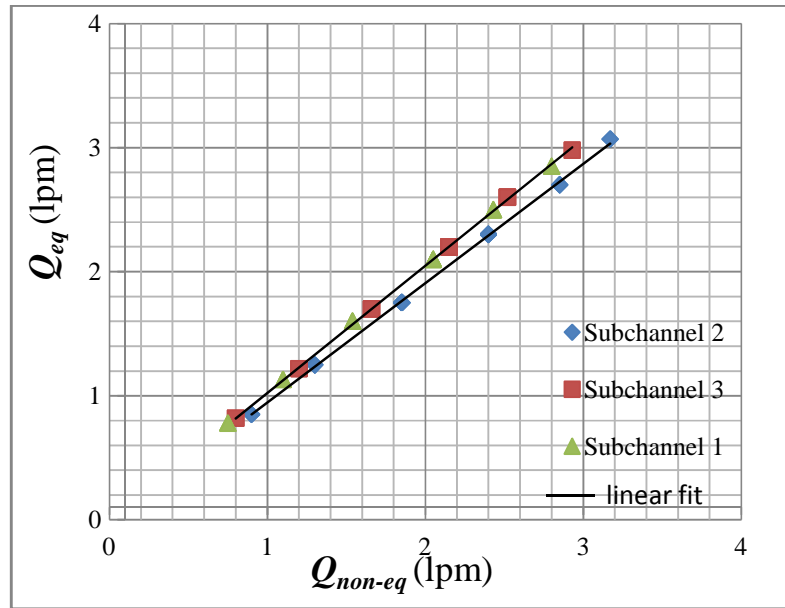
### 6.3 Results and discussion

The flow redistribution (non-equilibrium flow to equilibrium flow) due to void drift among the subchannels of AHWR rod bundle was measured by varying superficial liquid velocity at inlet ranging from 0 to 0.48 m/s and superficial gas velocity ( $J_g$ ) ranging from 0 to 1.38 m/s corresponding void fraction ranging from 0 to 0.8 which is same as that in prototype.

Figures 6.1 (a) and 6.1 (b) show variation of equilibrium flow (at outlet) with non-equilibrium flow (at inlet) for both gas and liquid phase respectively.



(a) Gas phase



(b) Liquid phase

**Fig. 6.1** Equilibrium flow vs non equilibrium flow for gas and liquid phase

The non-equilibrium flow approaches towards equilibrium flow as going downstream of test section. The gas volumetric flow rate is more in subchannel 2 as compared to subchannel 3 and subchannel 1 while liquid volumetric flow rate is less in sub channel 2 as compared to subchannel 3 and subchannel 1. This is because ratio of flow area of subchannel 2 ( $A_2$ ) to the total area ( $A_t = A_1 + A_2 + A_3$ ) is more for subchannel 2 ( $A_2/A_t = 0.40$ ) as compared to subchannel 3 ( $A_3/A_t = 0.29$ ) and subchannel 1 ( $A_1/A_t = 0.31$ ). It means that voids drift towards subchannels having more open area (i.e. subchannel 2) which is agreed with existing literature [(Lahey and Schraub (1969), Lahey et al. (1972), Gonzalez-Santalo et al. (1972); Lahey (1986); Sato et al. (1987), Tapucu et al. (1988), Gencay et al. (2001), Sadatomi et al. (1994), Sadatomi et al. (2004) ].

Figures 6.2 (a) and 6.2 (b) show variation of equilibrium void fraction (at outlet) with non-equilibrium (at intlet) void fraction.

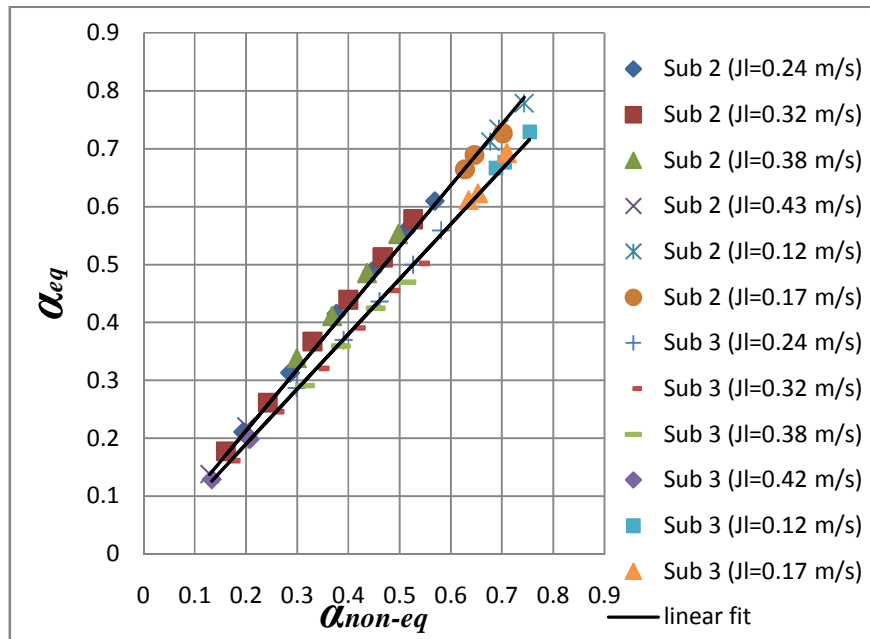


Fig. 6.2 (a) Equilibrium void fraction vs non equilibrium void fraction for subchannel 3-2

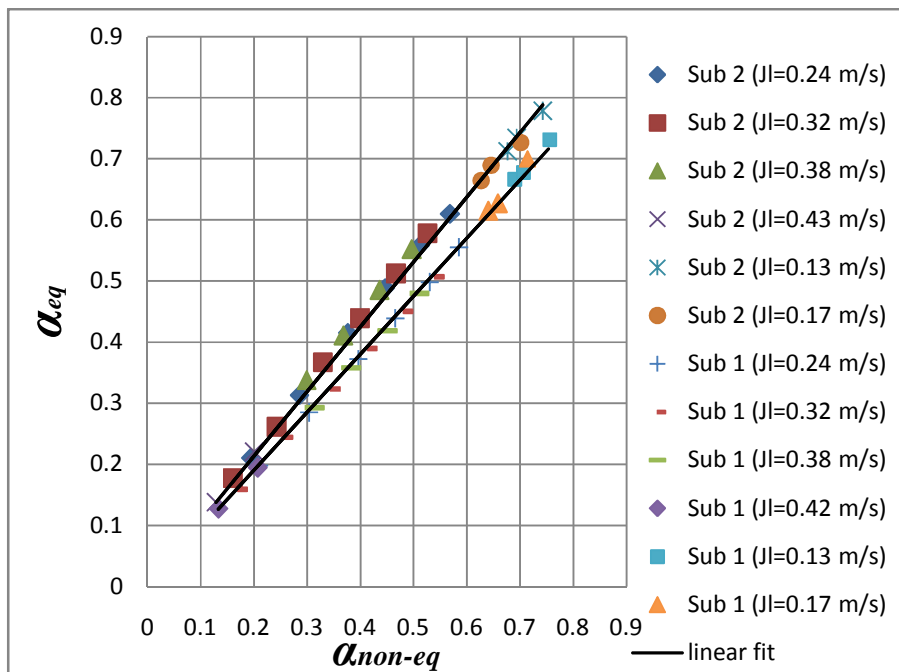


Fig. 6.2 (b) Equilibrium void fraction vs non equilibrium void fraction for subchannel 11-2

The main findings of these experiments are as follows.

- (1) The equilibrium void fraction is more in subchannel 2 as compared to subchannel 3 and subchannel 1. This is because ratio of flow area of subchannel 2 ( $A_2$ ) to the total area ( $A_t=A_1+A_2+A_3$ ) is more for subchannel 2 ( $A_2/A_t=0.40$ ) as compared to subchannel 3 ( $A_3/A_t = 0.29$ ) and subchannel 1 ( $A_1/A_t=0.31$ ).
- (2) The variation in equilibrium and non-equilibrium void fraction is very less with respect to liquid superficial velocity.
- (3) In both the cases of void drift i.e. subchannel 1-2 and subchannel 3-2, the difference in equilibrium and non-equilibrium void fraction of individual subchannels is less when void fraction is equal to 0.3 and this difference is more at void fraction greater than 0.3. This means that voids drift more in slug-churn as compared to bubbly flow.

#### **6.4 Determination of void diffusion coefficient**

The void diffusion coefficient ( $D$ ) is determined by substituting void fraction difference in equilibrium and non-equilibrium condition and net gas mass flux due to void drift in void settling model given in equation (6.1). Figures 6.3 (a) and 6.3 (b) show the variation of void diffusion coefficient between the subchannels with average void fraction.

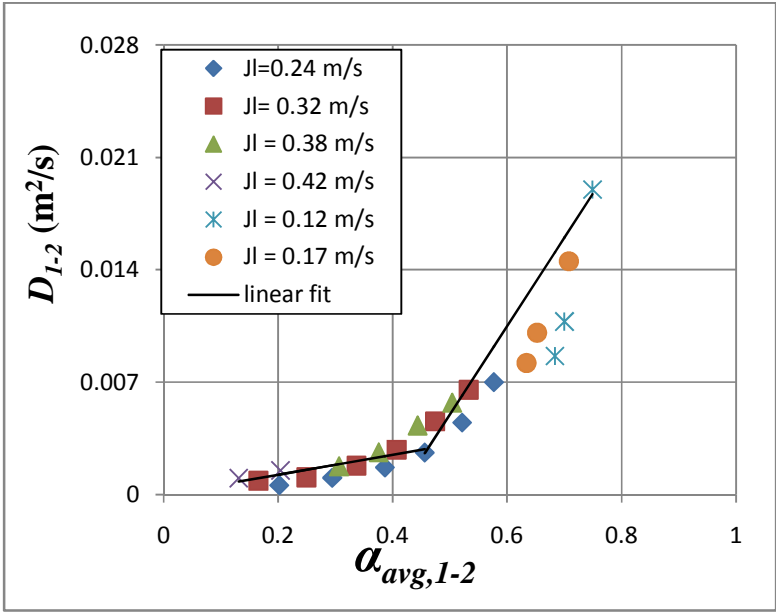


Fig. 6.3 (a). Variation of void diffusion coefficient between the subchannel 1-2 with average void fraction 1-2

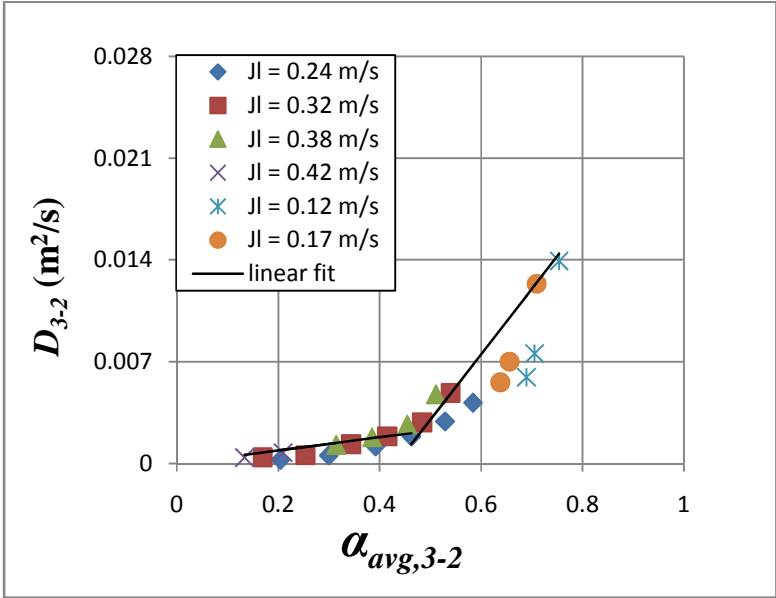


Fig. 6.3 (b). Variation of void diffusion coefficient between the subchannel 3-2 with average void fraction 3-2

The main findings are as follows.

1. The void diffusion coefficient is more or less constant or little increases with increase in average void fraction up to  $\alpha \approx 0.45$ . Beyond void fraction  $\alpha \approx 0.45$ , there is a steep increase in void diffusion coefficient with increase in average void fraction.
2. The trends of void diffusion coefficient found to be same for subchannel 1-2 and subchannel 3-2.
3. Also the magnitude of diffusion coefficient found to be increase with increase in superficial liquid velocity.

### **6.5 Assessment of existing model to simulate equilibrium void fraction distribution due to void drift**

An attempt has been made to study the capability of existing models to predict the measured equilibrium void fraction distribution. Rowe et al. (1990) and Carlucci et al. (2003) proposed model to evaluate the void fraction distribution in a hydraulically equilibrium flow. The model of equilibrium void fraction distribution by Rowe et al. (1990) is given by

$$\alpha_i = \alpha_{avg} + \alpha_{avg} (1 - \alpha_{avg}) \left(1 - \frac{D_{h,avg}}{D_{h,i}}\right) \quad (6.7)$$

Carlucci et al. (2003) modified Rowe et al. (1990) model by including constant  $K$  and factor of mass-flux and pressure  $F_{G,p}$ , which is given by

$$\alpha_i = \alpha_{avg} + K\alpha_{avg}F_{G,p}(1 - \alpha_{avg})\left(1 - \frac{D_{h,avg}}{D_{h,i}}\right) \quad (6.8)$$

In this section, we evaluate the equilibrium void fraction models like Rowe et al. (1990), Carlucci et al. (2003) against the data obtained from present experiments of equilibrium void fraction as discussed above. For evaluation, we have compared the measured (experimental) equilibrium void fraction  $\alpha_{exp}$  with equilibrium void fraction  $\alpha_{cal}$ . The error analysis has been done to find out maximum, minimum and average error between measured and calculated (predicted) value of two phase turbulent mixing rate. The error analysis shows how predicted value by equilibrium void fraction models differs from experimental values.

$$\text{Max. Error } E_{\max,i} = \max\left(\frac{\alpha_{i,cal} - \alpha_{i,exp}}{\alpha_{i,exp}} \times 100\right) \quad (6.9)$$

$$\text{Min. Error } E_{\min,i} = \min\left(\frac{\alpha_{i,cal} - \alpha_{i,exp}}{\alpha_{i,exp}} \times 100\right) \quad (6.10)$$

The average error is calculated as

$$\text{AverageError} = \frac{\sum_{i=1}^n E_i}{n} \% \quad (6.11)$$

where  $n$  = no. of data points and

$$E_i = \left( \frac{\alpha_{i,cal} - \alpha_{i,exp}}{\alpha_{i,exp}} \times 100 \right) \quad (6.12)$$

The capability of existing models to predict the measured equilibrium void fraction distribution as shown in Figures 6.4 and 6.5

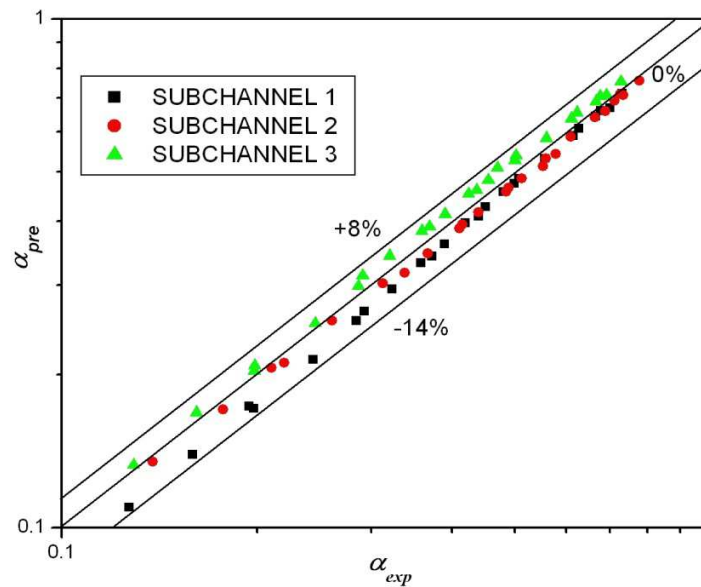


**Fig. 6.4** Comparison of the predictions of Rowe et al. Model (1990) against subchannels experiments for equilibrium void fraction in two phase flow.

The calculated equilibrium void fraction by Rowe et al. (1990) model shows discrepancy, when compared against measured equilibrium void fraction as seen in Figure 6.4. The error calculated between predicted and experiment is very less. The calculated equilibrium void fraction differs from measured equilibrium void fraction for subchannel

1 by an average error of -7 %.The calculated equilibrium void fraction differs from measured equilibrium void fraction for subchannel 2 by an average error of -4 %.The calculated equilibrium void fraction differs from measured equilibrium void fraction for subchannel 3 by an average error of 5 %.

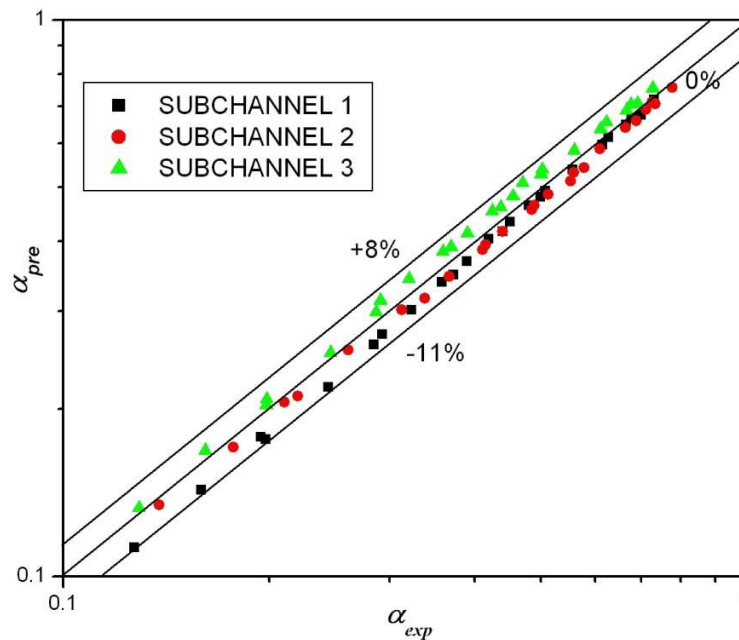


**Fig. 6.5** Comparison of the predictions of Carlucci et al. model (2003) against subchannels experiments for equilibrium void fraction in two phase flow.

The calculated equilibrium void fraction by Carlucci et al. (2003) model shows discrepancy, when compared against measured equilibrium void fraction as seen in Figure 6.5. The same trend is found in this model because this model is derived from Rowe et al. (1990) model. The calculated equilibrium void fraction differs from measured equilibrium void fraction for subchannel 1 by an average error of -5 %.The calculated equilibrium void fraction differs from measured equilibrium void fraction for subchannel

2 by an average error of -4 %.The calculated equilibrium void fraction differs from measured equilibrium void fraction for subchannel 3 by an average error of 5 %.

The above comparison indicates that Rowe et al. (1990) and Carlucci et al. (2003) models could predict void fraction distribution in a hydraulically equilibrium flow with an average error of  $\pm 5$  %.

In addition to these models, Lahey model (1972) is also compared against present experimental data which is shown in Figure 6.6. Lahey et al. (1972) derived model based on Levy's (1963) model is given by

$$\frac{(\alpha_i - \alpha_j)}{\alpha_{avg}} = \frac{(G_i - G_j)}{G_{avg}} \tag{6.13}$$

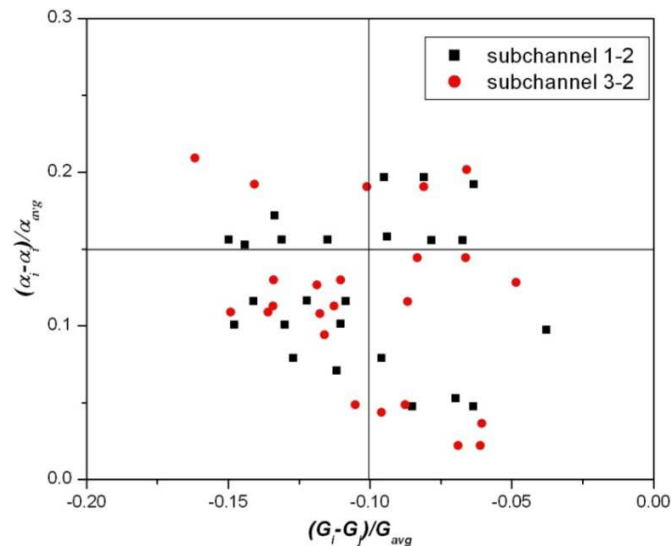


**Fig. 6.6** Comparison of ratio of equilibrium void fraction difference to average void fraction vs ratio of equilibrium mass flux difference to average mass flux in two phase flow.

The result indicates that the ratio of equilibrium void fraction difference to the average void fraction is not proportional to ratio of equilibrium mass flux difference to average mass flux between subchannels. This trend is also found by previous subchannel experiments of void drift; for two subchannel experiment by Sadatomi (1994) and for multi-subchannel experiment by Sadatomi (2004).

## **6.6 Closure**

The void drift among the subchannels of AHWR rod bundle is measured for different superficial liquid velocity and found that voids drift towards subchannels having more open area. Also voids drift is more in slug-churn as compared to bubbly flow. In addition to it, the diffusion coefficient is also determine by substituting net mass flux due to void drift and void fraction difference in equilibrium and non-equilibrium condition. An assessment of existing models against our experimental data has been carried out and found that these models predict present data quite accurately.

## CHAPTER 7

# *STUDY OF SINGLE AND TWO PHASE DIVERSION CROSS FLOW IN AHWR ROD BUNDLE*

---

---

### **7.1 Introduction**

In this chapter results of single phase and two phase diversion cross flow for AHWR rod bundle are discussed. The diversion cross flow is an inter-subchannel mixing phenomena which occurs only due to radial pressure difference between adjacent subchannels. The necessary condition for diversion cross flow to occur is that, at the inlet of the mixing section, the time-averaged radial pressures difference between the subchannels is not zero i.e.  $\Delta P_{1-2} = \Delta P_{3-2} \neq 0$ . The measured inlet water flow rate for single phase flow and measured air-water mixture was introduced into all three subchannels, such that difference in radial pressure between the subchannels should exist. Under this condition, flow rate of each phase at outlet of the separators were again measured through respective subchannel lines rotameters. This difference in flow rate at inlet and outlet of individual subchannel of test section will give net change in flow rate due to diversion cross flow.

This flow redistribution occurs in the presence of radial pressure difference between the subchannels. The radial pressure difference between the subchannels is generally related

to density and cross flow velocity between the subchannels by a factor “K” which is called as transverse resistance coefficient or cross flow resistance coefficient represented as

$$K = \frac{\Delta P}{\frac{1}{2} \rho V_{dc}^2} \quad (7.1)$$

Where  $\Delta P$  is radial pressure difference between subchannels

$\rho_l$  = Density of liquid and  $V_{dc}$  = diversion cross flow velocity

Using cross flow momentum equation based on two fluid model, to take care of the gap to centroidal distance in the subchannel; the transverse resistance coefficient or cross flow resistance is modified as

$$K = \frac{S}{\delta} \frac{\Delta P}{\rho V_{dc}^2} \quad (7.2)$$

where S is gap between the subchannels and  $\delta$  is centroidal distance between subchannels.

The lateral velocity due to diversion cross flow in single phase flow can be calculated as

$$V_{dc} = J_{dc} \quad (7.3)$$

The lateral velocity due to diversion cross flow in two phase flow can be calculated as

$$V_{dc} = \frac{J_{dc}}{1 - \alpha} \quad (7.4)$$

Where  $J_{dc} = (Q_{in} - Q_{out})/A$  is superficial liquid velocity due to diversion cross and  $\alpha$  average void fraction between the subchannel

Also an assessment of existing models against present experimental data has been carried out. In the view of this, a new model for cross flow resistance (K) of single and two phase flow condition, applicable to AHWR has been presented.

## 7.2 Experiments conducted

Experiments were carried out to determine transverse cross flow resistance for single phase flow by varying axial velocity from 0 to 1 m/s and for two phase flow, the superficial axial liquid velocity was varied from 0 to 0.64 m/s and superficial axial gas velocity was varied from 0 to 1.8 m/s corresponding void fraction in two phase flow ranging from 0 to 0.8 which is same as that in prototype. In order to set a cross flow in the test section, Kawahara et al. (2007) method was used. In the present experiment, we fixed the inlet flow rate ratio in the subchannels  $Q_2/Q_t = 0.6$  and  $Q_1/Q_t = Q_3/Q_t = 0.2$  for every run. The experiments repeated three times and error found was within  $\pm 1\%$ . The experimental test matrix for single and two phase diversion cross flow is given in Tables 7.1 and 7.2 respectively.

**Table 7.1** Experimental test matrix for single phase diversion cross flow

| S. no | Velocity in subchannel<br>3<br>m/s | Velocity in subchannel<br>2<br>m/s | Velocity in subchannel<br>1<br>m/s |
|-------|------------------------------------|------------------------------------|------------------------------------|
| 1     | 0.08                               | 0.18                               | 0.09                               |
| 2     | 0.11                               | 0.26                               | 0.12                               |
| 3     | 0.16                               | 0.36                               | 0.17                               |
| 4     | 0.2                                | 0.47                               | 0.22                               |
| 5     | 0.28                               | 0.64                               | 0.3                                |
| 6     | 0.38                               | 0.87                               | 0.42                               |
| 7     | 0.47                               | 1.1                                | 0.52                               |

**Table 7.2** Experimental test matrix for two phase diversion cross flow

| S. no | Superficial<br>Liquid<br>velocity<br>$J_l$ in sub 3 | Superficial<br>gas<br>velocity<br>$J_g$ in sub 3 | Superficial<br>Liquid<br>velocity<br>$J_l$ in sub 2 | Superficial<br>gas<br>velocity<br>$J_g$ in sub 2 | Superficial<br>Liquid<br>velocity<br>$J_l$ in sub 1 | Superficial<br>gas<br>velocity<br>$J_g$ in sub 1 |
|-------|---|--|---|--|---|--|
| 1     | 0.08  | 0.44 to 0.78                                     | 0.17  | 1.00 to 1.8                                      | 0.09  | 0.48 to 0.86                                     |
| 2     | 0.11  | 0.44 to 0.78                                     | 0.26  | 1.00 to 1.8                                      | 0.12  | 0.48 to 0.86                                     |
| 3     | 0.16  | 0.04 to 0.40                                     | 0.36  | 0.10 to 0.97                                     | 0.17  | 0.05 to 0.48                                     |
| 4     | 0.20  | 0.04 to 0.40                                     | 0.47  | 0.10 to 0.97                                     | 0.22  | 0.05 to 0.48                                     |
| 5     | 0.27  | 0.04 to 0.40                                     | 0.64  | 0.10 to 0.97                                     | 0.30  | 0.05 to 0.48                                     |

The cross flow resistance coefficient between subchannel 1-2 and subchannel 3-2 for single and two phase was calculated by using equation (7.2) with the measured radial pressure difference by DPTs, lateral velocity, gap to centroidal distance ratio and density of fluid.

The lateral velocity due to diversion cross flow in single phase and two phase flow is calculated by using equations (7.3) and (7.4) respectively.

### 7.3 Results and discussion

The cross flow resistance is measured for single phase flow by varying axial velocity from 0 to 1 m/s and for two phase flow, the superficial axial liquid velocity was varied from 0 to 0.64 m/s and superficial axial gas velocity was varied from 0 to 1.8 m/s

corresponding void fraction in two phase flow ranging from 0 to 0.8 which is same as that in prototype.

### 7.3.1 Single phase diversion cross flow

Figure 7.1 shows the variation of transverse resistance coefficient ( $K_{sp}$ ), for single phase water flows. The transverse resistance coefficient ( $K_{sp}$ ) is plotted against a ratio of diversion cross flow velocity to the axial velocity ( $V_{dc}/V_{axial}$ ).

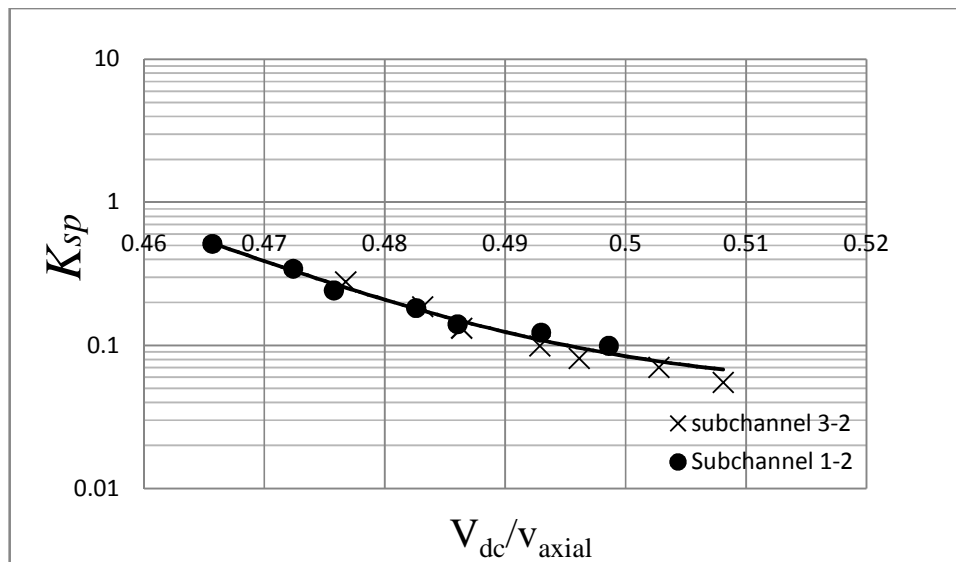


**Fig. 7.1** Transverse resistance coefficient in single phase flow vs Ratio of cross flow velocity to the axial velocity

The single phase Transverse resistance coefficient coefficient ( $K_{sp}$ ) are well correlated with ( $V_{dc}/V_{axial}$ ) by the regression curve and is given by

$$K_{sp} = 7 \times 10^9 \exp(-50.5 V_{dc}/V_{axial}) \quad (7.5)$$

Where  $K$ = transverse resistance coefficient,  $V_{dc}$ = Diversion cross flow velocity,  $V_{axial}$ = Axial flow velocity

### 7.3.2 Two phase diversion cross flow

Figure 7.2 shows variation of transverse resistance coefficient ( $K_{tp}$ ), for two phase flows. The transverse resistance coefficient ( $K_{tp}$ ) is plotted against a ratio of diversion cross flow velocity to the axial velocity ( $V_{dc}/V_{axial}$ ).

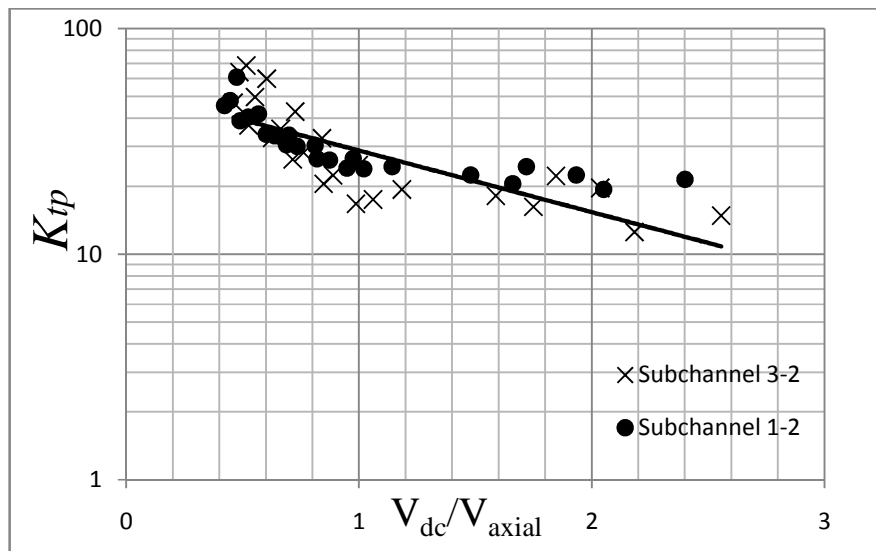


**Fig. 7.2** Transverse resistance coefficient in two phase flow vs Ratio of cross flow velocity to the axial velocity.

The two phase transverse resistance coefficient ( $K_{tp}$ ) are well correlated with ( $V_{dc}/V_{axial}$ ) by the regression curve and is given by

$$K_{tp} = 54 \exp(-0.63 V_{dc}/V_{axial}) \tag{7.6}$$

The main findings are as follows.

1. The cross flow resistance coefficient decreases with increase in ratio of cross flow velocity to the axial velocity both in single and two phase flow condition.
2. Also cross flow resistance coefficient in two phase flow is higher as compared to single phase flow.

#### **7.4 Assessment of existing model to simulate diversion cross flow resistance**

In computer codes such as COBRA, the transverse resistance coefficient is assumed to be constant all along the gap between the subchannels e.g. 0.15 [Rowe (1973)], 0.5 [Rowe (1973)], 1.0 [Tappacu (1988)], 2.5 [Shoukri, (1985)]. The experiment performed by Tapucu [1976] shows that cross flow resistance coefficient is not constant and it is function ratio of the lateral flow velocity to the donor channel axial velocity, the recipient channel axial velocity, and of the gap clearance and thickness of the slot.

Kim and Park (1975) proposed a correlation for predicting cross flow resistance is function of ratio of the lateral flow velocity to the donor channel axial velocity, Reynolds number of recipient channel and ratio of pitch to diameter. Kawahara et al. (2007) proposed a correlation for predicting cross flow resistance is a function of ratio of cross flow velocity to the average mean velocity between the subchannel. Iwamura (1986) proposed a correlation relating cross-flow resistance is proportional void fraction and cross-flow Reynolds number.

An attempt has been made to study the capability of existing models to predict the measured single phase and two phase diversion cross flow resistance. The error analysis has been done to find out maximum, minimum and average error between measured and calculated (predicted) value of cross flow resistance coefficient.

$$\text{Max. Error } E_{\max,i} = \max \left( \frac{K_{cal} - K_{exp}}{K_{exp}} \times 100 \right) \quad (7.7)$$

$$\text{Min. Error } E_{\min,i} = \min \left( \frac{K_{cal} - K_{exp}}{K_{exp}} \times 100 \right) \quad (7.8)$$

The average error is calculated as

$$\text{AverageError} = \frac{\sum_{i=1}^n E_i}{n} \% \quad (7.9)$$

where n= no. of data points and

$$E_i = \left( \frac{K_{cal} - K_{exp}}{K_{exp}} \times 100 \right) \quad (7.10)$$

**(i) Evaluation of single phase diversion cross flow model**

Table 7.3 and Table 7.4 shows prediction due to Kawahara et al. (2007) and Kim and Park (1995) model compared against experimental data of subchannel 1-2 and subchannel 3-2.

**Table 7.3** Comparison of prediction by Kawahara et al. (2007) model and measured value of transverse resistance coefficient in single phase diversion cross flow

| Subchannel 1-2 |                |                 |         |                 | Subchannel 3-2 |                 |         |                 |
|----------------|----------------|-----------------|---------|-----------------|----------------|-----------------|---------|-----------------|
| S. no          | Measured value | Predicted value | Error % | Average error % | Measured value | Predicted value | Error % | Average error % |
| 1              | 0.513          | 0.0301          | -94     | -84             | 0.278          | 0.0288          | -90     | -73             |
| 2              | 0.343          | 0.0293          | -91     |                 | 0.187          | 0.0281          | -85     |                 |
| 3              | 0.243          | 0.0289          | -88     |                 | 0.132          | 0.0277          | -79     |                 |
| 4              | 0.183          | 0.0281          | -85     |                 | 0.099          | 0.0270          | -73     |                 |
| 5              | 0.141          | 0.0278          | -80     |                 | 0.081          | 0.0267          | -67     |                 |
| 6              | 0.123          | 0.0270          | -78     |                 | 0.070          | 0.0260          | -63     |                 |
| 7              | 0.099          | 0.0264          | -73     |                 | 0.055          | 0.0255          | -54     |                 |

**Table 7.4** Comparison of prediction by Kim and Park (1995) model and measured value of transverse resistance coefficient in single phase diversion cross flow

| Subchannel 1-2 |                |                 |         |                 | Subchannel 3-2 |                 |         |                 |
|----------------|----------------|-----------------|---------|-----------------|----------------|-----------------|---------|-----------------|
| S. no          | Measured value | Predicted value | Error % | Average error % | Measured value | Predicted value | Error % | Average error % |
| 1              | 0.513          | 1.6E-30         | -100    | -100            | 0.278          | 2.8E-31         | -100    | -100            |
| 2              | 0.343          | 5.5E-31         | -100    |                 | 0.187          | 1.0E-31         | -100    |                 |
| 3              | 0.243          | 3.2E-31         | -100    |                 | 0.132          | 6.1E-32         | -100    |                 |
| 4              | 0.183          | 1.1E-31         | -100    |                 | 0.099          | 2.2E-32         | -100    |                 |
| 5              | 0.141          | 6.4E-32         | -100    |                 | 0.081          | 1.3E-32         | -100    |                 |
| 6              | 0.123          | 2.2E-32         | -100    |                 | 0.070          | 4.7E-33         | -100    |                 |
| 7              | 0.099          | 9.1E-33         | -100    |                 | 0.055          | 2.1E-33         | -100    |                 |

The results indicate that Kawahara et al. (2007) and Kim and Park (1995) model predict significantly lower than measured values.

In addition to it, a new model is proposed for transverse resistance coefficient which is given by equation (7.5). The prediction due to this model has been compared against present experimental data as shown in Table 7.5.

**Table 7.5.** Comparison of present model against experimental data of subchannel 1-2 and subchannel 3-2

| Subchannel 1-2 |                |                 |         |                 | Subchannel 3-2 |                 |         |                 |
|----------------|----------------|-----------------|---------|-----------------|----------------|-----------------|---------|-----------------|
| S. no          | Measured value | Predicted value | Error % | Average error % | Measured value | Predicted value | Error % | Average error % |
| 1              | 0.51331        | 0.42865         | -16     | -8.6            | 0.27843        | 0.24498         | -12     | -0.42           |
| 2              | 0.34334        | 0.30544         | -11     |                 | 0.18661        | 0.17742         | -5      |                 |
| 3              | 0.24266        | 0.25746         | 6       |                 | 0.13202        | 0.15078         | 14      |                 |
| 4              | 0.18253        | 0.18239         | 0       |                 | 0.09949        | 0.1086          | 9       |                 |
| 5              | 0.15314        | 0.15329         | 0       |                 | 0.08356        | 0.09203         | 10      |                 |
| 6              | 0.13197        | 0.10795         | -18     |                 | 0.07214        | 0.06591         | -9      |                 |
| 7              | 0.10314        | 0.0813          | -21     |                 | 0.05647        | 0.05032         | -11     |                 |

The results indicate that the present model can predict the transverse resistance coefficient predicts quite accurately.

**(ii) Evaluation of two phase diversion cross flow model**

Table 7.6 and Table 7.7 shows Kawahara et al. (2007) model and Iwamura et al. (1986) model compared against experimental data of subchannel 1-2 and subchannel 3-2.

**Table 7.6** Comparison of prediction by Kawahara et al. (2007) model against measured value of transverse resistance coefficient in two phase diversion cross flow

| Subchannel 1-2 |                |                 |         |                 | Subchannel 3-2 |                 |         |                 |
|----------------|----------------|-----------------|---------|-----------------|----------------|-----------------|---------|-----------------|
| S. no          | Measured value | Predicted value | Error % | Average error % | Measured value | Predicted value | Error % | Average error % |
| 1              | 60.92          | 0.13            | -99.78  | -99.56          | 68.65          | 0.12            | -99.83  | -99.54          |
| 2              | 41.87          | 0.10            | -99.76  |                 | 59.99          | 0.09            | -99.85  |                 |
| 3              | 33.70          | 0.07            | -99.79  |                 | 42.89          | 0.07            | -99.84  |                 |
| 4              | 30.32          | 0.06            | -99.82  |                 | 32.67          | 0.05            | -99.84  |                 |
| 5              | 26.55          | 0.04            | -99.84  |                 | 24.83          | 0.04            | -99.84  |                 |
| 6              | 24.45          | 0.03            | -99.87  |                 | 19.36          | 0.03            | -99.84  |                 |
| 7              | 24.47          | 0.25            | -98.96  |                 | 22.25          | 0.22            | -98.99  |                 |
| 8              | 22.46          | 0.21            | -99.06  |                 | 19.69          | 0.19            | -99.03  |                 |
| 9              | 21.43          | 0.15            | -99.30  |                 | 14.82          | 0.13            | -99.11  |                 |
| 10             | 48.04          | 0.15            | -99.70  |                 | 64.20          | 0.13            | -99.80  |                 |
| 11             | 40.55          | 0.11            | -99.72  |                 | 49.71          | 0.10            | -99.79  |                 |
| 12             | 33.53          | 0.08            | -99.75  |                 | 35.97          | 0.08            | -99.78  |                 |
| 13             | 30.06          | 0.07            | -99.78  |                 | 28.26          | 0.06            | -99.78  |                 |
| 14             | 26.16          | 0.05            | -99.81  |                 | 22.38          | 0.05            | -99.78  |                 |
| 15             | 23.91          | 0.04            | -99.84  |                 | 17.49          | 0.04            | -99.79  |                 |
| 16             | 22.44          | 0.32            | -98.57  |                 | 18.18          | 0.28            | -98.43  |                 |
| 17             | 20.51          | 0.27            | -98.69  |                 | 16.24          | 0.24            | -98.50  |                 |
| 18             | 19.39          | 0.19            | -99.01  |                 | 12.55          | 0.17            | -98.64  |                 |
| 19             | 45.60          | 0.16            | -99.65  |                 | 47.00          | 0.14            | -99.70  |                 |
| 20             | 39.04          | 0.13            | -99.68  |                 | 37.30          | 0.11            | -99.70  |                 |
| 21             | 34.07          | 0.09            | -99.73  |                 | 32.78          | 0.08            | -99.74  |                 |
| 22             | 30.52          | 0.07            | -99.76  |                 | 26.30          | 0.07            | -99.74  |                 |
| 23             | 26.46          | 0.06            | -99.79  |                 | 20.53          | 0.05            | -99.75  |                 |
| 24             | 24.07          | 0.04            | -99.82  |                 | 16.74          | 0.04            | -99.76  |                 |

**Table 7.7** Comparison of prediction by Iwamura et al. (1986) model against measured value of transverse resistance coefficient in two phase diversion cross flow

| Subchannel 1-2 |                |                 |         |                 | Subchannel 3-2 |                 |         |                 |
|----------------|----------------|-----------------|---------|-----------------|----------------|-----------------|---------|-----------------|
| S. no          | Measured value | Predicted value | Error % | Average error % | Measured value | Predicted value | Error % | Average error % |
| 1              | 60.92          | 16.38           | -73.11  | -41.97          | 68.65          | 16.29           | -76.26  | -33.08          |
| 2              | 41.87          | 20.15           | -51.87  |                 | 59.99          | 20.26           | -66.22  |                 |
| 3              | 33.70          | 21.49           | -36.24  |                 | 42.89          | 21.66           | -49.49  |                 |
| 4              | 30.32          | 21.22           | -30.03  |                 | 32.67          | 21.41           | -34.48  |                 |
| 5              | 26.55          | 19.76           | -25.57  |                 | 24.83          | 20.00           | -19.43  |                 |
| 6              | 24.45          | 17.62           | -27.94  |                 | 19.36          | 17.82           | -7.99   |                 |
| 7              | 24.47          | 26.11           | 6.69    |                 | 22.25          | 26.31           | 18.26   |                 |
| 8              | 22.46          | 23.70           | 5.55    |                 | 19.69          | 23.89           | 21.35   |                 |
| 9              | 21.43          | 17.19           | -19.81  |                 | 14.82          | 17.29           | 16.64   |                 |
| 10             | 48.04          | 10.62           | -77.89  |                 | 64.20          | 10.62           | -83.46  |                 |
| 11             | 40.55          | 13.94           | -65.62  |                 | 49.71          | 13.94           | -71.97  |                 |
| 12             | 33.53          | 15.50           | -53.76  |                 | 35.97          | 15.62           | -56.56  |                 |
| 13             | 30.06          | 15.89           | -47.13  |                 | 28.26          | 16.05           | -43.19  |                 |
| 14             | 26.16          | 15.46           | -40.90  |                 | 22.38          | 15.67           | -29.95  |                 |
| 15             | 23.91          | 14.07           | -41.14  |                 | 17.49          | 14.20           | -18.81  |                 |
| 16             | 22.44          | 20.35           | -9.33   |                 | 18.18          | 20.54           | 12.93   |                 |
| 17             | 20.51          | 18.78           | -8.46   |                 | 16.24          | 18.96           | 16.80   |                 |
| 18             | 19.39          | 14.42           | -25.62  |                 | 12.55          | 14.51           | 15.62   |                 |
| 19             | 45.60          | 6.38            | -86.01  |                 | 47.00          | 6.33            | -86.53  |                 |
| 20             | 39.04          | 8.69            | -77.74  |                 | 37.30          | 8.73            | -76.59  |                 |
| 21             | 34.07          | 12.52           | -63.26  |                 | 32.78          | 12.61           | -61.52  |                 |
| 22             | 30.52          | 13.14           | -56.94  |                 | 26.30          | 13.28           | -49.53  |                 |
| 23             | 26.46          | 12.85           | -51.46  |                 | 20.53          | 13.03           | -36.53  |                 |
| 24             | 24.07          | 12.13           | -49.62  |                 | 16.74          | 12.21           | -27.08  |                 |

The results indicate that kawahara et al. (2007) and Iwamura et al. (1986) predict significantly less compared to measured values.

In addition to it, model is proposed for transverse resistance coefficient given by equation (7.6) is also compared against present experimental data and found that it predicts quite accurately as shown in Table 7.8.

**Table 7.8** Comparison of present model against experimental data of subchannel 1-2 and subchannel 3-2.

| Subchannel 1-2 |                |                 |         |                 | Subchannel 3-2 |                 |         |                 |
|----------------|----------------|-----------------|---------|-----------------|----------------|-----------------|---------|-----------------|
| S. no          | Measured value | Predicted value | Error % | Average error % | Measured value | Predicted value | Error % | Average error % |
| 1              | 60.92          | 40.05           | -34.25  | -2.16           | 68.65          | 39.03           | -43.15  | 4.49            |
| 2              | 41.87          | 37.76           | -9.83   |                 | 59.99          | 36.92           | -38.45  |                 |
| 3              | 33.70          | 34.76           | 3.14    |                 | 42.89          | 34.18           | -20.32  |                 |
| 4              | 30.32          | 32.38           | 6.78    |                 | 32.67          | 31.78           | -2.72   |                 |
| 5              | 26.55          | 29.21           | 10.01   |                 | 24.83          | 28.79           | 15.96   |                 |
| 6              | 24.45          | 26.30           | 7.55    |                 | 19.36          | 25.60           | 32.23   |                 |
| 7              | 24.47          | 18.28           | -25.31  |                 | 22.25          | 16.88           | -24.14  |                 |
| 8              | 22.46          | 15.97           | -28.88  |                 | 19.69          | 14.97           | -23.96  |                 |
| 9              | 21.43          | 11.90           | -44.47  |                 | 14.82          | 10.79           | -27.19  |                 |
| 10             | 48.04          | 40.75           | -15.18  |                 | 64.20          | 39.75           | -38.09  |                 |
| 11             | 40.55          | 38.80           | -4.30   |                 | 49.71          | 38.10           | -23.35  |                 |
| 12             | 33.53          | 36.12           | 7.73    |                 | 35.97          | 35.55           | -1.17   |                 |
| 13             | 30.06          | 33.99           | 13.09   |                 | 28.26          | 33.41           | 18.23   |                 |
| 14             | 26.16          | 31.14           | 19.03   |                 | 22.38          | 30.85           | 37.87   |                 |
| 15             | 23.91          | 28.38           | 18.69   |                 | 17.49          | 27.69           | 58.31   |                 |
| 16             | 22.44          | 21.27           | -5.24   |                 | 18.18          | 19.85           | 9.19    |                 |
| 17             | 20.51          | 18.97           | -7.55   |                 | 16.24          | 17.94           | 10.50   |                 |
| 18             | 19.39          | 14.83           | -23.51  |                 | 12.55          | 13.64           | 8.71    |                 |

|    |       |       |       |  |       |       |        |  |
|----|-------|-------|-------|--|-------|-------|--------|--|
| 19 | 45.60 | 41.38 | -9.26 |  | 47.00 | 40.40 | -14.05 |  |
| 20 | 39.04 | 39.67 | 1.62  |  | 37.30 | 38.77 | 3.93   |  |
| 21 | 34.07 | 36.96 | 8.49  |  | 32.78 | 36.38 | 10.99  |  |
| 22 | 30.52 | 34.99 | 14.67 |  | 26.30 | 34.41 | 30.83  |  |
| 23 | 26.46 | 32.22 | 21.76 |  | 20.53 | 31.66 | 54.22  |  |
| 24 | 24.07 | 29.70 | 23.37 |  | 16.74 | 29.01 | 73.28  |  |

### 7.5 Closure

In this chapter, results of single phase and two phase cross flow for AHWR rod bundle are discussed. The cross flow resistance coefficient decreases with increase in ratio of cross flow velocity to the axial velocity both in single and two phase flow condition. Also the cross flow resistance coefficient in two phase flow is higher as compared to single phase flow. An assessment of existing models against present experimental data has been carried out and found that none of these models predict cross flow resistance coefficient for AHWR rod bundle. In the view of this, a new model applicable to AHWR has been presented which predicts cross flow resistance coefficient quite accurately.

## CHAPTER 8

### *CONCLUSION AND FUTURE WORK*

---

---

#### **8.1 Conclusion**

In the present work, an inter-subchannel mixing phenomenon has been investigated in the subchannels of AHWR rod bundle due to its importance for reactor thermal margin and safety. An assessment of turbulent mixing models has been carried out and found that there is large discrepancy between predictions by models and existing experimental data relevant to conventional BWRs. This is because turbulent mixing phenomena are highly geometry and operating condition dependent. The average errors in existing models as compared to test data are found to be more than 1000 %. Because of large error in the models, a new model for turbulent mixing was proposed from first principle. The model could predict within average error of  $\pm 4\%$  for all the test data available for triangular-triangular, square-square, rectangular-rectangular subchannel array. The model was tested even for steam-water high pressure data and found that it can predict within average error of  $\pm 9.94\%$ . However, the AHWR rod bundle is completely different from conventional BWRs. In addition being a natural circulation BWR, the flow velocity in the subchannel can vary over a wide range unlike that of conventional BWRs. The existing

test data and models applicable to conventional BWRs, are not applicable to AHWR condition. This has necessitated measurement in 1:1 condition of AHWR rod bundle and develops AHWR specific models can later use for AHWR thermal margin and safety analysis.

Study of inter-subchannel mixing phenomena for AHWR rod bundle gives important conclusion which are enlisted here

### **I. Single phase turbulent mixing**

1. The turbulent mixing rate increase with increase in flow velocity in the subchannel.
2. The turbulent mixing rate between subchannels is higher for higher  $S/\delta$  and vice versa.
3. The capability of existing correlations to predict the measured single phase turbulent mixing rate and found that none of these correlations are able to predict measured turbulent mixing rate accurately.
4. An empirical model is derived based on these experimental data and found that there is good agreement i.e.  $\pm 7\%$  between predicted and measured values.

### **II. Two phase turbulent mixing**

1. The liquid phase turbulent mixing rate is more or less constant up to average void fraction of 0.3 which is in bubbly flow regime, and then increases and reaches to a maximum at void fraction equal to 0.55 which is in slug-churn flow regime; afterwards it decreases till it reaches void fraction equal to 0.8.

2. The gas phase turbulent mixing rate increases with increase in average void fraction and reaches maximum at void fraction equal to 0.65. Afterwards, it decreases till it reaches void fraction equal to 0.8.
3. The turbulent mixing rate between subchannels is nearly same for two phase flow conditions unlike that in single phase flow condition. The reason behind is that two phase fluctuation is more as compared to single phase flow due to bubble induced turbulence which homogenizes the turbulent mixing rate.
4. The test data were compared with existing models. It was found that existing models could not predict the measured turbulent mixing rate in the rod bundle of AHWR.
5. Also capability of present model is evaluated to predict the measured two phase turbulent mixing rate. It was found that the present models could predict the measured turbulent mixing rate in the rod bundle of reactor within range (average error) of  $\pm 2\%$ .

### **III. Void drift**

1. Significant amount of void drift is observed to the subchannel having more open area.
2. The variation in equilibrium and non-equilibrium void fraction is insignificant with respect to liquid superficial velocity.
3. The difference in equilibrium and non-equilibrium void fraction of individual subchannel is found to be less in bubbly flow regime and is more in slug-churn flow regime.
4. The void diffusion coefficient is more or less constant or little increases with increase in average void fraction up to  $\alpha \approx 0.45$ . After void fraction  $\alpha \approx 0.45$ , there is a steep increase in void diffusion coefficient with increase in average void fraction increases.

5. The capability of existing correlation is checked to predict the measured equilibrium void fraction. The test data were compared with existing models in literature. It was found that existing models could predict the measured equilibrium void fraction in the rod bundle of reactor within range (average error) of +8 % to -14 %.

#### **IV Diversion cross flow**

1. The cross flow resistance coefficient decreases with increase in ratio of cross flow velocity to the axial velocity both in single and two phase flow condition.
2. Also cross flow resistance coefficient in two phase flow is higher as compared to single phase flow.
3. It is well correlated with ratio of cross flow velocity to the axial velocity both in single and two phase flow condition.

In addition to above, our results indicates that

- i. The turbulent mixing and void drift both are found to be dependent on void fraction and flow regimes even for low mass flux condition typical to AHWR geometry.
- ii. The magnitude of turbulent mixing rate and diffusion coefficient is found to be higher for AHWR subchannels geometry compared to conventional BWRs geometry for the same mass flux.
- iii. Also the magnitude of turbulent mixing rate and diffusion coefficient found to be increase with increase in superficial liquid velocity.

## 8.2 Future Work

A rigorous study has been performed to investigate inter-subchannel mixing phenomena i.e. turbulent mixing, void drift and diversion cross flow for AHWR rod bundle which include assessment of models, experiments performed for subchannel analysis and develop model for the same. However no research is fully complete and gives future direction. Some important points enlisted here

1. The experiment was performed for AHWR rod bundle with no spacer. However literature suggests spacers enhances mixing between subchannels. So experiment can perform including spacer which is important to predict CHF accurately.
2. This experiment is performed with water and air as working fluid to scale up steam water system. It is interesting to know the effect of heating on mixing between subchannels of AHWR rod bundle.
3. The computer code like COBRA can be modified by introducing models so developed for inter-subchannel mixing for AHWR rod bundle.
4. Local measurement of turbulent mixing, void drift and diversion cross flow is also important for subchannel mixing phenomena. So experiment can perform to measure turbulent mixing, void drift and diversion cross flow locally in the rod bundle by using advance technique

## References

1. **R.T. Lahey, Jr., and F.J. Moody**, The Thermal Hydraulics of Boiling Water Nuclear Reactor, 2<sup>nd</sup> ed., ANS, La Grange Park (1993).
2. **A. Hotta, H. Shirai, M. Azuma, M. Sadatomi, A. Kawahara, H. Ninokata**. “A modified equilibrium void distribution model applicable to subchannel-scale vapor–liquid cross flow model for conventional square and tight lattice BWR fuel bundles”. *Nuclear Engineering and Design*, 235: 983–999 (2005).
3. **K. Petrunik**, “Turbulent Mixing Measurement for Single Phase Air, Single Phase Water, and Two Phase Air-Water Flows in Adjacent Rectangular Subchannels,” M.Sc Thesis, University of Windsor, Ontario (1968)
4. **F. B. Walton**, “Turbulent Mixing Measurements for Single-Phase air, Single-Phase Water and Two-Phase Air-Water Flows in Adjacent Triangular Subchannels,” M.Sc. Thesis, Department of Chemical Engineering, University of Windsor (1969).
5. **D.S. Rowe and C.W. Angel**, “Cross flow mixing between parallel flow channel during boiling, Part III: Effect of spacer on mixing between two channels”, Bettelle Northwest, BNWL-371, (1969).

6. **K. P. Galbraith and J. G. Knudsen**, “Turbulent Mixing Between Adjacent Channels for Single-Phase Flow in a Simulated Rod Bundle,” *AICHE Symp. Ser.*, 68, 118, 90 (1971).

7. **K. S. Singh**, “Air-Water Turbulent Mixing in Simulated Rod Bundle Geometries,” Ph.D. Thesis, Department of Chemical Engineering, University of Windsor (1972).

8. **F.S. Castellana, W.T. Adams, J.E. Casterline**, “Single-phase subchannel mixing in a simulated nuclear fuel assembly”, *Nuclear Engineering and Design*. 26, 242 (1974).

9. **J. T. Rogers and A. E. E. Tahir**, “Turbulent Interchange Mixing in Rod Bundles and the Role of Secondary Flows,” *ASME 75-HT-31*, American Society of Mechanical Engineers (1975).

10 **J. M. Kelly and N. E. Todreas**, “Turbulent Interchange in Triangular Array Bare Rod Bundles,” COO- 2245-45TR, Massachusetts Institute of Technology (1977)

11. **M. Sadatomi, A. Kawahara, K. Kano and Y. Sumi**, Single and Two-Phase of Turbulent Mixing Rate between Adjacent Subchannels in a Vertical 2×3 Rod Array Channel, *International Journal of Multiphase Flow*, 30, pp. 481-498, (2004).

12. **A. Kawahara, M. Sadatomi, H. Kudo and K. Kano**, “Single and two phase turbulent mixing rate between subchannels in triangle tight lattice rod bundle,” *JSME International Journal, Series B*, 49, No. 2., pp. 287-295, (2006).
13. **K. Rehme**, “The Structure of Turbulence in Rod Bundles and the Implications on Natural Mixing Between the Subchannels,” *Int. J. Heat Mass Transfer*, 35, 567 (1992); [http://dx.doi.org/10.1016/0017-9310\(92\)90291-Y](http://dx.doi.org/10.1016/0017-9310(92)90291-Y).
14. **W. J. Seale**, “Turbulent Diffusion of Heat Between Connected Flow Passages, Part 1: Outline of Problem and Experimental Investigation,” *Nucl. Eng. Des.*, 54, 183 (1979); [http://dx.doi.org/10.1016/0029-5493\(79\)90166-3](http://dx.doi.org/10.1016/0029-5493(79)90166-3).
15. **K.F. Rudzinski**, “Two-Phase Turbulent Mixing for Air-Water Flows in Adjacent Triangular Subchannels”. M.Sc. Thesis, Department of Chemical Engineering, University of Windsor. (1970).
16. **A. Kawahara, M. Sadatomi and Y. Sato**, “Two-phase turbulent mixing between subchannels in a simulated rod bundle geometry-the effect of the number of gaps between subchannels,” *Proc. 2<sup>nd</sup> Japanese-German Symp. on multi phase flow*. Tokyo, Japan. September 25-27, pp. 55-64, (1997b).
17. **S. G. Bues**, “Two Phase Turbulent Mixing Model for Flow in Rod Bundle”. *Report WAPD-T-2438*. Bettis Atomic Power Laboratory. (1972).

18. **M.S. Kazimi, J.E. Kelly**, “Formulation of Two Fluid Model for Mixing in LWR Bundle”. *Thermal Hydraulics of Nuclear Reactor*, pp 433–439 (1983).
19. **L.N. Carlucci, Hammouda, D.S. Rowe**. “Two Phase Turbulent Mixing And Buoyancy Drift in Rod Bundle”. *Nuclear Engineering and Design*, 227: 65–84 (2003).
20. **A. Kawahara, M. Sadatomi and Y. Sato**, “Prediction of turbulent mixing rate of both gas and liquid Phases between adjacent subchannels in a two phase slug churn flow,” *Nuclear Engineering and Design*, Vol. 202, pp. 27-38, (2000).
21. **R.T. Lahey and F.A. Schraub**, “Mixing, flow regime and void fraction for two-phase flow in rod bundle”, two phase flow and heat transfer in rod bundle, ASME winter annual meeting, Los Angeles, California. pp. 1-14 (1969).
22. **R.T. Lahey Jr., B.S. Shiralkar, D.W. Radcliffe, E.E. Polomik**, “Out-of pile subchannel measurements in a nine rod bundle for water at 1000 psia,” in G. Hetzroni et al. (eds.), *Progress in Heat Transfer*, Vol. 6, Pergamon, London, pp. 345-363 (1972).
23. **J.M. Gonzalez-Santalo, P. Griffith**, Two-phase flow mixing in rod bundle subchannels, ASME Paper 72-WA/NE-19, pp. 1-13 (1972).

24. **R.T. Lahey Jr.**, “Subchannel measurements of the equilibrium quality and mass flux distribution in a rod bundle”, Proc.8th Int. Heat Transfer Conf., San Francisco, pp.2399-2404 (1986).
25. **Y. Sato, M. Sadatomi, H. Tsukashima**, “Two-phase flow characteristics in interconnected subchannels with different cross-sectional areas”, Proc. ASME-JSME Thermal Engineering Joint Conf., ASME, New York, pp. 389-395 (1987).
26. **Y. Sato, M. Sadatomi**, “Two-phase gas-liquid flow distributions in multiple channels”, Proc. Japan-US Seminar on Two phase Flow Dynamics, Ohtso, pp. E4 1-10 (1988).
27. **S. Gencay, A. Teyssedou and P. Tye**, “Lateral mixing mechanism in vertical and horizontal interconnected subchannel two phase flow”. Nuclear. Technology (ANS). 138, 140-161–37 (2001).
28. **M. Sadatomi, A. Kawahara, Y. Sato**, “Flow redistribution due to void drift in two-phase flow in a multiple channel consisting of two subchannels”. *Nuclear Engineering and Design*. 148, 463–474 (1994).
29. **M. Sadatomi, A. Kawahara, T. Kuno, K. Kano**, “Two-Phase Void Drift Phenomena in a  $2 \times 3$  Rod Bundle: Flow Redistribution Data and their Analysis”. *Nuclear Technology* (ANS) 152, 23–37 (2004).

30. **M. Sadatomi, A. Kawahara, K. Kano**, “Flow characteristic in hydraulically equilibrium two phase flow in vertical 2×3 rod bundle channel”. *International journal of multiphase flow*. 30,1093–1193 (2004).
- 31 **A. Kawahara, M. Sadatomi, K. Kano, Y. Sasaki, H. Kude**, “Void Diffusion Coefficient In Two-Phase Void Drift For Several Channels Of Two- And Multi-Subchannel Systems”, *Multi phase Science and Technology*, 18, pages 31-54 (2006)
32. **J.S. McNown**, ASCE Trans. 119-1103 (1954).
33. **T.G. Chapman**, “Pressure Equalization by Fluid Exchange Between Parallel Flow Channels”, ORNL-TM-456 (1963).
34. **R.T. Dittrich and C.C. Graves**, Flight Propulsion Research Laboratory, Cleveland, Ohio, NACA-TN-3663 (1956).
35. **R.T. Dittrich**, Flight Propulsion Laboratory, Cleveland, Ohio, NACA-TN-3924 (1958).
36. **A. Tapucu**, “Studies On Diversion Cross-Flow Between Two Parallel Channels Communicating By A Lateral Slot. I: Transverse Flow Resistance Coefficient” *Nuclear Engineering and Design* 42, 297-306 (1976).

37. **A. Kawahara, T. Higuchi, M. Sadatomi and H. Kudo** , “Single- and Two-Phase Diversion Cross-Flows Between Triangle Tight Lattice Rod Bundle Subchannels -Data on Flow Resistance and Interfacial Friction Coefficients for the Cross-Flow”, *Journal of power and energy system*, Vol.1 no. 1, 111-122 (2007).
38. **T. Iwamura, H. Adachi, M. Sobajima**, “Air-Water Two-Phase Cross Flow Resistance in Rod Bundle, *Journal of Nuclear Science and Technology*”, Vol. 23[7], pp. 658-660 (1986).
39. **S Kim and G.C. Park**, “Numerical Determination of Lateral Loss Coefficient for Subchannel Analysis in Nuclear Fuel Bundle”. *Journal of Korean nuclear society*, vol 27 no 4, 491-502 (1995).
40. **A. Tapucu, M. Geçkinli, N. Troche, and R. Girard**, “Experimental Investigation of Mass Exchanges Between Two Laterally Interconnected Two-Phase Flows,” *Nuclear Engineering and Design*, 105, 295 (1988)
41. **N. E. Todreas and M. S. Kazimi**, *Nuclear Systems II*, Massachusetts Institute of Technology (1976).
42. **A. Dasgupta, D.K. Chandraker, P.K. Vijayan and D. Saha**, “Steady State Subchannel Analysis of AHWR fuel cluster”. BARC/2006/E/018 (2006).

43. **D.K. Chandraker**, “Study on critical power for Advanced Heavy Water Reactor,” Ph.D. Thesis, Department of Nuclear Engineering, Tokyo Institute of Technology (2012).

44. **D.K. Chandraker, A.K. Nayak, P.K. Vijayan** “Development and Validation of Methodology for Dryout Modeling in BWR Fuel Assemblies and Application to AHWR Design.” BARC newsletter, issue no 33, pp 19-27 (2013)

45. **P. Griffith and Rose G.**, “Course notes on two phase flow”, MIT Summer Course notes, (1964).

46. **G. Wallis, Eleventh Advanced Seminar**, “Two-Phase Gas Liquid Flows”, A.I.Ch.E., New York, pp 1-33 (1967).

47. **D. Chisholm**, “Void fraction during two-phase flow”. *J. Mech. Eng. Sci.* 15, 235–236 (1973).

48. **J.T., Rogers and R.G. Rosehart**, Mixing by Turbulent Interchange in Fuel Bundle, Correlation and Interface. ASME, 72-HT-53, (1972).

## APPENDIX 1

### Carlucci et al. (2003) model

Carlucci et al. (2003) developed a model based on the principle that total phasic turbulent mixing rate is sum of homogenous turbulent mixing rate and incremental turbulent mixing rate.

The total liquid turbulent mixing rate is given by

$$W'_l = W'_{l,\text{hom}} + \Delta W'_{l,\text{tph}} \quad (1)$$

where

$$W'_{l,\text{hom}} = (1-x)W'_{\text{hom}} \quad (2)$$

The total gas turbulent mixing rate is given by

$$W'_g = W'_{g,\text{hom}} + \Delta W'_{g,\text{tph}} \quad (3)$$

where

$$W'_{g,\text{hom}} = xW'_{\text{hom}} \quad (4)$$

The homogenous turbulent mixing rate is calculated from following equation

$$W_{\text{hom}} = \mu_{\text{hom}} a_w \left( \frac{S}{d} \right)^{b_w} \left( \frac{GD}{\mu_{\text{hom}}} \right)_{\text{hom}}^{0.9} \quad (5)$$

$a_w$  and  $b_w$  are constant. For triangular geometry  $a_w = 0.0018$  and  $b_w = -0.4$  and square or rectangular geometry  $a_w = 0.005$  and  $b_w = 0.106$ .

The homogenous dynamic viscosity is given by

$$\mu_{\text{hom}} = \left( \frac{x}{\mu_g} + \frac{1-x}{\mu_l} \right)^{-1} \quad (6)$$

In this model, incremental turbulent mixing rate equation was obtained by fitting the data of Walton (1969), Singh (1972), and Rudzinski (1970) for triangular and square array subchannel geometry, which is given by following equation

For liquid phase

$$\Delta W_{l,ph} = 0.0515 \exp \left[ -0.5 \left( \frac{\alpha - 0.53}{0.1794} \right)^2 \right] \quad (7)$$

For gas phase

$$\Delta W_{g,ph} = 0.00264 \exp \left[ -8.332 \left\{ \ln \left( 1 - 1.9412 (\alpha - 0.75884) \right) \right\}^2 \right] \quad (8)$$

The above correlations are applicable for smooth bundles having no obstruction with low mass flux (100-2000 kg/m<sup>2</sup>s) and low pressure range (0.1-0.34 MPa). To show the effects of mass flux, pressure, obstruction (spacer) and gap spacing, Carlucci et al. (2003) modified above model by introducing various factors. The modified model is shown below

The total liquid turbulent mixing rate is given by

$$W'_l = W'_{l,hom} + W'_{l,inc} \quad (9)$$

where

$$W'_{l,hom} = F_{obs} (1-x) W'_{hom} \quad (10)$$

and

$$W'_{l,inc} = \frac{F_{G.P} F_{gap} \Delta W'_{l,ph}}{F_{obs}} \quad (11)$$

The total gas turbulent mixing rate is given by

$$W'_g = W'_{g,hom} + W'_{g,inc} \quad (12)$$

where

$$W'_{g,hom} = F_{obs} \chi W'_{hom} \quad (13)$$

and

$$W'_{g,inc} = \frac{F_{G,P} F_{gap} \Delta W'_{g,tph}}{F_{obs}} \quad (14)$$

The gap factor and obstruction factor is calculated by the following relation

$$F_{gap} = 1.287 \left[ 1 - \exp(-1.5 \times 10^6 \times S^2) \right] \quad (15)$$

and

$$F_{obs} = 1 + a_{obs} k \exp(-b_{obs} \frac{z}{D}) \quad (16)$$

respectively. In the above equation,  $k$  is obstruction loss factor which is proportional to square of obstruction flow area to total flow area and  $a_{obs}$  and  $b_{obs}$  are constant and their values are given as 3.3 and 0.13 respectively.

### **Bues (1972) model**

In Bues' model, the total turbulent mixing rate is formulated for two regimes. A physical model is developed for the first region i.e. bubbly-slug region and it is combined with an empirical fit for the second region i.e. annular region

In bubbly-slug regime, the turbulent mixing rate is given by

$$W'_I = W'_{l, sph} + B_1 \left( \frac{AG}{D} \right) \frac{\rho_l}{\rho_g} \left( \frac{s-1}{s} \right) x \quad (17)$$

where the single phase liquid turbulent mixing rate is given by

$$W'_{l, sph} = 0.0035 \mu_l \text{Re}_l^{0.9} \quad (18)$$

The empirical constant is expressed as

$$B_1 = 0.04 \left( \frac{S}{D} \right)^{1.5} \quad (19)$$

The slip ratio

$$s = \frac{x}{1-x} \cdot \frac{1-\alpha}{\alpha} \cdot \frac{\rho_l}{\rho_g} \quad (20)$$

The peak mixing is assumed to take place at a quality  $x_p$  which is given by

$$x_p = \left[ \frac{0.4 \{ \rho_l (\rho_l - \rho_g) g D \}^{0.5}}{G} + 0.6 \right] \times \frac{1}{\left[ \left( \frac{\rho_l}{\rho_g} \right)^{0.5} + 0.6 \right]} \quad (21)$$

Substituting  $x=x_p$  in equation (17), then the peak mixing rate is expressed as

$$W'_p = W'_{l, sph} + B_1 \left( \frac{AG}{D} \right) \frac{\rho_l}{\rho_g} \left( \frac{s-1}{s} \right)_{x=x_p} x_p \quad (22)$$

In annular flow regime, the turbulent mixing rate is given by

$$W'_{II} = W'_{g, sph} + (W'_p - W'_{g, sph}) \left( \frac{1 - \left( \frac{x_0}{x_p} \right)}{\frac{x}{x_p} - \left( \frac{x_0}{x_p} \right)} \right) \quad (23)$$

The single phase gas turbulent mixing rate is given by

$$W'_{g, sph} = 0.0035 \mu_g \text{Re}_g^{0.9}; \quad (24)$$

The empirical parameter is expressed as

$$\frac{x_0}{x_p} = 0.57 \text{Re}^{0.0417} \quad (25)$$

According to Lahey and Moody (1993), the turbulent mixing of q-phase in a two phase flow is given by

$$W'_q = \rho_q \alpha_{gap,q} S \left( \frac{\varepsilon}{l} \right)_{tph} \quad (26)$$

Therefore we can write, the turbulent mixing of liquid in a two phase flow is given by

$$W'_l = \rho_l (1 - \alpha) S \left( \frac{\varepsilon}{l} \right)_{tph} \quad (27)$$

and the turbulent mixing of gas in a two phase flow is given by

$$W'_g = \rho_g \alpha S \left( \frac{\varepsilon}{l} \right)_{tph} \quad (28)$$

For finding out the liquid turbulent mixing rate and gas turbulent mixing rate from the total turbulent mixing rate, Kawahara et al. (2000) derived the velocity fluctuation of two phase from this model which are as follows

The velocity fluctuation of two phase for first region is given by

$$\left( \frac{\varepsilon}{l} \right)_{l,tph} = \frac{\rho_l}{\rho_{tph}} \left( \frac{\varepsilon}{l} \right)_{l,sph} \theta_l \quad (29)$$

where the velocity fluctuation of single phase is expressed as

$$\left( \frac{\varepsilon}{l} \right)_{l,sph} = \frac{0.0035 \mu_l \text{Re}_l^{0.9}}{\rho_l S} \quad (30)$$

The mean two phase density is given by

$$\rho_{tph} = \rho_g \alpha + \rho_l (1 - \alpha) \quad (31)$$

The multiplier is expressed as

$$\theta_l = \left\{ 1 + (\theta_{p,l} - 1) \left( \frac{s}{1-s} \right)_{x=x_p} \frac{s-1}{s} \frac{x}{x_p} \right\}; \quad (32)$$

where

$$\theta_{p,l} = \frac{W'_p}{W'_{l,sph}} \quad (33)$$

The velocity fluctuation of two phase for second region is given by

$$\left( \frac{\varepsilon}{l} \right)_{II,tph} = \frac{\rho_l}{\rho_{tph}} \left( \frac{\varepsilon}{l} \right)_{g,sph} \theta_g \quad (34)$$

where the velocity fluctuation of single phase due to turbulent mixing is given by

$$\left( \frac{\varepsilon}{l} \right)_{g,sph} = \frac{0.0035 \mu_g \text{Re}_g^{0.9}}{\rho_g S} \quad (35)$$

The multiplier  $\theta_g$  is given by

$$\theta_g = 1 + (\theta_{p,g} - 1) \left( \frac{1 - \left( \frac{x_0}{x_p} \right)}{\frac{x}{x_p} - \left( \frac{x_0}{x_p} \right)} \right) \quad (36)$$

### **Kazimi and Kelly (1983) model.**

Kazimi and Kelly's model is based on Bues' model which shows dependence of mixing rate on flow regimes. They proposed a correlation between the velocity fluctuation due to two phase turbulent mixing and the velocity fluctuation due to single phase turbulent mixing which are as follows.

$$\left(\frac{\varepsilon}{l}\right)_{tph} = \left(\frac{\varepsilon}{l}\right)_{sph} \theta \quad (37)$$

where  $\theta$  is the two phase multiplier which depend on quality are as follows

$$\text{If } 0 < x < x_p \text{ then } \theta = 1 + (\theta_p - 1) \left( \frac{1 - \left(\frac{x_0}{x_p}\right)}{\frac{x}{x_p} - \left(\frac{x_0}{x_p}\right)} \right) \quad (38)$$

$$\text{and if } 0 < x < x_p \text{ then } \theta = 1 + (\theta_p - 1) \left( \frac{x}{x_p} \right) \quad (39)$$

In equation 37, the empirical parameter is calculated from following relation

$$\frac{x_0}{x_p} = 0.57 \text{Re}^{0.0417} \quad (40)$$

and value of  $\theta_p$  is taken as equal to 5

The correlation for velocity fluctuation due to single phase turbulent mixing rate is given by Roger and Rosehart (1972)

$$\left(\frac{\varepsilon}{l}\right)_{sph} = \frac{1}{2} \lambda \text{Re}^{-0.1} \left( 1 + \frac{D_j}{D_i} \right) \frac{D_i}{d} \cdot \frac{G_i}{\rho} \quad (41)$$

where

$$\lambda = 0.0058 \left( \frac{S}{d} \right)^{-1.46} \quad (42)$$

### **Kawahara et al. (2000) model**

Kawahara et al. deduced a model for slug churn flow regime. In this model, the liquid phase turbulent mixing rate is the sum of three independent component mixing rate due to turbulent diffusion, convective transfer and pressure difference as given by

$$W_l' = W_{l,td}' + W_{l,ct}' + W_{l,pd}' \quad (43)$$

For turbulent mixing rate due to turbulent diffusion and convective transfer, Kawahara et al. modified Sadatomi et al. model for the single phase turbulent mixing by multiplying  $(1-\alpha)$  which are as follows

$$W_{l,TD}' = \rho_l \left( \frac{F_i^*}{\varepsilon_{Dli}} + \frac{F_j^*}{\varepsilon_{Dli}} \right)^{-1} (1-\alpha) \quad (44)$$

where the subchannels geometry factor for square or rectangular geometry is given by

$$F_i^* = \frac{\pi}{4} + \frac{p/d}{\sqrt{\left(\frac{p}{d}\right)^2 - 1}} \tan^{-1} \theta \left( \frac{p/d + 1}{\left(\frac{p}{d}\right)^2 - 1} \right) \quad (45)$$

and the subchannel geometry factor for triangular geometry is given as

$$F_i^* = -\frac{1}{2} \sin^{-1} \left( \frac{p/d}{\sqrt{3}} \right) + \frac{p/d}{\sqrt{(p/d)^2 - 1}} \tan^{-1} \left( \frac{\left( \frac{p/d}{\sqrt{3}} + 1 \right) \tan \left[ \frac{1}{2} \sin^{-1} \left( \frac{p/d}{\sqrt{3}} \right) \right]}{\sqrt{(p/d)^2 - 1}} \right) \quad (46)$$

According to Elder (1959), the turbulent diffusivity of liquid is given by

$$\frac{\rho_l \mathcal{E}_{Dli}}{\mu_l} = 0.040 \text{Re}_{li} \sqrt{f_i} \quad (47)$$

where Reynolds number and friction factor are given by

$$\text{Re}_{li} = \frac{\rho_l u_{li} D_i}{\mu_l}; \quad (48)$$

$$u_{li} = \frac{j_{li}}{1 - \alpha} \quad (49)$$

and

$$f_i = 0.079 \text{Re}_{li}^{-0.25} \quad (50)$$

For convective transfer

$$W_{i,ct}^* = \beta_{ct} S G_i (1 - \alpha) \quad (51)$$

For square geometry, Stanton number is given as

$$\beta_{ct} = 0.0018 \left( \frac{S}{d} \right)^{-0.52} \quad (52)$$

For triangular geometry, Stanton number is given as

$$\beta_{ct} = 0.000023 \left( \frac{S}{d} \right)^{-1.86} \quad (53)$$

The turbulent mixing rate due to pressure difference fluctuation is given as

$$W'_{ipd} = \rho_l (\sum S) (1-\alpha) \sqrt{\frac{2\rho_l}{K_l} \Delta P'_{RMS}} \quad (54)$$

The RMS value of pressure difference fluctuation is given as

$$\Delta P'_{RMS} = \sqrt{2(1-\gamma)P'_{RMS}}; \quad (55)$$

The value of the correlation coefficient  $\gamma$  depends on number of gap and flow pattern. In slug churn region, the mean value of  $\gamma$  for 1-centre gap was equal to 0.97, for 2-side gap was equal to 0.92, for 3 gap was equal to 0.97.

The RMS value of static pressure difference fluctuation is

$$P'_{RMS} = 2.3P'_{pipe,RMS} \quad (56)$$

where

$$P'_{pipe,RMS} = -38\alpha^5 + 51\alpha^4 - 22\alpha^3 + 7.6\alpha^2 - 0.28\alpha + 0.10 \quad (57)$$

Proportionality constant  $K_l$  calculated by following formula

For 1-center gap:

$$K_{l1c} = 0.71 \times 10^6 (1-\alpha) \text{Re}_{IPD}^{-1.58} \quad (58)$$

For 2-side gap:

$$K_{l2s} = 1.93 \times 10^6 (1-\alpha) \text{Re}_{IPD}^{-1.58} \quad (59)$$

For 3-gap:

$$K_{l3S} = 1.18 \times 10^6 (1 - \alpha) \text{Re}_{IPD}^{-1.58} \quad (60)$$

If size is different from the channel used in the experiment than  $K_l$  is calculated by following relationships

$$K_l = 4.0 \times 10^9 (1 - \alpha) S^{1.41} \text{Re}_{IPD}^{-1.58} \quad (61)$$

The Reynolds number is given as

$$\text{Re}_{l,pd} = \frac{2S\rho_l(\tilde{V}_l)_{pd}}{\mu_l} \quad (62)$$

where the lateral fluctuating velocity is given as

$$\tilde{V}_l = \frac{W'_{l,pd}}{\rho_l(\sum S)} \quad (63)$$

Calculation of  $W'_{l,pd}$  requires an iterative method because  $K_l$  is a function of Reynolds number which again depends on  $W'_{l,pd}$ .

For predicting the gas phase turbulent mixing, they assumed that both gas phase turbulent mixing and liquid phase turbulent mixing are related to each other. In this model, the axial gas volumetric fraction  $\beta$  was related by lateral gas volumetric fraction  $\tilde{\beta}$ , which are as follows

$$(1 - \tilde{\beta}) = -4.10(1 - \beta)^4 + 6.85(1 - \beta)^3 - 2.36(1 - \beta)^2 + 0.61(1 - \beta) \quad (64)$$

The axial gas volumetric fraction  $\beta$  is given as

$$\beta = \frac{j_g}{j_g + j_l} \quad (65)$$

The lateral gas volumetric fraction  $\tilde{\beta}$

$$\tilde{\beta} = \frac{\tilde{V}_g}{\tilde{V}_g + \tilde{V}_l}; \quad (66)$$

where

$$\tilde{V}_l = \frac{W_l'}{\rho_l (\sum S)} \quad (67)$$

and

$$\tilde{V}_g = \frac{W_g'}{\rho_g (\sum S)} \quad (68)$$

## APPENDIX 2

### Incorporation of gap and centroidal distance between subchannels:

As discussed in 5.5.1, the equation for liquid mixing number in two phase flow can be represented by

$$N_{l,mix} = F_{l,gc} \times K_l \quad (1)$$

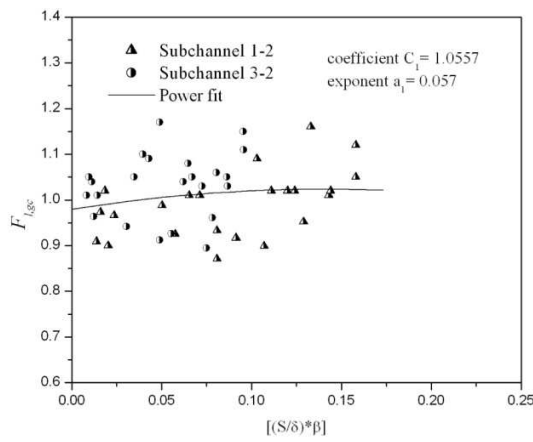
Where

$$K_l = C_l \left[ \text{Re}_{mix} \right]^{a_l} \quad (2)$$

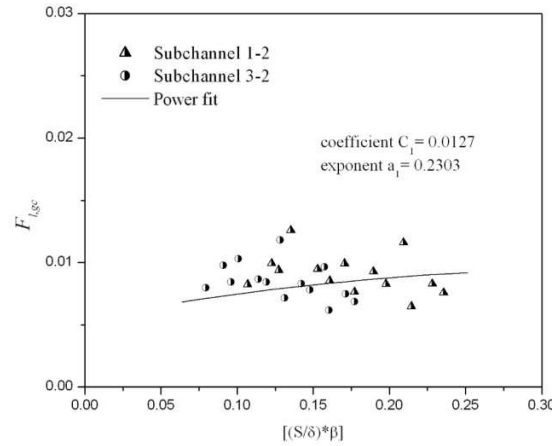
The equation of gap to centroid factor for liquid mixing rate can be expressed as best fit by

$$F_{l,gc} = \left( \frac{N_{l,mix}}{K_l} \right) = C_1 \left[ \left( \beta_{liq} \right) \left( \frac{S}{\delta} \right) \right]^{a_1} \quad (3)$$

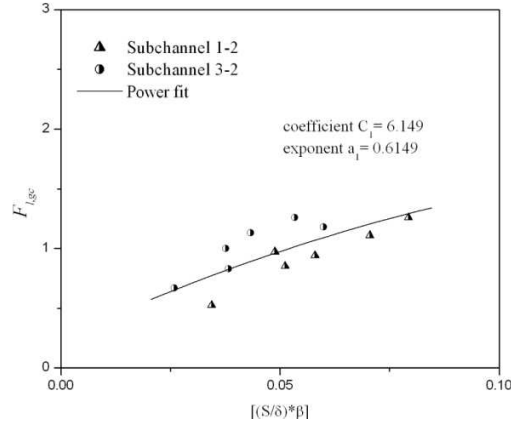
The coefficient ( $C_1$ ) and exponent ( $a_1$ ) were obtained by the test data of present subchannel experiments of plotted on dimensionless gap to centroid factor against combined gap to centroidal distance ratio and volumetric liquid fraction against combined gap to centroidal distance ratio and volumetric liquid as shown in Figure 1 (a), 1 (b), and 1 (c)..



(a)  $0 \leq \alpha \leq 0.3$



(b)  $0.3 \leq \alpha \leq 0.55$



(c)  $0.55 \leq \alpha \leq 0.8$

**Figure 1** The coefficient  $C_1$  and exponent  $a_1$  for various subchannel geometry in liquid phase mixing rate

As discussed in 5.5.2, the equation for gas phase can be represented by

$$N_{g,mix} = F_{g,gc} \times K_g \quad (4)$$

where

$$K_g = C_g \left[ \beta_{gas} \times \ln(\text{Re}_{mix}) \right]^{a_g} \quad (5)$$

The equation of gap to centroid factor for gas mixing rate can be expressed as best fit by

$$F_{g,gc} = \left( \frac{N_{g,mix}}{K_g} \right) = C_1 \times e^{a_1 \times (\beta_{liq}) \left( \frac{S}{d} \right)} \quad (6)$$

The coefficient ( $C_1$ ) and exponent ( $a_1$ ) were obtained by the test data of present subchannel experiments plotted on dimensionless gap to centroid factor against combined

gap to centroidal distance ratio and volumetric liquid fraction as shown in Figure 2 (a), 2

(b),

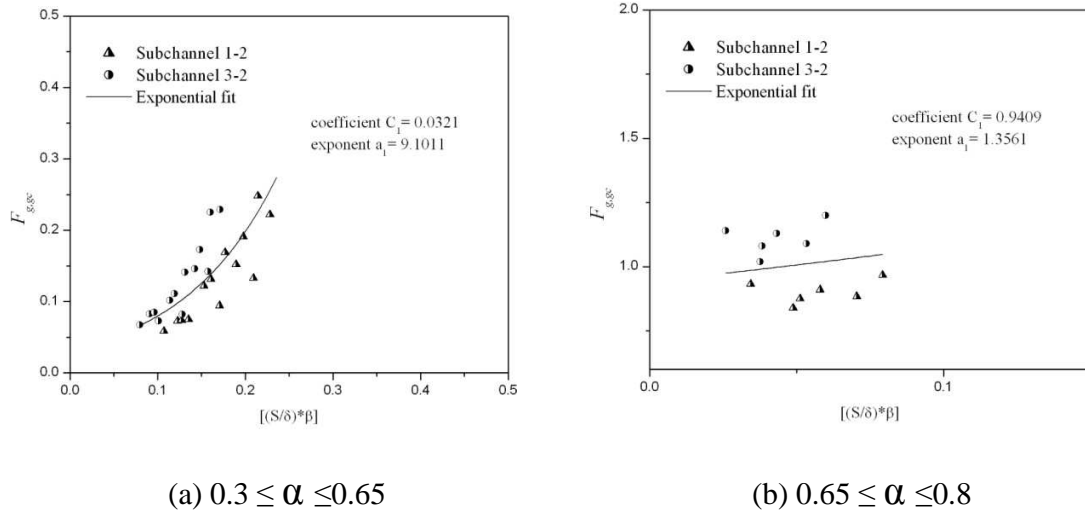


**Figure 2** The coefficient  $C_1$  and exponent  $a_1$  for various subchannel geometry in gas phase mixing rate

### (ii) Modeling of pressure effect

As discussed in 5.5.1 and 5.5.2, the effect of pressure is represented by the following expression

$$F_p = \left( \frac{\sigma_{H.T.}}{\sigma_{R.T.}} \right)^n \quad (7)$$

Where  $n=2$  is the best fit for pressure correction factor

$\sigma_{H.T.}$  = surface tension at high temperature at a corresponding saturation pressure,

$\sigma_{R.T.}$  = surface tension at reference temperature i.e. ambient temperature at a corresponding saturation pressure.

The pressure factor for ambient condition reduces to one as surface has same value in numerator and denominator.

## APPENDIX 3

### Uncertainty analysis

The uncertainty in the experimental data has been determined by standard error analysis method described by Bevington and Robinson (2003). The method for error analysis is as follows:

If  $R$  is a function of  $x$  and  $y$ , written as  $R(x,y)$ , then the uncertainty in  $R$  is obtained by taking the partial derivatives of  $R$  with respect to each variable, multiplication with the uncertainty in that variable, and addition of these individual terms in quadrature (i.e. square, added and then square rooted)

$$R = R(x, y) \tag{1}$$

$$\partial R = \sqrt{\left(\frac{\partial R}{\partial x} \partial x\right)^2 + \left(\frac{\partial R}{\partial y} \partial y\right)^2 + \dots} \tag{2}$$

#### (i) Error analysis of single phase turbulent mixing

The measurement error in volumetric flow rate for water is  $\pm 2\%$  and volumetric flow rate for air rotameter is  $\pm 1\%$ . The measurement error in concentration is  $\pm 2\%$ . Based on the measured data, the error in estimated turbulent mixing rate in single phase flow is found to be  $\pm 6.2\%$ .

**(ii) Error analysis of two phase turbulent mixing**

The measurement error in volumetric flow rate for water is  $\pm 2\%$  and volumetric flow rate for air rotameter is  $\pm 1\%$ . The measurement error in concentration is  $\pm 3\%$ . Based on the measured data, the error in estimated liquid and gas turbulent mixing rate in two phase flow is found to be  $\pm 7.5\%$  and  $\pm 5.25\%$ .

**(iii) Error analysis of void drift**

The measurement error in volumetric flow rate for water is  $\pm 2\%$  and volumetric flow rate for air rotameter is  $\pm 1\%$ . Based on the measured data, the error in estimated void diffusion coefficient by void settling model (Lahey and Moody (1993)) and void fraction by Chisholm correlation (1973) is found to be  $\pm 0.1\%$  and  $\pm 4.15\%$  respectively.

**(iv) Error analysis of diversion cross flow**

The measurement error in volumetric flow rate for water is  $\pm 2\%$  and volumetric flow rate for air rotameter is  $\pm 1\%$ . The accuracy of differential pressure transmitters is  $\pm 0.2\%$ . Based on the measured data, the error in estimated transverse resistance coefficient in single phase flow and two phase flow is found to be  $\pm 2.25\%$  and  $\pm 3.15\%$  respectively.